

**PHYSICOCHEMICAL CHARACTERIZATION OF
THE SORPTION BEHAVIOR OF Cs⁺ AND Sr²⁺
IONS ON NATURAL KAOLINITE AND
CLINOPTILOLITE MINERALS**

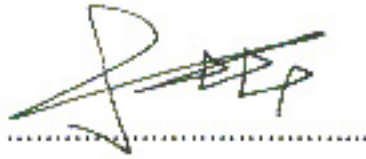
**A Thesis Submitted to
the Graduate School of Engineering and Sciences of
İzmir Institute of Technology
in Partial Fulfillment of the Requirement for the Degree of**

MASTER OF SCIENCE

in Chemistry

**by
Dilek AKAR**

**January 2005
İZMİR**



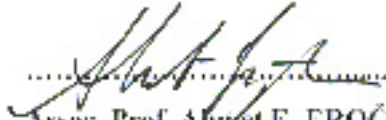
Date of Signature

14.01.2005

Asst. Prof. Tatal SUAIWAN

Supervisor

Department of Chemistry

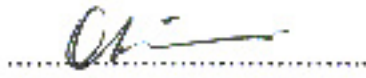


14.01.2005

Assoc. Prof. Ahmet E. EROGLU

Co-supervisor

Department of Chemistry

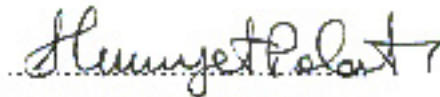


14.01.2005

Prof. Dr. Çetin GÜLER

Ege University,

Facult of Science, Department of Chemistry



14.01.2005

Assoc. Prof. Hüriyet POLAT

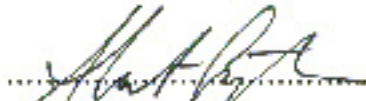
Department of Chemistry



14.01.2005

Assoc. Prof. Serdar ÖZÇELİK

Department of Chemistry



14.01.2005

Assoc. Prof. Ahmet E. EROGLU

Head of Department of Chemistry

Assoc. Prof. Semahat ÖZDEMİR

Head of the Graduate School

ACKNOWLEDGEMENT

I would like to thank the people who have assisted me in preparing this thesis. First I would like to express my grateful thanks to my supervisor Assist. Prof. Dr. Talal SHAHWAN for his guidance, motivations and endless supports during this project. Also I am grateful to my co-supervisor Assoc. Prof. Dr. Ahmet E. EROĞLU for his valuable criticisms and help throughout my thesis.

I am also thankful to Research Scientist Sinan YILMAZ for his help in the AAS measurements, and the Center of Material Research for their assistance in the SEM/EDS and XRPD measurements. Thanks also to Research Assistant Betül ÖZTÜRK for her help in the FTIR measurements.

Special thanks go to all friends, research assistants, technicians in İzmir Institute of Technology for their helps and friendships.

Finally I would like to thank my family for their supports and motivations. Especially I want to extend my appreciation to Murat AKAR for his endless help in preparing my thesis.

ABSTRACT

In this study, aspects of the thermodynamics and kinetic profile of the sorption behavior of Cs^+ and Sr^{2+} ions on natural minerals of kaolinite and clinoptilolite originating from Sındırgı and Manisa regions were investigated.

Radioactive wastes that are caused by the increasing usage and production of radioactive substances give rise to big problems rising day by day. Natural substances such as clay minerals and zeolites decrease the dispersion of radioactive isotopes by sorption. Therefore they can be able to retard the radioactive pollution that is caused by radioisotopes, and the reach of these radioisotopes to the underground waters.

^{137}Cs ($t_{1/2} = 30.1$ y) and ^{90}Sr ($t_{1/2} = 28.8$) are radioisotopes that are important as radioactive wastes due to their long half-lives, and that produce with high yields at the end of nuclear fission reactions.

The experiments were performed using the batch technique at four different initial concentrations, two different temperatures, and time period ranging from 5 minutes up to 48 hours.

The experimental findings revealed that the percentage sorption of Cs^+ on clinoptilolite ranged 91-94, on kaolinite ranged 28-40, and that the percentage sorption of Sr^{2+} on clinoptilolite ranged between 48-93 and 12-47 for the kaolinite case. In order to check the stability of sorption of Sr^{2+} and Cs^+ ions fixed by kaolinite and clinoptilolite, desorption experiments were performed as well with tap water. The results indicated that in the case of Cs^+ sorption on kaolinite the percentage desorption amounted to 40, but was smaller than 7 in the case of clinoptilolite. The desorption percentage of Sr^{2+} from clinoptilolite did not exceed 5, while it is amounted to 12 in kaolinite case, indicating a more stable fixation by clinoptilolite.

The results showed that sorption of both Sr^{2+} and Cs^+ on both minerals followed pseudo-second order kinetics, with the rate constants indicating faster sorption on kaolinite. The activation energies were 11.6 and 15.3 kJ/mol for Cs^+ sorption on kaolinite and clinoptilolite, respectively. Alternatively, the activation energy values for Sr^{2+} sorption on kaolinite and clinoptilolite were 8.5 and 17.3 kJ/mol, respectively. Freundlich and D-R isotherm models were found to adequately describe the adsorption data of Sr^{2+} and Cs^+ on both minerals.

Cs^+ sorption showed a spontaneous and exothermic behavior on both minerals with ΔH^0 being -6.3 and -11.4 kJ/mol for Cs^+ uptake by kaolinite and clinoptilolite, respectively. On the other hand, Sr^{2+} sorption showed a spontaneous and endothermic behavior on both minerals with ΔH^0 being 11.22 and 9.8 kJ/mol for Sr^{2+} sorption on kaolinite and clinoptilolite, respectively. To check the effect of interlayer expansion on the uptake capacity of kaolinite, the clay was intercalated with DMSO, to overcome the tight H-bonding interconnecting the layers of the clay. Expanding the interlayer space of kaolinite from 0.71 nm to 1.12 nm using DMSO intercalation, lead to an increase in the sorption capacity of kaolinite, with the increase being more significant in Sr^{2+} case. Compared with the percentage sorption on natural kaolinite, the percentage sorption of Cs^+ on DMSO-intercalated kaolinite for the initial concentrations of 100 and 500 mg/L of CsCl, increased, respectively, from 35 to 41 , and from 27 to 33 . On the other hand, the percentage sorption of Sr^{2+} on DMSO-intercalated kaolinite for the initial concentrations of 100 and 500 mg/L of $\text{Sr}(\text{NO}_3)_2$, increased from 17 to 58 , and from 22 to 45 , respectively.

SEM/EDS characterization was carried out to investigate structural changes accompanying the sorption process. SEM analysis indicated that both minerals has a well-defined crystal structure. The EDS findings revealed some localization in the sorbed Sr^{2+} and Cs^+ on the surfaces of both minerals and demonstrated the higher fixation ability of clinoptilolite.

ÖZ

Bu çalışmada Cs^+ ve Sr^{2+} iyonlarının, Sındırgı ve Manisa'dan çıkarılan kaolinit ve klinoptilolit minerallerince tutulmaları, kinetik ve termodinamik açılarından incelendi. Deneyler, 5 dakikadan 48 saate kadar değişen çalkalama süreleri, dört farklı başlangıç konsantrasyonu ve iki farklı sıcaklık ortamlarında gerçekleştirilmiştir.

Radyoaktif maddelerin artan üretim ve kullanımı sonucunda oluşan radyoaktif atıklar gün geçtikçe büyüyen bir sorun olarak ortaya çıkmaktadır. Jeolojik oluşumlarda bulunan kil mineralleri ve zeolitler gibi doğal maddeler radyoaktif izotopların dağılımını sorpsiyon yoluyla azaltarak yer altı sularına ulaşmalarını ve meydana getirebilecekleri radyoaktif kirlenmeyi önemli ölçüde önleyebilmektedir.

^{137}Cs ($t_{1/2} = 30.1$ y) ve ^{90}Sr ($t_{1/2} = 28.8$ y) izotopları nükleer fizyon sonucunda yüksek verimle oluşan ve uzun yarı-ömürleri nedeniyle radyoaktif atıklar bakımından önemli olan radyoizotoplardır.

Elde edilen sonuçlar, kaolinit ve klinoptilolit üzerindeki tutulma yüzdelerinin Cs^+ için sırasıyla 28-40 ve 91-94 arasında değiştiğini, Sr^{2+} için sırasıyla 12-47 ve 48-93 arasında değiştiğini göstermiştir. Kaolinit ve klinoptilolit minerallerince adsorplanmış olan Sr^{2+} ve Cs^+ iyonlarının tutulmasının kararlılığını kontrol etmek için çeşme suyu ile desorpsiyon deneyleri gerçekleştirildi. Sonuçlara göre, Cs^+ iyonunun kaolinit kilinden salınımı %40'lara ulaşırken, aynı iyonun klinoptilolit'ten salıverme oranı sadece %7 civarında kalmaktadır. Öbür yandan, Sr^{2+} iyonunun klinoptilolit'ten salıverilme yüzdeleri %5'i geçmezken, kaolinit'ten salınan Sr^{2+} iyonu %12'i geçmemektedir.

Kinetik çalışmalar, Sr^{2+} ve Cs^+ iyonlarının her iki mineral üzerinde de ikinci dereceden hız izleyerek tutulduğunu göstermiştir, ve hız sabitleri kaolinit üzerindeki tutulmanın daha hızlı olduğunu göstermektedir. Cs^+ iyonunun kaolinit ve klinoptilolit mineralleri üzerinde tutulmasına ait aktivasyon enerjisi değerleri sırasıyla 11.6 ve 15.3 kJ/mol'dür. Sr^{2+} iyonunun kaolinit ve klinoptilolit üzerinde tutulmasına ait aktivasyon enerjisi değerleri ise sırasıyla 8.5 ve 17.3 kJ/mol'dür.

Freundlich ve D-R izotermilerinin Sr^{2+} ve Cs^+ iyonlarının her iki mineral üzerinde adsorpsiyonuna ait verileri iyi temsil ettiği bulunmuştur. Termodinamik verilere göre, Cs^+ iyonunun her iki mineral üzerindeki tutulması da kendiliğinden ve ekzotermik bir davranış gösterir ve Cs^+ iyonunun kaolinit ve klinoptilolit minerallerince tutulmasına ait entalpi değerleri sırasıyla -6.3 ve -11.4 kJ/mol'dür. Öbür yandan, Sr^{2+}

iyonunun her iki mineral üzerindeki tutulması kendiliğinden ve endotermik bir davranış göstermiştir ve Sr^{2+} iyonunun kaolinit ve klinoptilolit üzerinde tutulmasına ait entalpi değerleri sırasıyla 11.22 ve 9.8 kJ/mol olarak saptanmıştır.

Kaolinitin yapısını oluşturan tabakalar H-bağları sayesinde sulu ortamlarda genişlememektedir. Bu bağları kırıp tabakalar arası boşluğu genişletmek amacı ile DMSO molekülleri kullanılmıştır. Bunun sonucunda, kaolinitin tabakalar arası boşluğu 0.71nm'den 1.12 nm'e artmıştır. Bu işlem kilin sorpsiyon kapasitesinde bir miktar artış sağlamıştır. Doğal kaolinitin sorpsiyon kapasitesi ile karşılaştırıldığında, 100 ve 500 mg/L CsCl başlangıç konsantrasyonları için Cs^{+} 'un DMSO ile muamele edilmiş kaolinitdeki sorpsiyon kapasitesi, sırasıyla, 35'den 41'e, ve 27'den 33'e artmıştır. Diğer yandan, 100 ve 500 mg/L $Sr(NO_3)_2$ başlangıç konsantrasyonları için Sr^{2+} 'un DMSO ile muamele edilmiş kaolinitdeki sorpsiyon kapasitesi, sırasıyla, 17'den 58'e ve 22'den 45'e artmıştır.

SEM/EDS karakterizasyonu adsorpsiyonla birlikte meydana gelen yapısal değişiklikleri araştırmak amacıyla gerçekleştirilmiştir. SEM analizi her iki mineralin de düzgün bir kristal yapısına sahip olduğunu göstermiştir. EDS bulguları adsorplanmış olan Sr^{2+} ve Cs^{+} iyonlarının her iki mineralin yüzeyinde de tam bir homojen dağılım göstermediklerini ortaya koymuştur ve klinoptilolit daha yüksek adsorpsiyon kapasitesine sahip olduğunu göstermiştir.

TABLE OF CONTENTS

LIST OF FIGURES	XI
LIST OF TABLES.....	XIII
CHAPTER 1 INTRODUCTION	1
1.1 The Sorption Process	1
1.1.1 Basic Definitions.....	1
1.1.2 The Liquid – Solid Interface.....	4
1.2 Radioactive Isotopes in the Geosphere.....	7
1.2.1 Radioactive Wastes.....	7
1.2.2 Cesium	13
1.2.3 Strontium	13
1.3 Clay Minerals and Zeolites.....	14
1.3.1 Clay Minerals.....	15
1.3.1.1 Kaolinite.....	17
1.3.2 Zeolites.....	18
1.3.2.1 Clinoptilolite	19
1.4 The Present Study	20
1.4.1 Literature Survey	20
1.4.2 Aims of the Present Study	22
1.4.3 Methods Applied.....	23
1.4.3.1 Atomic Absorption Spectrometry (AAS)	23
1.4.3.2 Scanning Electron Microscopy/Energy Dispersive X-ray Spectroscopy (SEM/ EDS)	25
1.4.3.3 X-ray Diffraction (XRD)	26
CHAPTER 2 EXPERIMENTAL.....	29
2.1 Preparation of Samples	29
2.1.1 Pretreatment of Kaolinite and Clinoptilolite.....	29
2.1.2 DMSO-Intercalation of Kaolinite	30
2.1.3 The Sorption Experiments	31

2.2 Desorption Studies	31
2.3 Analysis of the Aqueous Solutions	31
2.4 Analysis of the Solid Phases	32
2.4.1 XRPD	32
2.4.2 SEM/EDS	32
CHAPTER 3 MATHEMATICAL RELATIONS	33
3.1 The Distribution Ratio	33
3.2 Adsorption Isotherms	34
3.2.1 Langmuir Isotherm Model	34
3.2.2 Freundlich Isotherm Model	35
3.2.3 Dubinin-Radushkevich Isotherm Model (D-R)	36
3.3 Thermodynamic Parameters	37
3.4 Kinetic Equations	39
3.4.1 First-Order Kinetics	39
3.4.2 Second-Order Kinetics	40
3.4.3 Intra-Particle Diffusion Model	42
3.4.4 Activation Energy	42
CHAPTER 4 RESULTS AND DISCUSSION	44
4.1 Characterization of Natural Kaolinite and Clinoptilolite Minerals	44
4.1.1 XRPD Characterization	44
4.1.2 SEM / EDS Characterization	46
4.1.3 FTIR Characterization	47
4.2 Kinetic Analysis of Sorption	49
4.2.1 Determination of Rate Equations and Activation Energies	53
4.2.2 Determination of Diffusion Parameter	57
4.3 Sorption Isotherm Models	61
4.3.1 Freundlich Isotherm Model	62
4.3.2 D-R Isotherm Model	66
4.4 Determination of Thermodynamic Parameters	69
4.5 Desorption Studies	72

4.6 Surface Characterization.....	73
4.6.1 Characterization of Cs- and Sr-Loaded Kaolinite.....	73
4.6.2 Characterization of Cs- and Sr-Loaded Clinoptilolite	79
CHAPTER 5 CONCLUSIONS	82
REFERENCES	84
APPENDICES	90

LIST OF FIGURES

<u>Figure</u>	<u>Page</u>
Figure 1.1. Schematic picture of Stern and Gouy layers	5
Figure 1.2. Diagram of a radioactive waste repository (EBS).....	9
Figure 1.3. Retardation mechanisms.....	12
Figure 1.4. Manufacture of phyllosilicates	16
Figure 1.5. The ideal kaolinite structure	18
Figure 1.6. Crystal structure representation of clinoptilolite viewed down [001] with [010] vertical.....	20
Figure 1.7. Illustration of Bragg's law.....	27
Figure 2.1. DMSO treatment of kaolinite	30
Figure 4.1. XRPD diagram of natural kaolinite (K = kaolinite, Q = quartz).....	45
Figure 4.2. XRPD diagram of natural clinoptilolite (C = clinoptilolite)	45
Figure 4.3. Typical SEM images of natural kaolinite.....	47
Figure 4.4. Typical SEM images of natural clinoptilolite	47
Figure 4.5. FTIR spectra of natural kaolinite used in our studies.....	48
Figure 4.6. FTIR spectrum of clinoptilolite used in this work	49
Figure 4.7. Variation of the sorbed amount of Cs ⁺ (μmol/g) on kaolinite with time at 25°C	51
Figure 4.8. Variation of the sorbed amount of Sr ²⁺ (μmol/g) on kaolinite with time at 25°C	51
Figure 4.9. Variation of the sorbed amount of Cs ⁺ (μmol/g) on clinoptilolite with time at 25°C	52
Figure 4.10. Variation of the sorbed amount of Sr ²⁺ (μmol/g) on clinoptilolite with time at 25°C.....	52
Figure 4.11. Corresponding linear fit for the variation of the sorbed amount of Cs ⁺ on kaolinite with time, using the pseudo-second order equation at 25C	54
Figure 4.12. Corresponding linear fit for the variation of the sorbed amount of Sr ²⁺ on kaolinite with time, using the pseudo-second order equation at 25C	54
Figure 4.13. Corresponding linear fit for the variation of the sorbed amount of Cs ⁺ on clinoptilolite with time, using the pseudo-second order equation at 25C.....	55
Figure 4.14. Corresponding linear fit for the variation of the sorbed amount of Sr ²⁺ on clinoptilolite with time, using the pseudo-second order equation at 25C.....	55
Figure 4.15. Intraparticle diffusion plots of sorbed Cs ⁺ on kaolinite at 25 ⁰ C and 60 ⁰ C.....	59

Figure 4.16. Intraparticle diffusion plots of sorbed Sr ²⁺ on kaolinite at 25°C and 60°C	59
Figure 4.17. Intraparticle diffusion plots of sorbed Cs ⁺ on clinoptilolite at 25°C and 60°C	60
Figure 4.18. Intraparticle diffusion plots of sorbed Sr ²⁺ on clinoptilolite at 25°C and 60°C	60
Figure 4.19. Freundlich isotherm model plots of Cs ⁺ sorbed by kaolinite at 25°C and 60°C	64
Figure 4.20. Freundlich isotherm model plots of Sr ²⁺ sorbed by kaolinite at 25°C and 60°C	64
Figure 4.21. Freundlich isotherm plots of Cs ⁺ sorbed by clinoptilolite at 25°C and 60°C	65
Figure 4.22. Freundlich isotherm plots of Sr ²⁺ sorbed by clinoptilolite at 25°C and 60°C	65
Figure 4.23. D-R isotherm plots of Cs ⁺ sorbed by kaolinite at 25°C and 60°C	67
Figure 4.24. D-R isotherm plots of Sr ²⁺ sorbed by kaolinite at 25°C and 60°C	67
Figure 4.25. D-R isotherm plots of Cs ⁺ sorbed by clinoptilolite at 25°C and 60°C.....	68
Figure 4.26. D-R isotherm plots of Sr ²⁺ sorbed by clinoptilolite at 25°C and 60°C.....	68
Figure 4.27. EDS mapping images showing the distribution of elements Al, Si, and Cs on the surface of Cs-loaded kaolinite	75
Figure 4.28. EDS mapping images showing the distribution of elements Al, Si, and Sr on the surface of Sr-loaded kaolinite	76
Figure 4.29. XRPD diagrams of: (a) natural kaolinite, (b) DMSO-treated kaolinite, (c) DMSO-intercalated kaolinite after loading with Cs ⁺ ions	78
Figure 4.30. EDS mapping images showing the distribution of elements Al, Si, and Cs on the surface of Cs-loaded clinoptilolite	80
Figure 4.31. EDS mapping images showing the distribution of elements Al, Si, and Sr on the surface of Sr-loaded clinoptilolite.....	81

LIST OF TABLES

<u>Table</u>	<u>Page</u>
Table 1.1. Properties of physisorption and chemisorption	2
Table 1.2. Characteristic interactions associated with categories of adsorption	3
Table 1.3. Some radionuclides of importance in radioactive waste considerations	8
Table 1.4. CEC-values of minerals	15
Table 1.5. Spectroscopic flames for AAS with their properties	24
Table 1.6. X-ray wavelengths (in Å) and K filters for common anode materials	28
Table 2.1. Concentrations of Na, K, Ca, Mg in tapwater used in sorption studies.....	29
Table 4.1. EDS results of the atomic percentages of O, Na, Mg, Al, Si, K, Ca in natural kaolinite and clinoptilolite minerals obtained from spot analysis at 3 different points selected randomly on the surface of minerals.	46
Table 4.2. % Sorption values at different initial concentrations.....	50
Table 4.3. The values of k_2 and $[C]_e$ obtained from the linear fits of the experimental data to the second order rate equation	57
Table 4.4. The linear correlation coefficients (R-values) obtained from Langmuir isotherm plots.....	62
Table 4.5. Freundlich parameters, n and k, obtained from the plots of Cs^+ and Sr^{2+} uptake by kaolinite and clinoptilolite at 25°C and 60°C.....	63
Table 4.6. D-R parameters, K, C_m , and E, obtained from the plots of Cs^+ and Sr^{2+} uptake by kaolinite and clinoptilolite at 25°C and 60°C.....	66
Table 4.7. The R_d values (mL/g) corresponding to Cs^+ sorption on kaolinite and clinoptilolite	69
Table 4.8. The R_d values (mL/g) corresponding to Sr^{2+} sorption on kaolinite and clinoptilolite	70
Table 4.9. Values of ΔH^0 , ΔS^0 , and ΔG^0 calculated from the sorption data of Cs^+ and Sr^{2+} on kaolinite and clinoptilolite.....	70
Table 4.10. The percentage desorption values for Cs^+ sorption on both kaolinite and clinoptilolite	72
Table 4.11. The percentage desorption values for Sr^{2+} sorption on both kaolinite and clinoptilolite	73
Table 4.12. EDS findings of the atomic percentages of O, Si, Al, Ca, Mg, Na, K, and Cs in Cs-loaded kaolinite	75
Table 4.13. EDS findings of the atomic percentages of O, Si, Al, Ca, Mg, Na, K, and Sr in Sr loaded kaolinite	76

Table 4.14. EDS findings of the atomic percentages of Al, Si, O, Na, K, Mg, Ca, and Cs in Cs-loaded clinoptilolite.....	79
Table 4.15. EDS findings of the atomic percentages of Al, Si, O, Na, K, Mg, Ca, and Sr in Sr loaded clinoptilolite.....	80

CHAPTER 1

INTRODUCTION

1.1 The Sorption Process

1.1.1 Basic Definitions

Sorption is the term used to refer to a variety of processes by which a chemical species is fixed on a solid substrate. In the course of a sorption process, the retarded chemical species is termed *sorbate*, whereas the solid substrate is named *sorbent*. Sorption is an important process for the transport of radionuclides through soil media. The presence of aluminosilicate minerals, which includes various types of clay and zeolite minerals act as a natural barriers that retards the transportation of various radionuclides and other potentially harmful ions into the aqueous environment.

The existence of numerous fine particles generated by chemical or physical deterioration of macroscopic solid compounds, low particle settling velocity facilitating the transport, high specific surface area, strong capacities to fix radionuclides are the factors connected with sorption of trace levels radionuclide which determines the transport of radionuclides through the geosphere. (Hakem et al. 1996 p. 225)

In literature, there is no unique definition among researchers / scientists regarding the type of processes that could be classified under the general term of sorption, which is usually confused with the term “adsorption”. Sorption process can take a number of forms that could include fixation of the sorbate at the surface of the sorbent through chemical bonding, electrostatic interactions, or even weaker types of forces like van der Waals forces. The term sorption is used also to describe processes in which the sorbate is ‘absorbed’ within the bulk structure (channels, pores, interlayer space, ...etc) of the sorbent. This term is also occasionally applied to refer to processes in which the sorbate forms a ‘coprecipitate’ with ions in the sorption medium and deposit on the sorbent interface.

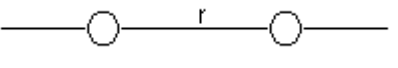
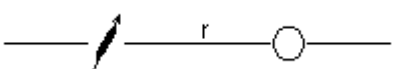
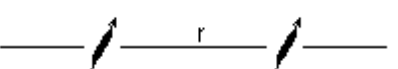
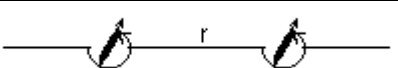
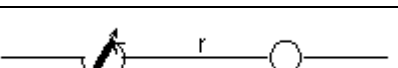
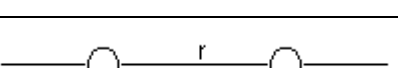
Classically, the term ‘adsorption’ is used to describe two kinds of forces of interaction between the *adsorbate* and the *adsorbent*. These are broadly described as physisorption (physical adsorption) or chemisorption (chemical adsorption). The basic characteristics of each of those types are outlined in Table 1.1 (Rouquerol 1999 p. 10). The forces which give rise to physisorption are the same with the forces responsible for the condensation of vapours and deviations from ideal gas behavior. The forces which cause chemisorption are the same as those responsible for the production of chemical compounds.

Table 1.1. Properties of physisorption and chemisorption

Physisorption	Chemisorption
<ul style="list-style-type: none"> • Multilayer adsorption • Low degree of specificity • Physisorbed molecule keeps its identity and on desorption it returns to its original form • Always exothermic but the energy involved is not much larger than the condensation energy of adsorbable substance (< ~40 kJ/mol) • Physisorption systems generally reach the thermodynamic equilibrium rapidly 	<ul style="list-style-type: none"> • Monolayer adsorption • Depend on the reactivity of adsorbent and adsorbable substance • Chemisorbed molecule loses its identity and cannot be recovered by desorption • Energy involved in chemisorption is the same order of magnitude as the energy change of a comparable chemical reaction (can reach several hundreds of kJ/mol when chemical bond formation takes place between the adsorbate and the adsorbent) • In chemisorption system an activation energy is involved and at low temperatures the system may not reach the equilibrium due to insufficient thermal energy

As far as sorption of radionuclides and heavy metals on soil constituents are considered, the vast majority of studies performed in this context (Atun et al.1996, Grütter et al. 1990, Jinzhou et al. 1996, Shahwan and Erten 2002) report energies of interaction that lie within the range of physisorption and relatively weak electrostatic interactions (ion-exchange processes). A variety of interactions that can be classified under such categories are given in Table 1.2 (JR Weber et al.1991 p. 501). It is reported that physisorption type of interaction is considered to prevail for energies of adsorption varying from several kJ/mol up to about 40 kJ/mol, a value above which some sort of chemical bonding is considered to develop (Levine et al. 1988 p.372, Özcan A.S. and Özcan A. 2004 p. 7). In physisorption, the adsorbed molecule might not be firmly affixed to a certain site on the surface of the solid and thus could freely move over different sites on the surface.

Table 1.2. Characteristic interactions associated with categories of adsorption

Category of Interaction	Representation of Interaction	Interaction Range
ELECTROSTATIC		
Ion-Ion		$1 / r$
Ion-Dipole		$1 / r^2$
PHYSICAL		
Dipole-Dipole (Coulombic)		$1 / r^3$
Keesom Energy		$1 / r^6$
Dipole-Induced Dipole (Debye energy)		$1 / r^6$
Instantaneous Dipole- Induced Dipole (London dispersion energy)		$1 / r^6$

Electrostatic interactions refer to the interaction between the sorbate ion and the charge present on the aluminosilicate sorbent. The charge on the sorbent can be of pH-

dependence (arising from protonation-deprotonation of aluminol Al-OH and silanol Si-OH groups), or pH independent, like the one stemming from isomorphous substitution that usually causes the emerging of a negative charge on the structure of the solid (Shahwan, 2000 p. 15).

Moreover, the charge of the positive sorbate ion might stimulate a counter negative charge at the solid interface with solution leading to the development of ion-dipole interactions. Moreover, physisorption processes could include interactions between dipole moments which arise from charge separation within a neutral molecule and can be permanent or induced for both adsorbate and adsorbent molecules. The extent to which such interactions would be effective is dependent on the magnitude and direction of the dipole moments and the separating distance between the interacting species.

1.1.2 The Liquid – Solid Interface

The interaction of cations in the hydrosphere with soil components is subject to various types of factors. Such factors are related with the properties of groundwater (temperature, pH, E_h), the speciation of these cations and their concentration, the structural characteristics of the soil components like porosity, surface area, swelling, grain size, in addition to factors that include the period of contact, the degree of mixing, and the ratio of soil to aqueous solution.

For a cation in the bulk of a solution to be fixed by the surface of the solid, three processes usually take place (Liu et al 1995 p. 839); film diffusion, particle diffusion, and chemical exchange reaction. Film diffusion (FD) is the diffusion of the cation through the solution film surrounding the soil particles. Particle diffusion (PD) is the diffusion of the same cation through the hydrated interlayer space of soil particles. Once the cation is close enough to the sorbing site, the chemical exchange reaction (CR) takes place.

The type of diffusion in an ion exchange process is affected by soil particle size and nuclide concentration. Film diffusion occurs usually with a low concentration and small-sized particles. Soil mineral composition affects the amounts of exchanging cations. Also many factors such as ion exchange, soil particle radius, and organic constituents affect the rates of ion exchange on soils. Usually the rate of ion exchange declines with increasing charge of the exchanging species. (Liu et al. 1995 p. 839)

At the soil-solution interface, the charged surface and oppositely charged ions in aqueous phase, counter-ions, develop an electrical double layer. The thickness of the double layer and its surface charge is affected mainly by ionic strength of the medium (Hakem et al. 1996 p. 226).

Double layer contains Gouy (diffuse) layer and Stern layer. In Gouy layer ions in the solution side of double layer are diffuse, that is, the greatest concentration of counter ions are near the surface where the electrostatic forces are largest and most able to overcome the thermal processes. At greater distances lesser concentrations are present since the electrostatic forces are weakened. Stern (or fixed) layer contains a layer of adsorbed ions at surface and forms an inner, compact layer extending into a distance close to the surface of the colloid (Polat p. 15, 26). A schematic representation of these layers is given in Fig. 1.1 (Shahwan 2000 p. 18).

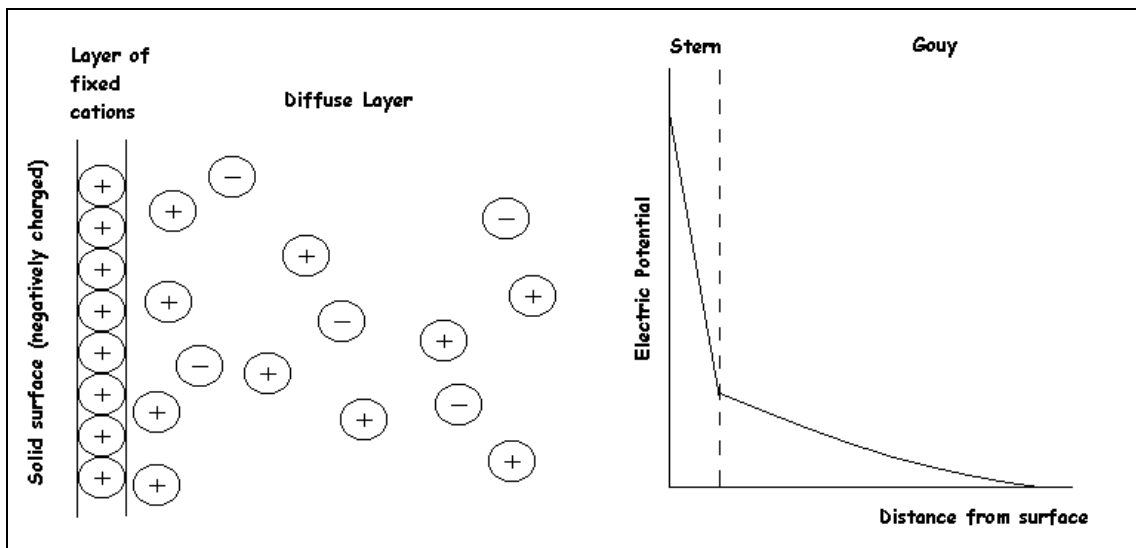
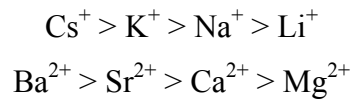


Figure 1.1. Schematic picture of Stern and Gouy layers

In the above figure the affinity of solid surface which is negatively charged to ions in solution shows the extent to which surface would favour sorbing ions. The affinity depends on two interactions which are Coulombic interactions and ion-dipole and ion-induced dipole interactions. Coulombic interactions take place between counter ion and the fixed groups of exchanger and the second class of interactions occur between counter ions and water molecules. If the Coulombic interactions are weaker than ion-dipole and ion-induced dipole interactions, the following affinity series is observed:



This sequence shows that the ion with bigger hydrated radii prefers to displace with ions of smaller hydrated radii. If the first type interactions preponderate the second type interactions, the selectivity may be reversed. For most clays normal sequence is observed, while for some zeolites reversed affinity is observed. (Shahwan 2000 p. 18). Affinity depends on concentration and oxidation state of adsorbate. As the adsorbate ion concentration of solution increases, the number of ions which show tendency to migrate to solid surface increases. And also with the increasing oxidation state of adsorbate ion, affinity of solid surface to them increases. (Shahwan 2000 p. 18)

Prediction of the extent of partitioning of a sorbing cation between aqueous solution and soil surface requires the development of equilibrium constants that cover wide ranges of sorption conditions. However, due to the variety of experimental conditions that could affect such partitioning, and the resulting complications in modelling sorption, the development of such equilibrium constants is never easy. Alternatively, empirical distribution ratios that are valid over a given set of experimental conditions are developed. Mathematically, the distribution constant (R_d) refers to the ratio of concentration of a trace constituent on the solid to that in the liquid. When the distribution constants are used, several assumptions are valid (Jedinakova 1998 p. 16, 17):

1. the relation between the sorbed and aqueous concentrations of constituent is linear at least over the concentration range of interest
2. the sorption reaction is reversible
3. the sorption reaction is fast enough to achieve a local equilibrium
4. sorption controls the aqueous concentration of the radionuclide
5. parameters that affect the sorption do not change within the system of interest

This R_d empirical constant is suitable when the site is well characterized both chemically and hydrologically. But this approach often fails in correlating with field measurements of actual radionuclide transport and R_d 's are sometimes unrealistic when considering the range of nonlinear geochemical parameters. Among these parameters

are; temperature, pH, fluid composition, ionic strength, mineral structure, substrate reactivity, organic complexation, etc. These parameters can significantly affect radionuclide transport mechanisms and kinetics. (Parkman et al. 1998 p. 1481, Westrich et al. 1998 p. 8)

In porous media, the retardation factor defines the relative motion of the sorbing constituent of groundwater compared to a non-sorbing constituent and is a dimensionless parameter. Retardation factor is defined with the following equation (Jedinakova 1998 p. 16, 17):

$$R = 1 + (\rho + \theta) * R_d \quad (1-1)$$

where ρ = dry bulk density of the porous medium through which groundwater is transported (g/cm^3)
 θ = Total porosity

1.2 Radioactive Isotopes in the Geosphere

1.2.1 Radioactive Wastes

The main sources of radionuclide contamination in the biosphere is caused by human activities in the form of nuclear fission and nuclear power reactors. Water sources are among the targets of contamination by radionuclides as a result of accidental leakage and/or planned radioactivity releases through weapon testing or improper handling of the radioactive wastes. Chemical forms of radionuclides, the content of inorganic and/or organic substances in water, and the hydrogeological situation all affect the behavior of radionuclides released into surface waters. (Atun et al. 1996 p. 435)

Table 1.3 shows some of important fission and activation products which are being introduced into the environment from the nuclear power plants, weapon testing, and applications in medicine, industry, and research. Each of such elements forms a potential threat to the biological environment due to long half-lives and/or strong radiations. (Shahwan 2000 p. 1). The table shows that the radioactive isotopes of Cs and Sr are among the ones with highest yield and possess long half-lives.

The term waste management defines the classification, control, movement, conditioning, storage, and disposal of wastes. The aim of radioactive waste management is to isolate the radioactive wastes in a manner that ensures no threat to man and his environment. There are two main options for the disposal of any material. The first way is to keep this material in the same place for as long as necessary which is known as containment and the second way is to allow natural processes to mobilize and disperse this material harmlessly which is commonly referred to as dilution and dispersion. (Shahwan 2000 p. 1, 2, 3)

Table 1.3. Some radionuclides of importance in radioactive waste considerations

Radionuclide	Half Life	Source	Fission Yield (%)
¹³⁵ Cs	3.0 x 10 ⁶ y	Nuclear Fission	6.54
¹³⁷ Cs	30.0 y	Nuclear Fission	6.18
⁸⁹ Sr	50.5 d	Nuclear Fission	4.82
⁹⁰ Sr	28.5 y	Nuclear Fission	5.77
¹⁴⁰ Ba	12.75 d	Nuclear Fission	6.21
¹³² Te	3.62 d	Nuclear Fission	4.31
¹³³ Xe	5.24 d	Nuclear Fission	6.70
¹²⁹ I	1.57 x 10 ⁷ y	Nuclear Fission	0.76
¹⁴⁰ La	1.68 d	Nuclear Fission	6.21
¹⁴⁴ Ce	284.9 d	Nuclear Fission	5.49
¹⁴³ Pr	13.58 d	Nuclear Fission	5.96
¹⁴⁷ Nd	10.98 d	Nuclear Fission	2.27
¹⁴⁷ Pm	2.623 y	Nuclear Fission	2.27
⁹³ Zr	1.5 x 10 ⁶ y	Fission + Activation	6.38
⁹⁹ Mo	2.748 d	Nuclear Fission	6.07
⁹⁹ Tc	2.13 x 10 ⁵ y	Nuclear Fission	6.07
⁵⁵ Fe	2.73 y	Activation	-
⁶⁰ Co	5.271 y	Activation	-
⁵⁹ Ni	7.5 x 10 ⁴ y	Activation	-

Both options are utilized in any single waste disposal system for radioactive waste management. In this system short lived radionuclides are contained in the same

place until a sufficient number of half-lives have passed, thus the concentration of these radionuclides in the waste is extremely low. For the very much longer-lived radionuclides, the system is envisaged to allow their slow mobilization and dispersion since it is impossible to achieve any equivalent number of half-lives. (Shahwan 2000 p. 2)

Storage of nuclear waste refers to the combination of natural and man-made barriers to gain long-term isolation of nuclear waste. Both natural and engineered barriers are used together in nuclear waste disposal since the uncertainty in inborn properties and performance of natural systems. And in these systems each barrier should provide safe isolation of nuclear waste by itself. A diagram of an engineered barrier systems (EBS) is shown in Fig. 1.2. (Jedinakova 1998 p. 13)

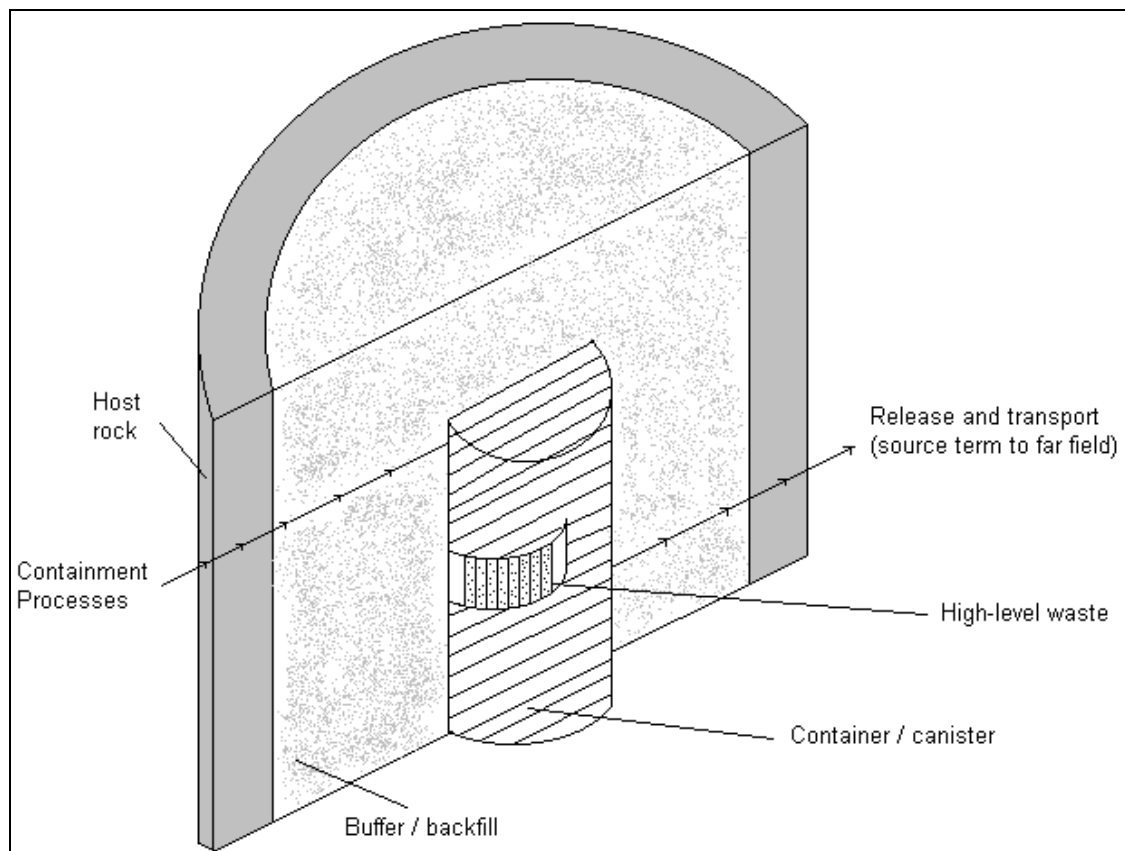


Figure 1.2. Diagram of a radioactive waste repository (EBS)

Starting from the innermost set of barriers, these contain the waste form or matrix, a container or canister, a backfill or buffer and finally the encircling geological formation as a host rock. (Shahwan 2000 p.6). Aluminosilicate components of soil like

clay minerals and zeolites might form part of the back filling materials. The functions of backfill or buffer materials are summarized below (Jedinakova 1998 p. 13):

1. to reduce possible tectonic forces on the container or canister
2. to stop the container or canister from settling within the emplacement tunnel
3. to conduct heat from the engineered barriers to keep near-field temperatures low
4. to supply a low-hydraulic conductivity, diffusional-transport barrier between the solidified waste form and host rock
5. to delay the diffusional-transport rate of dissolved radionuclides
6. to filter the fine particles and colloids which may form

The nuclear waste repository system is composed of two main zones: The near-field zone which contains all engineered barriers (i.e. solid matrix, buffering material, container) and a region of the surrounding rock which is modified by heat or chemical releases from the waste package. The far-field zone is the undisturbed natural geological system which is much larger physically and may have quite complex geological structure. The far-field zone is in a relatively steady state with respect to chemistry, hydrology and temperature compared with the near-field zone. The far-field zone controls the rate at which water can enter the near-field region and delays the transport and dilutes the concentration of radionuclides releasing from the near-field region. The output from far-field region releases to biosphere. (Shahwan 2000 p. 6, 7)

Radioisotopes may be transported from the repository to the biosphere by groundwater flowing through fractures in the surrounding rocks. If the travel time of water is sufficiently long compared with the half-life of the radioisotope, the extent of release of radioisotope to the biosphere is minimized. The migration of radionuclide by groundwater is affected by pH, redox potential (Eh), total salinity of water and the concentration of complexing agents, solubility of radionuclides and sorption on geological materials in direct contact with the flowing groundwater. (Shahwan 2000 p. 19, Cui and Eriksen 1997 p. 29, Parkman et al. 1998 p. 148, Westrich et al. 1998 p. 8). The extent of release of radionuclides from a waste into groundwater is controlled by one of four factors (Jedinakova 1998 p. 15):

1. dissolution rate of the waste form
2. sorption degree of the components of the waste matrix by barriers

3. transport rate of radionuclides away from the waste form
4. solubility of radionuclide containing solid

The enormous majority of radioisotopes which can be transported in groundwater are in the cationic form and may undergo reactions in aqueous medium which can affect their chemical forms and sorption properties. Among these reactions are (Shahwan 2000 p. 20):

1. hydration is the formation of aqua complexes by ion-dipole interactions. The energy related with hydration increases with decreasing ionic radii and with increasing positive charge of the cation.
2. hydrolysis reactions are the formation of hydroxo complexes since the repulsion of the protons by the cations when the charge of the cations is high. Hydrolysis depends on pH and increases with increasing charge and decreasing ionic radii of the cation.
3. condensation reactions are observed in the formation of polynuclear complexes where additional water molecules are removed. The formation of the covalent M-O-M bonds and of one molecule of water are the driving forces for this reactions.

The interaction of radionuclides in liquid with the encompassing solids in near-field and far-field zones affects the migration of these radionuclides to geosphere. Transportation of these radionuclides can be retarded when the interaction is strong and especially when the radionuclides are incorporated with the solids. Retardation mechanisms considered in appraising radionuclide migration from geologic repositories are (Shahwan 2000 p. 21, Jedinakova 1998 p. 15):

1. molecular filtration, ion-exclusion, diffusion into dead-end pore spaces that are purely physical processes
2. direct interactions with solid surface by physical adsorption, chemical adsorption or direct incorporation into the solid structure which is referred to as mineralization
3. indirect chemical reactions; e.g. precipitation which is observed due to increased concentration on the solid surface.

A schematic representation of these processes is shown in Fig. 1.3 (Shahwan 2000 p. 23):

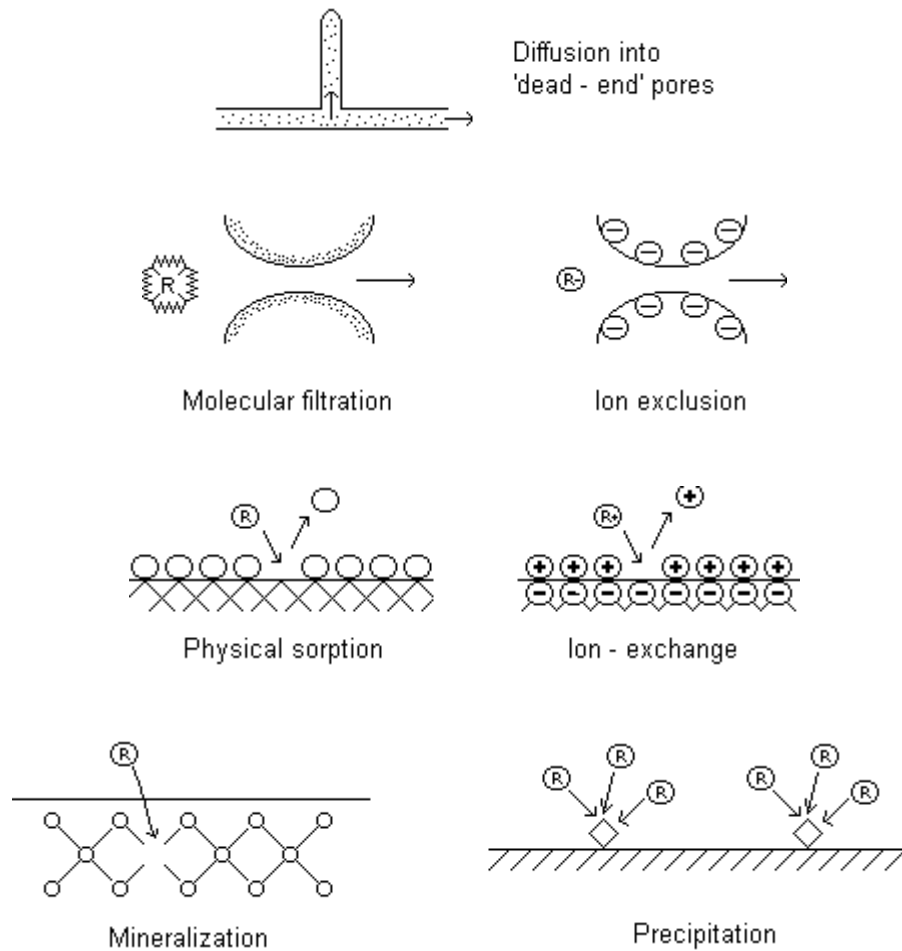


Figure 1.3. Retardation mechanisms

Among these mechanisms sorption and precipitation are considered the most important ones to decrease the release of radionuclide from near-field. Sorption is the process that causes the removal of solute from solution by attachment of that solute to the solid surface. Sorption reactions are means of satisfying the attractive forces, both physical and chemical, which are at the solid surface. It contains processes such as ion-exchange, surface complexation, specific adsorption and physical sorption. (Jedinakova 1998 p. 15)

The radionuclides of cesium (^{137}Cs) and strontium (^{90}Sr) are characterized by relatively long half lives, and their metabolic similarity to K and Ca, respectively, favors their uptake in plants after radiocontamination of agricultural fields. One of the

main pathways for radiation exposure is the intake of contaminated food. (Valcke et al. 1997a p. 205)

1.2.2 Cesium

Cesium is an alkali element ($z=55$) which has several radioactive isotopes. ^{133}Cs is the only one stable isotope that is naturally present in the environment. The most important radioactive isotopes of cesium are ^{134}Cs ($t_{1/2} = 2,06 \text{ y}$), ^{135}Cs ($t_{1/2} = 3,0 \times 10^6 \text{ y}$), and ^{137}Cs ($t_{1/2} = 30,17 \text{ y}$) which are produced in nuclear fission. (Shahwan and Erten 2002 p.115, Cui and Eriksen 1997 p.29). ^{135}Cs and ^{137}Cs are among the most hazardous nuclides because of their long half lives, high solubilities and relatively high fission yields which are 6.54 % and 6.18 % respectively. (Grütter et al. 1986 p. 677)

Exposure to low levels of stable or radioactive cesium occurs by breathing air, drinking waters which contain cesium, or eating food which was grown in contaminated soil. The Chernobyl accident caused widespread and continuous contamination by long-lived radionuclide ^{137}Cs . (Likar et al. 2001 p. 199). Exposure to high levels of stable cesium has not been shown to affect the health. But exposure to high amounts of radioactive cesium may damage cells and cause nausea, spewing, diarrhea, bleeding, coma, and even death. (WEB 1 (2001)) In a study of the diffusion and migration of ^{137}Cs in soil in Europe following Chernobyl accident, the presence of ^{137}Cs in the upper 10 cm of the soil was documented (Likar et al. 2001 p. 191).

1.2.3 Strontium

Strontium, Sr, is an alkali-earth element ($z = 38$), found in rocks, soil, coal, and oil. This element has 4 stable isotopes ^{84}Sr , ^{86}Sr , ^{87}Sr , ^{88}Sr . It has also several radioactive isotopes, with ^{90}Sr ($t_{1/2}=29.1 \text{ years}$) being the most common one. Sr is an important trace element in biological systems. Stable Sr in soil dissolves in water and goes deeper in the soil to the underground water. But the radioactive decay is the only way to diminish the amount of ^{90}Sr in the environment. (Parkman et al. 1998 p. 1481, 1482). ^{90}Sr is used as a power source for space equipment and navigational beacons as it creates heat when it decays. Moreover, this isotope is generated commercially in nuclear fission to use it in medicine and industry. When ^{90}Sr enters the body, it behaves

like Ca and incorporates with bone, bone marrow, soft tissues around the bone and teeth. (WEB 4 (2001))

People can be exposed to low levels of stable and radioactive strontium by breathing air, eating food that was grown in contaminated soil, or drinking water. It is highly unlikely that people exposed to stable strontium on trace levels would suffer harmful effects. Strontium chromate, which is stable strontium compound, can cause cancer. This is caused by chromium rather than strontium. High levels of radioactive Sr can damage bone marrow and produce anemia and hinder the blood from clotting properly (WEB 2 (2001)).

1.3 Clay Minerals and Zeolites

Clay minerals and zeolites belong to the family of soil fractions known as aluminosilicates. Aluminosilicate minerals may be classified into 3 groups according to their structural features (Goodman 1986 p.344):

1. Expanding layer structures such as smectites. These aluminosilicate minerals can greatly increase their surface area on solvation
2. Cage structures such as zeolites. These aluminosilicate minerals have internal surfaces accessible only to ions and molecules under a certain size.
3. Structures that the adsorption properties are determined only by their surfaces' chemical natures.

Many of aluminosilicate minerals carry a surface charge. This surface charge may arise from isomorphous cation substitution within the structure or protonation/deprotonation reactions at oxide or hydroxide surface groups. The former kind of reaction is pH independent and the latter reactions are pH dependent. Clay minerals which have layer structure are able to exchange cations (mainly Na^+ , K^+ , Mg^{2+} and Ca^{2+}) in positions between the layers, thus in those clays because of high specific surface area and the large number of exchange sites there is significant exchange capacity. Similarly, zeolites possess large cation exchange capacities by virtue of their networks of channels that can readily host cationic species.

Cation exchange capacity (CEC) refers to the total of all exchangeable cations in a solid and is usually reported as milliequivalents of cation per 100 g of mineral. The

CEC values of clays depend on clay type, depositional environment, crystal sizes, isomorphous substitutions and the nature of lattice structure of clay. Also CEC changes with the degree of crystallinity, surface area, presence of impurities. (Kleven et al. 1996 p.181, 194, Lim et al. 1980 p.223, 226)

Typical CEC-values of zeolites and kaolinite are expressed in the Table 1.4 in terms of meq/100g (Karnland and Pusch 1990 p. 11).

Table 1.4. CEC-values of minerals

Material	CEC (meq/100g)
Zeolites	100-300
Vermiculite	100-150
Montmorillonite	70-100
Chlorite	4-47
Hydrous mica	10-40
Kaolinite	3-15
Feldspar, quartz	1

1.3.1 Clay Minerals

Clay minerals are hydrous aluminum silicates having a particle size of less than 2 micrometers. The structure of a pure clay mineral contains two basic mineral-oxide layers which are stacked parallel units of silica and alumina sheets. The first layer is composed of silicon tetrahedral sheets and the second layer is formed of aluminum octahedral sheets. The type of the clay mineral is determined by the stacking of these two sheets into layer, the bonding between layers, and the substitution of other ions for Al and Si.

The broad group of hydrous silicates with layer structures are called phyllosilicate (phyllo = leaf like). Two-dimensional tetrahedra and octahedra of oxygen atoms or ions are the essential components of the phyllosilicate structure. In the center of the tetrahedra there are coordinating cations such as Si, Al³⁺, Fe³⁺. In the octahedra the coordinating cations are Al³⁺, Mg²⁺, Fe³⁺, or Fe²⁺. (Rouquerol 1999 p. 356) The

manufacture of phyllosilicates is part of a geological cycle which includes five stages, as presented schematically in Fig.1.4 (Cahn et al.1994 p.56):

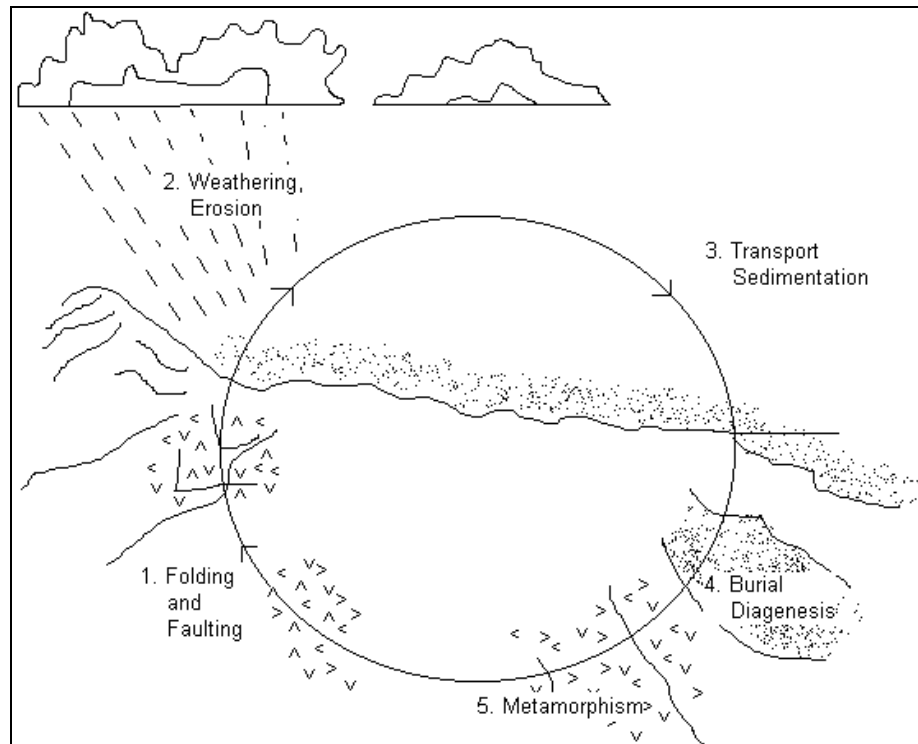


Figure 1.4. Manufacture of phyllosilicates

1. As a consequence of faulting, volcanic eruption, folding rocks are brought to the surface of the earth.
2. As a result of weathering rocks are broken down and the minerals in the rocks are modified at or near the surface.
3. By the action of wind and water some fragments of these minerals are transported.
4. Clay minerals are deposited and buried.
5. In order to complete the cycle clay minerals are transformed to metamorphic rocks.

Clay minerals have an important role in adjusting the mobility of ions which have both beneficial and toxic properties in soils and waters. Physical and chemical properties of the clay are affected by the nature of the adsorbed species. It is important to understand the adsorption processes and the nature of the adsorbed species on clay minerals in the chemical, agricultural, environmental, engineering, and construction industries. (Goodman 1986 p.342)

Turkey has plenty of clay deposits. Most of the kaolin deposits in Turkey are concentrated in the Marmara Sea Region, particularly in Balıkesir-Düvertepe region. The other kaolin deposits are in Nevşehir, Niğde, Bolu, Çanakkale, Eskişehir and the East Black Sea. Reserves can be variable in quality with kaolinite content between 40-80%. (Erten et al.1988 p.272, 273, ([WEB 5\(2003\)](#))).

1.3.1.1 Kaolinite

Kaolinite is the most known example of 1:1 type (two-sheet structure) clay minerals. Fig. 1.5 shows the ideal kaolinite structure ([WEB 6\(1999\)](#)). Kaolinite is a common mineral that is found in many geological formations. The general structural formula of kaolinite is $\text{Si}_4 \text{Al}_4 \text{O}_{10} (\text{OH})_8$ (Chorover et al. 2003 p.2200). This clay is composed of a tetrahedral SiO_4 layer apically bonded to an octahedral gibbsite (Al_2O_3) layer. Kaolinite structure includes both interlayer and inner OH groups. Interlayer OH groups form hydrogen bonds with the close silicon tetrahedral sheet. Inner OH groups are associated with empty octahedral aluminum sites. These OH groups are important in the surface electrostatics which affects the formation of host / guest complexes and therefore may play a significant role in appraising radionuclide transportation. (Westrich et al. 1998 p.10, 11, 12). Kaolinite is a non-expanding clay with a unit layer (or layer repeat distance) of approximately 7 Å (Rouquerol 1999 p.358).

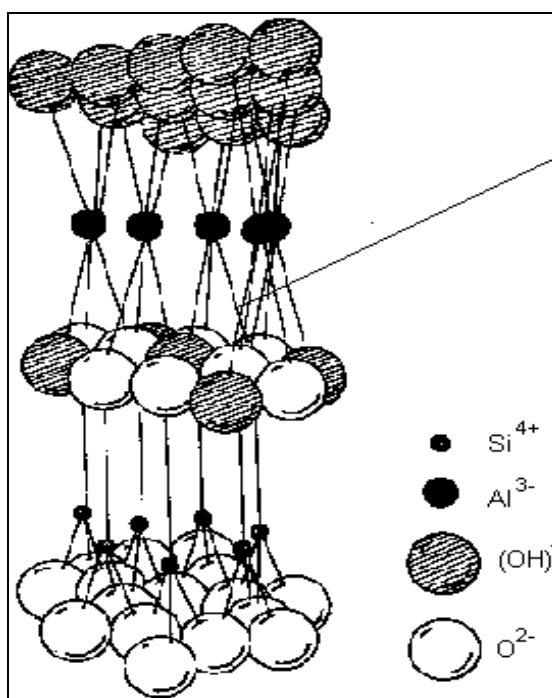


Figure 1.5. The ideal kaolinite structure

It is reported that intercalation of DMSO within the interlayer space of kaolinite causes the original basal spacing of kaolinite to rise from 0.72 nm to 1.12 nm. (Patakfalvi et al. 2003 p.46).

1.3.2 Zeolites

The aluminosilicate zeolites have been known for more than 200 years, but only about 50 years ago their high adsorption selectivity was first realized. They have reached high technological importance in catalysis, gas separation and drying, etc. In the breaking of paraffins, and the isomerization and disproportionation of aromatic compounds they find applications as industrial catalysts. (Rouquerol 1999 p.356)

TO_4 is the basic unit of a zeolite structure. In this formulation T is a silicon or aluminium atom/ion. The general structural formula of aluminosilicate zeolites is given by $\text{M}_{x/n} [(\text{AlO}_2)_x (\text{SiO}_2)_y] \cdot m \text{H}_2\text{O}$, where M is a non-framework, exchangeable cation. Aluminosilicate framework is anionic since it contains $(\text{AlO}_2)_x$ and $(\text{SiO}_2)_y$. The number of aluminium atoms in the T-positions govern the net negative charge of the framework. Therefore in order to balance the electric charge a corresponding number of M cations

are needed. It is impossible to obtain a zeolitic alumina, however some pure silica zeolites are known. Production of various zeolites is possible via the different arrangements of TO_4 tetrahedra with secondary building units. Among these secondary building units the two simplest are four and six tetrahedra rings, and the others include larger rings-up to 16 T atoms. (Rouquerol 1999 p. 378)

In zeolites there is little swelling or shrinking of the framework during adsorption or desorption due to the stiffness of the framework, it is this property of zeolites that differ them from clays and other aluminosilicates. Some zeolites are used for the treatment of radioactive wastes through their high exchange capacity, desirable selectivity for some radioisotopes, thermal, mechanical and radiation stability. (Rouquerol 1999 p.378 , Abusafa and Yücel 2002 p.103)

Deposits of natural zeolite minerals are found in many countries, including Japan, Russia, Italy, Greece, Turkey, Mexico, USA, Kenya and Australia. (Christie et al. 2002 p.16) In Turkey clinoptilolite is found in Bigadiç and Gördes regions with great amounts about five hundred million tons. (Toprak and Girgin 2000 p.344, Türkman et al. 2001 p.14)

1.3.2.1 Clinoptilolite

Clinoptilolite, the most widely available form of zeolites, possesses the structural formula $\text{Na}_6\text{Al}_6\text{Si}_{30}\text{O}_{72} \cdot 24 \text{H}_2\text{O}$ (Tanaka et al. 2003 p.713). Clinoptilolite, mordenite, erionite, and chabazite are types of natural zeolites that have been thought as effective materials for radioactive waste treatment processes. Clinoptilolite and mordenite including rocks have high cation-exchange capacities and selectivities for Cs, Sr, and Ba. Such attributes of these solids make them potential hosts for radioactive waste control. Clinoptilolite was reported to have high selectivity for ^{137}Cs and ^{90}Sr radioisotopes, and effectively to remove them from process waste waters (Abusafa and Yücel 2002 p.103, 104).

Clinoptilolite has the heulandite (HEU) type framework. It possesses intersecting open channels confined by ten- and eight-membered tetrahedral rings. The large ten-membered elliptic ring with dimensions about $7.0 \times 4.3 \text{ \AA}$ and the small eight-membered ring with dimensions about $4.6 \times 4.0 \text{ \AA}$ confine channels parallel to c-axis. Additional eight-membered ring channels are parallel to a-axis and cross-link the former channels. (Tanaka et al. 2003 p.713 , Armbruster 2001 p.14)

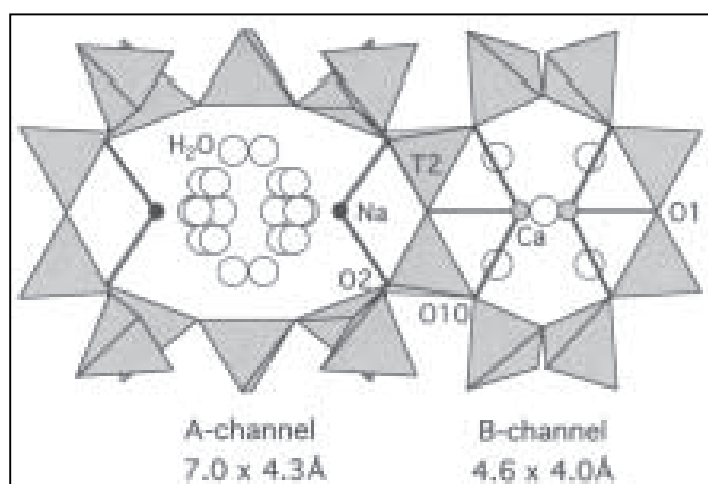


Figure 1.6. Crystal structure representation of clinoptilolite viewed down [001] with [010] vertical.

Figure 1.6 is representing the crystal structure of clinoptilolite. Sodium (small black sphere) resides in the larger A-channel and Ca (larger grey sphere) resides in the smaller B-channel. Sodium bonds to two framework oxygen atoms and five of the water molecules (large white spheres) in the A-channel. Calcium bonds to three framework oxygen atoms and five water molecules in the B-channel. (Woods and Gunter 2001 p. 428)

Clinoptilolite is negatively charged due to tetrahedrally coordinated aluminum, and this charge might be balanced by the exchangeable cations. Na^+ , K^+ , Ca^{2+} , and Mg^{2+} . For a particular zeolite the type, number and location of cations affect the selectivity and the rate of ion-exchange. (Abusafa and Yücel 2002 p.104)

1.4 The Present Study

1.4.1 Literature Survey

The sorption properties of Cs^+ and Sr^{2+} on various clay minerals and zeolites have been the subject of many studies performed in order to understand the effects of the factors affecting the sorption process and the mechanisms of retardation of metal ions by soil fractions. These factors include time, loading, temperature, pH, ionic

strength, particle size, etc. Most of these studies have been carried out by using radiotracer technique (Shahwan and Erten 2002, Mishra and Tiwary 1999, Wenming et al. 2001, Shahwan et al. 2002, Atun et al. 1996, Cui and Eriksen 1997, Grütter et al. 1990, Ishfaq et al. 1997, Bagosi and Csetenyi 1999). Part of such studies were devoted to investigate Cs^+ and Sr^{2+} sorption on kaolinite and clinoptilolite minerals (Abusafa and Yücel 2002, Parkman et al. 1998, Chorover et al. 2003, Lim et al. 1980, Valcke et al. 1997a, Valcke et al. 1997b, Westrich et al. 1998, Erten et al. 1988).

In a study of Cs and Sr uptake to kaolinite weathering in simulated tank waste leachate, it was reported that the Sr sorption was rapid and substantial, however the Cs sorption was slower and the extent of sorption was smaller than that of Sr (Chorover et al. 2003 p.2201). Dai-Chin Liu et. al, (1995) studied the characteristics of sorption kinetics of cesium and strontium in soils and concluded that Freundlich isotherm model provides a better fit of the sorption of Cs^+ and Sr^{2+} . In the same study, the kinetics of sorption of both cations on chosen soils were found to be a function of soil mineral composition, soil particle size and cation charge. (Liu et al. 1995 p.844)

The sorption behavior of Cs^+ on kaolinite was also investigated by Shahwan and Erten (2002). The uptake was examined as a function of time, cation concentration, temperature using the radiotracer method. In this study, it was reported that sorption involved kinetically rapid uptake steps, and that the sorption data were well represented by Freundlich and Dubinin-Radushkevich type isotherms. Cs^+ sorption on kaolinite was reported to be exothermic and spontaneous. The authors noted also that, the magnitudes of ΔG^0 suggest that ion-exchange is the primary sorption mechanism. Fast adsorption kinetics was also reported for Sr^{2+} uptake by kaolinite, which was also reported to fit Freundlich type isotherms (Shahwan and Erten 2002 p.117, 118, 119, 120)

The uptake of Cs^+ and Sr^{2+} on kaolinite was also studied by Westrich et al. (1998 p.17, 18, 19, 25, 26). The studies included characterization of kaolinite surfaces and sorption sites, adsorption measurements. According to the results of this study, Cs^+ is sorbed on edge and basal sites of kaolinite, with the aluminol edge binding sites being more reactive at typical soil pH than silanol edge sites or basal Si- or Al- sites. In addition it was found that Cs^+ is sorbed at aluminol edge sites as an inner – sphere complex and weakly sorbed as an outer – sphere complex on basal surfaces. It was also reported that some fraction of Cs^+ and Sr^{2+} are sorbed irreversibly on kaolinite and can not be easily desorbed from kaolinite surface. The fact that the surface sites of kaolinite

are the main fixation sites for Cs^+ was also confirmed in a study in which ToF-SIMS depth profiling was applied (Groenewold et al. 1998 p. 538)

In an investigation of the interaction of aqueous Sr^{2+} ions with the surface of kaolinite, it was concluded that Sr^{2+} is taken up into kaolinite surface in sites of octahedral geometry. Moreover, higher Sr^{2+} concentrations was reported to lead to longer Sr-O bonds formation suggesting weaker binding of Sr^{2+} to the kaolinite surface (Parkman et al.1998 p.1481, 1490, 1491).

Ivanov et. al, (2003) studied the effect of temperature on zeolite selectivity and reported that the equilibrium coefficient for Na^+ - Cs^+ exchange on clinoptilolite decreases significantly with temperature when the equivalent fractions of Cs^+ ions in the zeolite phase were very low. Moreover, it was indicated that the effect of temperature on zeolite selectivity increases significantly with decrease of equivalent fraction of the more strongly sorbed ionic component in the zeolite phase. (Ivanov et al. 2003 p.260, 262, 263)

In a study of ^{137}Cs removal from aqueous solutions using different cationic forms of a natural zeolite, the distribution coefficients of cesium on clinoptilolite were measured by radioactive tracer technique. In this study, Dubinin-Radushkevich isotherm model was found to represent the isotherms better (Abusafa and Yücel 2002 p.103). Another study on the same topic indicated that monovalent cations are more exchangeable for Cs^+ , with Na^+ -saturated mineral having the highest exchange capacity towards Cs^+ . On the other hand, divalent cations were more exchangeable for Sr^{2+} , with Ca^{2+} -saturated mineral possessing the highest exchange capacity. (Liu et al. 1995 p.841, 842, 844)

Valcke et. al, (1997) examined the radiocaesium ion-exchange behavior on natural clinoptilolite. The effect of competitive cations on sorption was also investigated. According to this study, K^+ and NH_4^+ ions are almost equally competitive in regard to radiocaesium ion-exchange. (Valcke et al. 1997a p.209, 211)

1.4.2 Aims of the Present Study

The aim of this study is to investigate the uptake of Cs^+ and Sr^{2+} ions by natural samples of kaolinite and clinoptilolite originating from Sındırgı and Manisa, respectively. The experiments were performed using the stable isotopes of these elements only. The primary parameters investigated include the time of contact,

concentration, temperature, ionic strength. These studies aim at elucidating detailed information regarding the kinetics of sorption, including the rate constants, rate order, and activation energies. In general, there is a scarcity in data available in literature regarding such parameters. Moreover the best fitting sorption isotherm models are examined using the most widely applied isotherm models. Sorption isotherms are helpful in demonstrating the extent of homogeneity of the sorption sites and the affinity of these sites towards the sorbed cations. The thermodynamic parameters, ΔH^0 , and ΔG^0 are calculated, the thing that can help in testing whether or not electrostatic binding forces are involved in sorption. Structural and morphological stability of kaolinite and clinoptilolite upon sorption is tested, and the sorption mechanism is discussed.

The experiments were entirely performed using the batch method. The characterization of the liquid and solid phases was carried out using Flame Atomic Absorption/Emission Spectroscopy (AAS/AES), X-ray Powder Diffraction (XRPD), and Scanning Electron Microscopy/Energy Dispersive Spectroscopy (SEM / EDS).

1.4.3 Methods Applied

1.4.3.1 Atomic Absorption Spectrometry (AAS)

Atomic Absorption Spectrometry (AAS) uses the absorption of radiation by free gaseous atoms in order to achieve qualitative detection and quantitative determination of elements (Welz and Sperling 1998 p.1). An atomic absorption spectrometer measures the absorbance which is the logarithm of the rate of incident light power (P_0) to transmitted light power (P) :

$$A = \log \frac{P_0}{P} \quad (1-5)$$

There is a relationship between P_0 and P when a light beam is decreased by the medium through which it passes:

$$P = P_0 \exp (-k L) \quad (1-6)$$

where k = absorption coefficient which is a function of wavelength of light,
number of atoms in the ground state per unit volume

L = path length in medium

There are two main components in an atomic absorption spectrometer: atom cell which creates atoms at the free gaseous ground state, and optical system to measure the signal. Atom cell dissolves the liquid sample and dissociates analyte elements into their free gaseous ground state form in which the atoms are available to absorb radiation coming from light source and to create a measurable signal which is proportional to concentration (Tyson and Haswell p.21). The atomizer, in which the analyte is atomized, is flame, graphite tube or quartz tube. In flame atomization fixed aliquot of measurement solution is converted into an aerosol in nebulizer and transported into the flame which must have enough energy to both vaporize and atomize the sample. Properties of flame types are presented in Table 1.5 (Welz and Sperling 1998 p.151).

Table 1.5. Spectroscopic flames for AAS with their properties

Oxidant	Fuel Gas	Max. Flame Temp. (°C)	Max. Burning Velocity (cm / s)	Remarks
Air	Acetylene	2250	158	Most commonly used flame
Nitrous oxide	Acetylene	2700	160	For difficultly volatilized and atomized substances
Air	Hydrogen	2050	310	Flame of high transparency; for easily ionized elements
Air	Propane / Butane	1920	82	For easily ionized elements

Radiation sources which generate electromagnetic radiation are hollow cathode lamps (HCLs) and electrodeless discharge lamps (EDLs) in AAS. In these sources the analyte element is volatilized and is excited thus it emits its spectrum. Monochromators separate analytical lines from other emission lines arising from the source and from broad band emission of atomizer. For dispersion of radiation diffraction gratings, prisms are used in AAS. (Welz and Sperling 1998 p.103, 113)

1.4.3.2 Scanning Electron Microscopy/Energy Dispersive X-ray Spectroscopy (SEM/ EDS)

SEM is the simplest and most accessible technique supplying images of structural differentiation in surface layers. Although SEM has some disadvantages as limited resolution, damaging polymer surfaces by electron beam, this technique is easy to use and involve easy sample preparation. SEM enables to image the surface and to distinguish some compositional difference (O'Connor and Sexton 1992 p.13, 15).

Prior to SEM/EDS analysis, the solid samples are sprinkled onto adhesive aluminum/carbon taps supported on metallic disks. Samples are then introduced to the machine operating under vacuum and SEM images are recorded. The images are obtained by using electron beams. In order to produce demagnified image of electron source lenses are utilized. Specimen is across scanned with this probe of electrons, as a result of sample-electron interaction signals are created. Then these signals are detected, amplified and utilized to modulate intensity of image tube.

The signal is produced when the electron beam, emitted by an electron gun, is scanned over the sample. When the sample is bombarded with electrons, many different interactions occur between them. Electrons are reflected from the sample and these electrons are collected by a detector in which they are converted into a small electrical signal. This signal includes a variety of information about a single point on the surface of sample. In order to obtain an image of the sample a large number of points over an area of sample is needed. The beam is moved point-by-point along a line and the reflected electron signal is collected. A line of 1000 points is completed, then the beam is moved quickly back to the start of that line. The beam is then shifted down one line width and repeats its scan. A complete scan includes 1000 lines in which they are 1000 points. (Lawes p.3, 6, 11)

There are two main types of sample/electron interactions: unscattered electrons and elastically scattered electrons. Elastically scattered electrons change direction but preserves almost all of their energy with < 1 eV loss. The angle through which the electron is deflected depends on how much energy it has, and how close it passes to the nuclei. Elastic scattering is more likely to be seen in samples of high atomic number, and with low accelerating voltage beams. Through inelastic scattering incident electrons transfer a large proportion of their kinetic energy to the target atoms. Inelastic scattering

is more likely to be seen in the lighter elements and gives useful information about the surface of sample and elemental composition of sample. (Lawes p.12, 16)

SEM is near-surface sensitive technique. The primary electron beam causes ionization of atoms on its path which in turn cause ejection of secondary electrons from the solid surface having energies between 0-20 eV and they are attracted to positively charged detector. Secondary electron images can be acquired about to 100 nm. Primary electron beam has the depth of penetration of 0.5-5 μm depending upon density of the solid. (O'Connor and Sexton 1992 p.13, 92)

In addition to SEM, Energy-dispersive X-ray spectrometry (EDX) is a complementary technique. The combination of SEM and EDX techniques has enabled observed phenomena to be attributed to a given element. (Welz and Sperling 1998 p.380, 381). Through the use of EDX, determination of thicknesses and compositions of layers on substrates is enabled. In this technique, X-rays are produced by the incident probe in a volume which is similar with these of backscattered electrons and thus the elements in a specimen within that volume can be identified by comparing the peaks with the characteristic energies of the elements. Internal corrections for the cross sections of different elements is automatically performed, thus the concentrations of the elements can be calculated. (O'Connor 1992 p.98, 99)

Moreover, in addition to spot analysis that enables the detection of various elements present in a certain point on the surface of a specimen, the distribution of various element across sections on the surface can also be mapped using EDX mapping analysis. The resulting map, which consists of bright points, shows the location of a particular element and brightness of the points gives information about the concentration of that element. (Lawes p.78, 79)

1.4.3.3 X-ray Diffraction (XRD)

The XRD analysis was performed to elucidate any possible structural changes that could accompany the sorption of Cs^+ and Sr^{2+} ions and to determine the mineralogical purity of the kaolinite and clinoptilolite.

X-ray diffraction is a many-sided analytical technique to identify crystalline solids such as metals, ceramics, geological materials, etc. which may be powders, sheets, single crystals, thin films, or irregular shapes based on the desired measurement.

The theoretical basis of X-ray diffraction stands on Bragg equation given by (Formica p.341, 342):

$$n \lambda = 2 d \sin \theta \quad (1-7)$$

where λ is the wavelength of incident light, n is the order of reflection ($n = 1,2,3,..$), d is the distance between parallel lattice planes, and θ is the Bragg angle which is the angle between the incident beam and a lattice plane (see Fig. 1.7 (Formica p.342)).

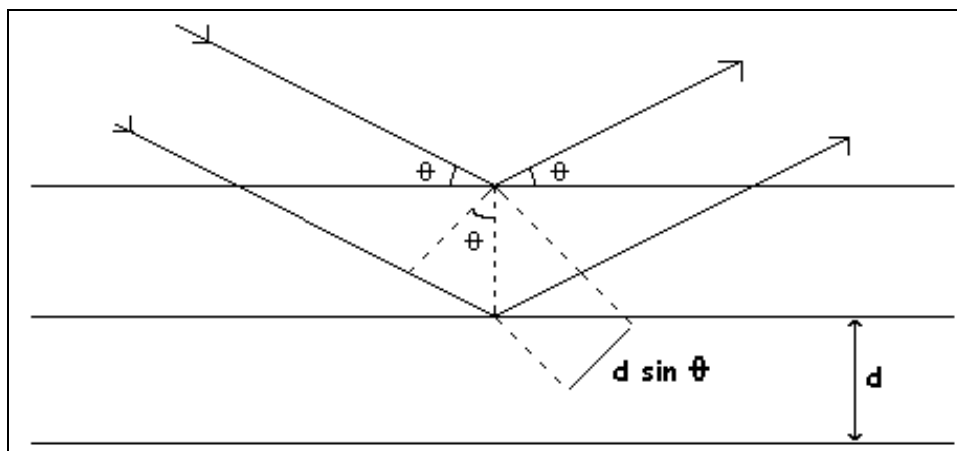


Figure 1.7. Illustration of Bragg's law

The samples can be analyzed in the powder form which is mounted on holders and then introduced for analysis. In an XRD device, X-rays are generated via bombarding a metal foil, which is commonly a Cu foil, through the use of electrons to emit polychromatic radiation which is then filtered via another metal foil (Ni foil) to generate monochromatic radiation. Then X-rays are focused on the sample, some of which pass through the sample and the others are diffracted by the planes of atoms to create beams at characteristic angles depending on X-ray wavelength, crystal orientation, structure of crystal. Pure substances give characteristic diffraction patterns like finger print. For example in the mixture of substances, each one gives its pattern independent from the others (Shahwan 2000 p.35, 36).

Table 1-6 shows the wavelengths of diffraction radiation. These wavelengths are specific to the material which creates X-rays. While wavelengths get smaller, radiation

becomes more energetic and penetrating. The longer the wavelength, the more spreading peaks in diffraction pattern. (Formica p.342)

Table 1.6. X-ray wavelengths (in Å) and K filters for common anode materials

Anode	K_{α1}	K_{α2}	K_β	K_β Filter
Chromium (Cr)	2.28970	2.29361	2.08487	Vanadium (V)
Cobalt (Co)	1.78897	1.79285	1.62079	Iron (Fe)
Copper(Cu)	1.54056	1.54439	1.39222	Nickel (Ni)
Molybdenum (Mo)	0.70930	0.71359	0.63229	Zirconium (Zr)

When the diffraction pattern of a sample is recorded, search-match procedure is used to determine the mineralogical composition of the samples. Quantitative analysis can be performed based on the fact that the amount of each phase in the sample is correlated with the area under the peak. However, this process is usually not simple and requires standard preparation.

CHAPTER 2

EXPERIMENTAL

2.1 Preparation of Samples

2.1.1 Pretreatment of Kaolinite and Clinoptilolite

The solid samples used in our studies were natural clinoptilolite and kaolinite. The samples were dry-sieved. The particle sizes of clinoptilolite and kaolinite used were $d < 38 \mu\text{m}$ and $75 < d < 600 \mu\text{m}$, respectively. Kaolinite was obtained from Sındırgı and clinoptilolite from Manisa regions located in the western part of Anatolia.

Prior to the sorption experiments, pretreatment of clinoptilolite and kaolinite was performed. The aim of this pretreatment step was to mimic the equilibrium existing between natural clinoptilolite and kaolinite with groundwater. 10 g of the minerals were introduced into beaker and 1 L of tap water, as substitute for groundwater, was added. The mixtures were shaken for 3-4 days. At the end of mixing, solid phases were filtered and dried overnight in an oven kept at $90 \text{ }^\circ\text{C}$. The solids were then used in the sorption experiments.

The concentrations of K^+ , Na^+ , Mg^{2+} , Ca^{2+} in the tap water were determined using AAS. The measurements were performed at the wavelengths (nm) 589, 766.5, 422.7, and 285.2 for the elements Na, K, Ca, and Mg, respectively. The average concentrations of those elements are given in Table 2.1:

Table 2.1. Concentrations of Na, K, Ca, Mg in tapwater used in sorption studies

Element	Na	K	Mg	Ca
Concentration (mg / L)	18	3	26	200

2.1.2 DMSO-Intercalation of Kaolinite

Kaolinite is non-expandable clay due to hydrogen bonding which tightly interlinks the kaolinite layers. By the intercalation of dimethylsulfoxide (DMSO), disaggregation of the lamellae of non-swelling kaolinite is achieved (Patakfalvi et al. 2003 p.46).

The experiments were performed by adding 100 ml of DMSO to 20 g of kaolinite and mixing the two at 65°C for 24 h. The mixture was filtered and the solid was washed with methanol for 5 days in order to remove the redundant DMSO by sedimentation. Washing with methanol was accomplished as follows: The filtered solid was mixed with 100 ml of methanol and the mixture was left for sedimentation until the following day. This process was repeated for 5 times. A schematic representation of this process is given in Fig. 2.1 (Patakfalvi et al. 2003 p.47)

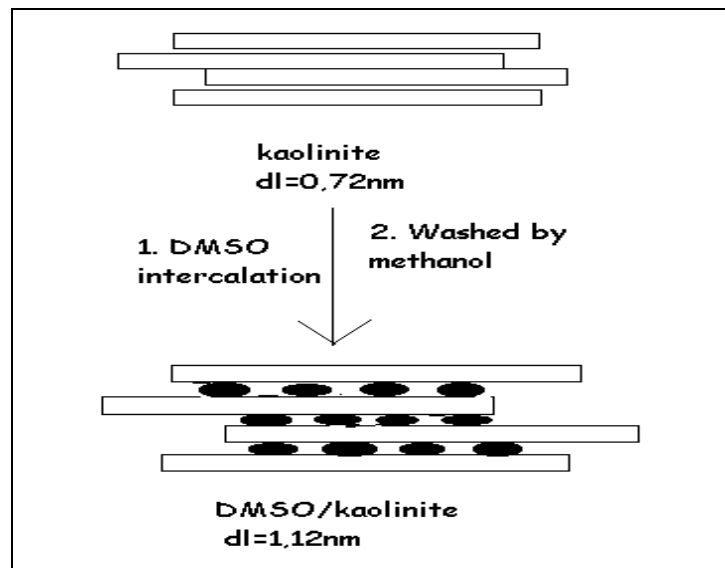


Figure 2.1. DMSO treatment of kaolinite

DMSO-intercalated kaolinite was then used in studies planned to elucidate the effect of interlayer expansion on the amounts of retarded Cs^+ and Sr^{2+} ions by kaolinite.

2.1.3 The Sorption Experiments

The sorption experiments were performed using 50 ml polyethylene tubes. The batch method was applied throughout the experiments. The initial concentrations of $\text{Sr}(\text{NO}_3)_2$ and CsCl solutions used in these experiments were 10 mg/L, 50 mg/L, 100 mg/L, and 500 mg/L. The amounts of solid and liquid phases were fixed at 0.5 g and 50 ml. The tubes were shaken using a Nuve ST 402 water bath shaker equipped with a microprocessor thermostat at 25 and 60 °C. The period of contact times were 5 min, 10 min, 30 min, 1 hour, 2 hours, 5 hours, 8 hours, 24 hours, 48 hours. At the end of each mixing period the solid phases were separated from the solution by filtration and dried overnight in an oven kept at 90 °C at the pH of 7.7 at which both kaolinite and clinoptilolite are negatively charged.

2.2 Desorption Studies

Following the sorption experiments, desorption studies have been carried out to investigate the stability of sorption. 10 ml tapwater was added to 0.1 g of Cs-, and Sr-loaded solid samples which were previously prepared at 25 °C, 48 hours and at 60 °C, 48 hours at initial concentrations of 10 mg/L and 50 mg/L CsCl / $\text{Sr}(\text{NO}_3)_2$. Then the tubes were shaken for 10 minutes, 4 hours, 24 hours, 7 days. At the end of mixing period the samples were filtered and aqueous phase concentrations of Cs/Sr were measured by AAS.

2.3 Analysis of the Aqueous Solutions

The filtrates obtained following the sorption process were analyzed using flame AAS. The instrument applied was a Thermo Elemental SOLAAR M6 Series atomic absorption spectrometer. Sr content in the aqueous solutions was determined by using a Sr hollow cathode lamp ($\lambda = 460.7$ nm), applied as source. The Cs content was determined by flame emission spectrometry. The wavelength was 852.1 nm. Na, K, Ca, and Mg determination was achieved using AES.

2.4 Analysis of the Solid Phases

2.4.1 XRPD

XRPD analysis of the mineral phases was performed using a Philips X'Pert Pro diffractometer. Samples of natural, Cs-sorbed, Sr-sorbed kaolinite/clinoptilolite were analyzed in the powder form. The samples were first ground, mounted on holders than introduced for analysis. The source is consisted of Cu K_{α} radiation ($\lambda = 1.54 \text{ \AA}$). Each samples was scanned within the 2 theta range of 2-60. The step size was 0.020 with a time per step duration of 0.60 s. The mineralogical compositions of the samples were determined using a search-match procedure.

2.4.2 SEM/EDS

SEM / EDS characterization was carried out using a Philips XL-30S FEG type instrument. Prior to analysis, the solid samples were sprinkled onto Al or C tapes which are adhesive and supported on metallic disks. Images of the sample surfaces were recorded at different magnifications with the highest being 20000x. EDS Elemental analysis was carried out on randomly selected points on the solid surface. Different locations were analyzed by spot signals in order to minimize any possible anomalies arising from the heterogeneous nature of the analyzed surface. In addition, mapping analysis have been used to detect any localization of Cs or Sr on aluminol or silanol groups of clinoptilolite / kaolinite. EDS mapping was conducted at a magnification of 500x and a voltage of 18 kV under vacuum conditions of 3.5×10^{-5} mBar.

CHAPTER 3

MATHEMATICAL RELATIONS

3.1 The Distribution Ratio

The distribution ratio (R_d) is used to quantify sorption. R_d values are characteristic for each element in solution and a certain solid, and through the use of distribution ratios the migration of sorbates can be calculated and modeled.

The distribution of a trace constituent between aqueous and solid phases is given by R_d as;

$$R_d = \frac{\text{concentration in the solid phase}}{\text{concentration in the solution}} \quad (3-1)$$

$$R_d = \frac{[C]_s}{[C]_l} \quad (3-2)$$

where $[C]_s$ can be calculated using the equation:

$$[C]_s = \frac{([C]^0 - [C]_l) \cdot V}{M} \quad (3-3)$$

Percentage sorption is frequently used in quantifying sorption. It is easily

$$\% \text{ Sorption} = \frac{[C]^0 - [C]_l}{[C]^0} \cdot 100 \quad (3-4)$$

where V = is the volume of solution (ml)

M = is the weight of solid material (g)

3.2 Adsorption Isotherms

An adsorption isotherm gives the relation between the amount of adsorbed ion by a unit mass of solid and the amount of that ion in solution, at a known temperature and under equilibrium conditions. In an adsorption isotherm, a gradient of unity shows the linearity of sorption, a gradient of less than unity shows nonlinear sorption behavior, i.e., K_d increases with decreasing concentration. (Poinssot et al. 1999 p.7). Linear sorption is achieved when the sorption sites are equivalent in terms of sorption energy. Isotherms can also be used to provide information about the affinity of sorption sites towards the sorbed ion.

Many models have been developed to represent the various types of adsorption processes. Among these models Langmuir, Freundlich and Dubinin-Radushkevich are the most frequently applied isotherm models.

3.2.1 Langmuir Isotherm Model

This model assumes the solid surfaces to have uniform sites, and no interaction between sorbed ions takes place, thus all adsorbed species can interact only with adsorption sites. This model is developed for the systems in which sorption leads to deposition of a single layer of solute ions on the sorbent surface and it assumes that the energy of sorption for each molecule is the same and independent of surface coverage. Also the rate of sorption is almost negligible when compared with the initial rate of sorption. (JR Weber et al. 1991 p.505, Ho and Mckay 2000 p.736)

Langmuir isotherm is given by;

$$[C]_s = \frac{K \cdot C_m \cdot [C]_l}{1 + K \cdot [C]_l} \quad (3-10)$$

where $[C]_s$ = amount of solute per unit mass of solid (meq/g)

C_m = maximum amount of solute that can be sorbed by the solid phase (meq/g), it corresponds to complete monolayer coverage

$[C]_l$ = equilibrium concentration of solute in solution (meq/ml)

K = a sorption coefficient related to the energy of sorption

The C_m , which represents the total number of surface sites per unit mass of adsorbent, would be equal for all adsorbates in the ideal case. Since there are differences in the adsorbate sizes, C_m may change for different compounds (Molva 2004). In order to obtain linear form the above equation can be rearranged:

$$[C]_s = C_m - \frac{[C]_s}{K \cdot [C]_l} \quad (3-11)$$

a straight line can be obtained by plotting $[C]_s$ versus $[C]_s/[C]_l$ whose slope is $1/K$ and the intercept is C_m .

3.2.2 Freundlich Isotherm Model

This model allows for energetically heterogeneous set of sorption sites with the sorption energy varying exponentially. It is the most widely used non-linear model to describe the dependence of sorption adsorbate concentration. The general expression of this isotherm model is given by:

$$[C]_s = k \cdot [C]_l^n \quad (3-12)$$

where $[C]_s$ = amount adsorbed per unit weight of solid at equilibrium (meq/g)
 $[C]_l$ = concentration of the adsorbate in solution at equilibrium (meq/ml)
 k and n are Freundlich constants

This equation can be linearized as:

$$\log [C]_s = \log k + n \log [C]_l \quad (3-13)$$

Plotting $\log [C]_s$ versus $\log [C]_l$ gives n as the slope and $\log k$ as the intercept. k is the amount adsorbed at equilibrium concentration and n denotes the extent to which sorption depends on concentration. The isotherm is concave and the adsorbates are bound with much weaker free energies when $n < 1$. If the value of $n > 1$, the isotherm is

convex and the presence of more adsorbate in the adsorbent increase the free energies of further sorption. (Molva 2004 p.18) The deviation of n from unity denotes a non-linear sorption which occurs on heterogeneous surfaces. The non-linear behavior of sorption means that, for $n < 1$ or $n > 1$, the energy barrier of sorption is increasing or decreasing exponentially with the increasing fraction of filled sites on the adsorbent. (Shahwan and Erten 2002 p.118, Oscarson et al. 1987 p.33, Ishfaq et al. 1997 p.179) If the parameter n is equal to 1, the Freundlich equation becomes linear and the value of Freundlich constant k becomes equal to the distribution ratio (R_d). (Shahwan 2000 p.41) In this case, the system has constant free energy at all adsorbate concentrations.

The parameter k is related to sorption capacity.(Atun and Kilislioglu 2003 p.610). If an adsorption system fits good to the Freundlich isotherm, we can conclude that there is nearly no limit to the adsorbed amount and there is a multilayer adsorption. (Molva 2004 p.18)

3.2.3 Dubinin-Radushkevich Isotherm Model (D-R)

This model is good at low concentration ranges and can be used to describe sorption on both homogeneous and heterogeneous surfaces. (Shahwan and Erten 2002 p.117)

D-R isotherm model is given by equation (Atun et al. 1996 p.437):

$$[C]_s = C_m * \exp(-K\Sigma^2) \quad (3-14)$$

- where
- $[C]_s$ = amount adsorbed per unit weight of solid (meq/g)
 - $[C]_m$ = sorption capacity of adsorbent per unit weight (meq/g)
 - K = constant related to the energy of sorption (mol^2/J^2)
 - Σ = Polanyi potential = $RT \ln(1 + 1/[C]_l)$ (J/mol)
 - $[C]_l$ = equilibrium concentration of solute in solution (meq/g)
 - R = gas constant (J/Kmol)
 - T = absolute temperature (K)

The linear form of the equation may be obtained by rearranging it:

$$\ln [C]_s = \ln C_m - K\Sigma^2 \quad (3-15)$$

By plotting $\ln [C]_s$ versus Σ^2 , K and $\ln C_m$ can be calculated from the slope and intercept, respectively. (Abusafa and Yücel 2002 p.111)

D-R model is used to obtain the maximum adsorption capacity (C_m) and mean adsorption energy (E) whose magnitude is useful for estimating the mechanism of adsorption. (Atun and Kilislioglu 2003 p.609) Polanyi defines the adsorption potential (Σ) as the free-energy change required to transfer one mole of ion from infinity in solution to the solid surface and it changes with the concentration of solution. Energy range of mean energy of sorption is within 8-16 kJ / mol for ion-exchange reactions. (Atun et al.1996 p.438)

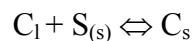
The parameter K is related to the adsorption mean free energy as (Ishfaq et al. 1997 p.180);

$$E = (-2K)^{-1/2} \quad (3-16)$$

Since D-R model does not require an energetically homogeneous surface or a constant adsorption potential, it is more common than Langmuir model. Because real surfaces are not homogeneous and binding sites are not uniform because of structural irregularities on surface. (Ishfaq et al. 1997 p.180)

3.3 Thermodynamic Parameters

An adsorption reaction can be simply represented by (Shahwan and Erten 2002 p.117):



where C_l = solute particle s in solution

S = sorption sites on the surface of the adsorbent

C_s = solute particles adsorbed on the adsorbent

In this representation, S is used to represent the accessible sorption sites which are assumed to possess equivalent energies. The overall summation of these sites gives

the exchange capacity of the solid. In real systems, the sorption sites are not totally homogeneous, and differ in their sorption energy. Most clays and aluminosilicates can be considered to possess roughly two kinds of sorption sites, one kind possesses high affinity but low capacity, and the other possesses a high capacity with low affinity toward sorbate specie.

The equilibrium constant for the above reaction is given as:

$$K = \frac{a_{Cs}}{a_s \cdot a_{Cl}} \quad (3-17)$$

Where a_{Cs} is the activity of solute particles adsorbed on the adsorbent, a_{Cl} is the activity of solute particles in solution, a_s is the activity of solid phase. The activity of the solid phase can be taken as unity at the reference state and the reaction 3-17 can be rearranged in terms of concentrations and activity coefficients γ as:

$$K = \frac{[C]_s}{[C]_l} \cdot \frac{\gamma_{Cs}}{\gamma_{Cl}} \quad (3-18)$$

Activity coefficients of dilute solutions are equal to unity, then the above expression becomes equivalent to distribution ratio (R_d).

Gibbs Free Energy of the adsorption system is calculated by the following reaction:

$$\Delta G = \Delta G^0 + RT \ln R_d \quad (3-19)$$

in which ΔG^0 = standard Gibbs free energy change

R = ideal gas constant

T = absolute temperature

Gibbs free energy does not change at equilibrium, thus the above reaction becomes:

$$\Delta G^0 = -RT \ln R_d \quad (3-20)$$

If the ΔG^0 values are negative, then the sorption process is spontaneous. The change in Gibbs free energy can be rearranged in terms of enthalpy change (ΔH^0) and entropy change (ΔS^0) as:

$$\Delta G^0 = \Delta H^0 - T \Delta S^0 \quad (3-21)$$

In order to calculate enthalpy of sorption, the following equation is used (Molva 2004 p.55):

$$\Delta H = \frac{R T_1 T_2 \cdot \ln \frac{K_2}{K_1}}{T_2 - T_1} \quad (3-22)$$

where K_1 and K_2 are equilibrium constant at T_1 and T_2 .

3.4 Kinetic Equations

3.4.1 First-Order Kinetics

For adsorption processes following the first-order kinetics, the following equation proposed by Lagergren can be employed (Kannan and Sundaram 2001 p.31, Mishra and Tiwary 1999 p.362):

$$\log (q_e - q_t) = \log q_e - \frac{kt}{2.303} \quad (3-23)$$

where q_e = amount adsorbed per unit mass of adsorbent at equilibrium (mg/g)

q_t = amount adsorbed per unit mass of adsorbent at time t (mg/g)

k = adsorption rate constant (1/min)

q_t is given by $(c_i - c_f) * v / m$ where c_i and c_f are the initial and final concentrations (mg/L), respectively and m is the mass of adsorbent (mg), v is the volume of solution (L).

3.4.2 Second-Order Kinetics

Adsorption processes obeying second-order kinetics should fit the rate equation (Ho and McKay 2000 p.736):

$$\frac{dq_t}{dt} = k (q_e - q_t)^2 \quad (3-24)$$

in which k = rate constant of sorption (g / mg*min)
 q_e = amount adsorbed at equilibrium (mg / g)
 q_t = amount adsorbed at time t (mg / g)

Rearranging;

$$\frac{dq_t}{(q_e - q_t)^2} = k dt \quad (3-25)$$

When equation (3-24) is integrated for the boundary conditions $t=0$ to $t=t$ and $q_t=0$ to $q_t=q_t$, the following a pseudo-second order equation results:

$$\frac{1}{q_e - q_t} = kt + \frac{1}{q_e} \quad (3-26)$$

Rearranging the above equation gives:

$$q_t = \frac{t}{\frac{1}{kq_e^2} + \frac{t}{q_e}} \quad (3-27)$$

if h (initial sorption rate) is equal to kq_e^2 , then:

$$q_t = \frac{t}{\frac{1}{h} + \frac{t}{q_e}} \quad (3-28)$$

which has a linear form of:

$$\frac{t}{q_t} = \frac{1}{h} + \frac{t}{q_e} \quad (3-29)$$

The value of h can be found from the intercept of t / q_t against t. The initial sorption rate increases with decreasing initial metal ion concentration. (Ho and Mckay 2000 p.736)

q_e, k and h can be expressed as a function of c₀ (Ho and Mckay 2000 p.738):

$$q_e = \frac{c_0}{A_q * c_0 + B_q} \quad (3-30)$$

$$k = \frac{c_0}{A_k * c_0 + B_k} \quad (3-31)$$

$$h = \frac{c_0}{A_h * c_0 + B_h} \quad (3-32)$$

where A and B are the empirical parameters for predicted q_e, k and h from c₀.

If we substitute 3-30 and 3-32 in equation 3-28, the rate of law for a pseudo-second order reaction is obtained as follows (Ho and Mckay 2000 p.738, 739):

$$q_t = \frac{t}{\frac{1}{\frac{c_0}{A_h c_0 + B_h}} + \frac{t}{\frac{c_0}{A_q c_0 + B_q}}} \quad (3-33)$$

$$q_t = \frac{c_0 t}{A_h c_0 + B_h + (A_q c_0 + B_q) t} \quad (3-34)$$

This is the generalised predictive model for sorbed ion at any contact time and initial metal ion concentration. The sorbed metal ion at any contact time increases with increasing metal ion concentration. (Ho and Mckay 2000 p.739)

3.4.3 Intra-Particle Diffusion Model

Diffusion is a process through which the adsorbate species are transported from the liquid phase into the solid phase and is often the rate limiting step of adsorption process in stirring batch shaker. Intra-particle diffusion model is given with below equation (Kannan and Sundaram 2001 p.27, 33, 34, Özcan A.S. and Özcan A. 2004 p.4):

$$q_t = k_p (t)^{1/2} + C \quad (3-35)$$

in which q_t = adsorbed amount at time t

k_p = intra-particle diffusion rate constant ($\text{mg} (\text{min})^{1/2} / \text{g}$)

C = intercept which gives information about the boundary layer thickness

Upon fitting the data to the above equation, if the linear correlation value is close to unity, then intra-particle diffusion process is effective. Also if the relation between \log (% removal) and \log (time) values give linear correlation, this reveals the presence of intra-particle diffusion process (Kannan and Sundaram 2001 p.27, 32, 34)

3.4.4 Activation Energy

Activation energy refers to the minimum kinetic energy that must be supplied to the system in order for a chemical process to take place. In sorption processes, the activation energy can be obtained using Arrhenius equation (Levine 1988 p.537, 538, 539, 540):

$$\ln \frac{k_2(T_2)}{k_2(T_1)} = - \frac{E_a}{R} \left(\frac{1}{T_2} - \frac{1}{T_1} \right) \quad (3-36)$$

where k = apparent rate constant which is given by $-kt = \ln[(q_e - q_t) / q_e]$

E_a = activation energy which can be calculated from the slope of $\ln k$ versus $1/T$ plot

R = gas constant

T = absolute temperature

If sorption is carried out at two different temperatures, for each the rate constant k is known, then the activation energy can be obtained using this equation.

CHAPTER 4

RESULTS AND DISCUSSION

4.1 Characterization of Natural Kaolinite and Clinoptilolite Minerals

The natural samples of kaolinite and clinoptilolite were characterized and analyzed to obtain their mineralogical and elemental constituents using XRPD and SEM/EDS techniques. The results are outlined in the following sections.

4.1.1 XRPD Characterization

The XRPD diagram of kaolinite is shown in Fig. 4.1 According to the features in the figure, natural kaolinite is seen to include quartz as an impurity. Kaolinite is characterized by its prominent peak occurring at $\sim 7 \text{ \AA}$, which corresponds to the interlayer space of the clay. Other kaolinite peaks corresponding to different reflections are also provided in the figure. The primary peak of quartz occurring near 3.03 \AA , seems to be the most intense peak. This usually stems from the high crystallinity of quartz phase, the thing giving rise to a higher 'cross section' of this mineral compared to kaolinite, which usually possesses poorer crystallinity and hence, in spite of existing in much larger amounts, it gives rise to features with lower intensities.

The XRPD diagram of clinoptilolite is demonstrated in Fig. 4.2 The mineral seems to be nearly pure. It must be stressed here that the limit of detection of XRPD ranges 5-10 percent composition, hence the possibility of existence of minor fractions of other minerals can not be completely excluded.

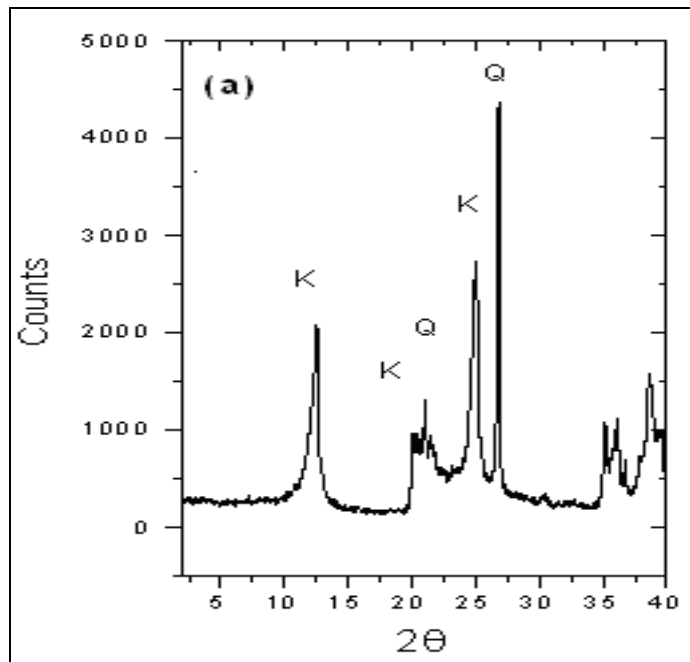


Figure 4.1. XRPD diagram of natural kaolinite (K = kaolinite, Q = quartz)

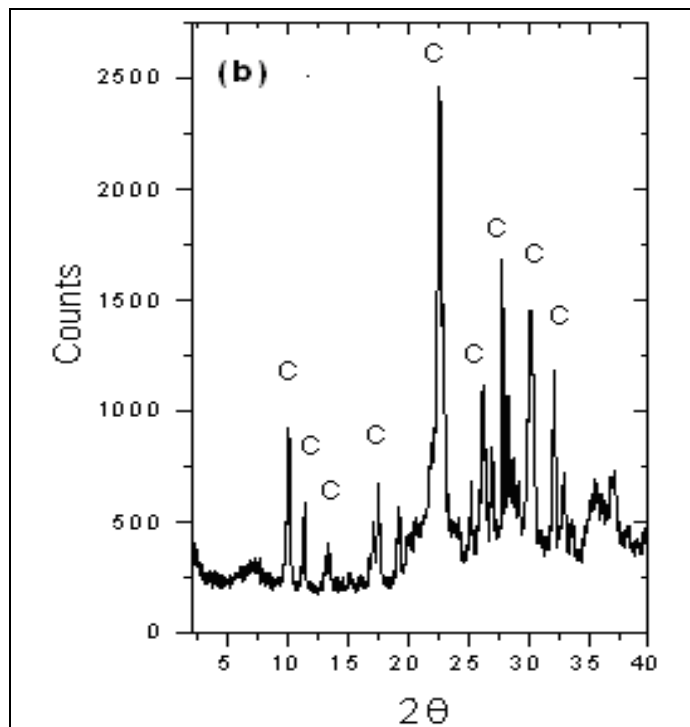


Figure 4.2. XRPD diagram of natural clinoptilolite (C = clinoptilolite)

4.1.2 SEM / EDS Characterization

SEM micro-characterization of kaolinite showed that the particles of this clay have a crystal structure of hexagonal shape (most of these particles appear to be broken) and edge size of approximately 500 nm. Typical SEM graphs of the clay are given in Fig. 4.3. Moreover, the EDS elemental analysis of the clay is provided in Table 4.1. The presence of the quartz fraction in the natural clay is verified by the higher Si content compared to Al, as in pure kaolinite ($\text{Si}_4 \text{Al}_4 \text{O}_{10} (\text{OH})_8$) the molar quantity of both is equal. But the fact that the ratio of Si/Al exceeds unity only slightly points out that quartz exists in a minor quantity.

Analysis of clinoptilolite using SEM revealed that the mineral is composed of crystals that vary in size and edge sharpness as shown in Fig. 4.4. The EDS results, which are given in Table 4-1, showed that the Si/Al ratio is somewhat less than their ratio in a pure clinoptilolite, $(\text{Na,K,Ca})_6 \text{Al}_6 \text{Si}_{30} \text{O}_{72} \cdot 24 \text{H}_2\text{O}$, thus suggesting structural imperfections in the lattice of the mineral. The elemental analysis indicated also that the cations hosted in the channels of the mineral are dominated by K and Ca.

Table 4.1. EDS results of the atomic percentages of O, Na, Mg, Al, Si, K, Ca in natural kaolinite and clinoptilolite minerals obtained from spot analysis at 3 different points selected randomly on the surface of minerals.

Sample	Element	Spot 1	Spot 2	Spot 3	Average	± S. D.
Kaolinite	O	65.94	67.47	67.11	66.84	0.80
	Na	0.45	0.52	0.44	0.47	0.04
	Mg	0.34	0.3	0.39	0.34	0.05
	Al	16.06	14.05	12.17	14.09	1.95
	Si	17.21	17.25	18.38	17.61	0.66
	K	0	0.21	0.21	0.14	0.12
	Ca	0	0.19	1.31	0.50	0.71
Clinoptilolite	O	62.54	61.17	62.11	61.94	0.70
	Na	0.55	0.45	0.68	0.56	0.12
	Mg	0.8	0.77	1.01	0.86	0.13
	Al	5.28	5.31	5.31	5.30	0.02
	Si	23.56	24.7	22.94	23.73	0.89
	K	1.49	1.72	1.63	1.61	0.12
	Ca	0.95	1.17	1.04	1.05	0.11

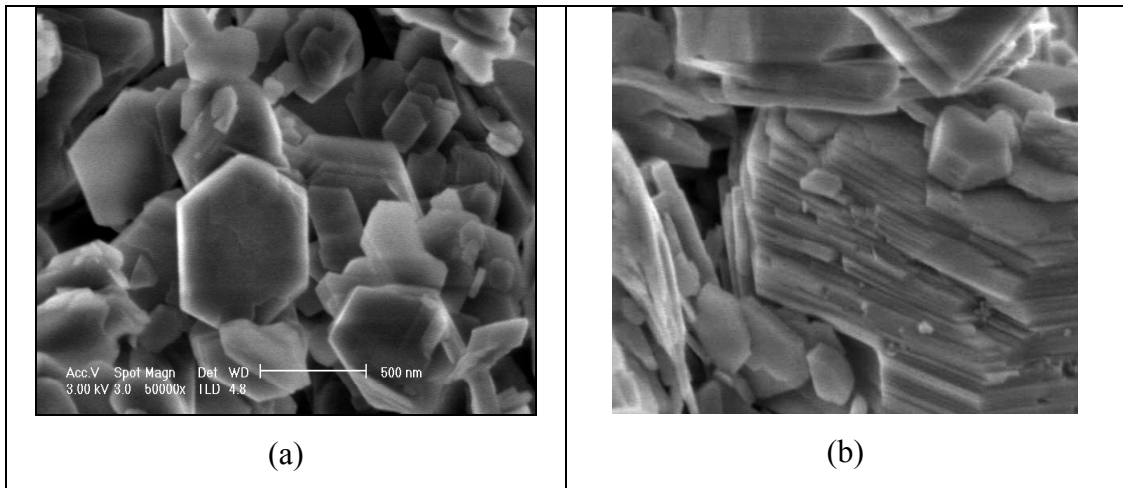


Figure 4.3. Typical SEM images of natural kaolinite

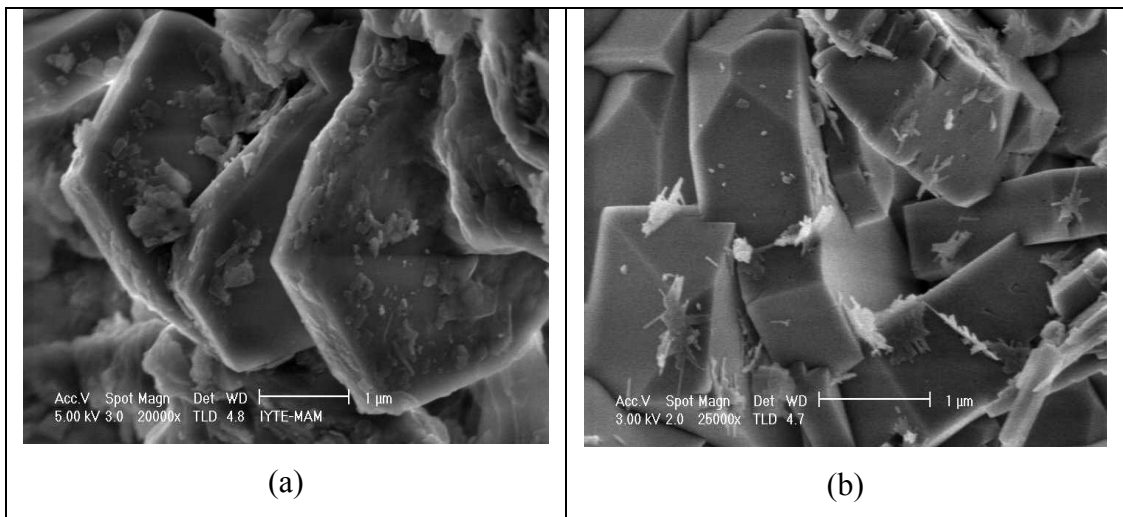


Figure 4.4. Typical SEM images of natural clinoptilolite

4.1.3 FTIR Characterization

Natural kaolinite and clinoptilolite samples were also characterized using Infrared Spectroscopy (FTIR). Various clay minerals can be identified using IR analysis based on their characteristic absorption features in the mid-IR spectral range. The identification was carried out through a comparison between the spectra of pure clays provided in literature (Russell and Fraser 1994 p. 45, 52-55), and those of the clays used

in the study. The FTIR spectra of kaolinite and clinoptilolite are given in Figures 4.5, 4.6 respectively.

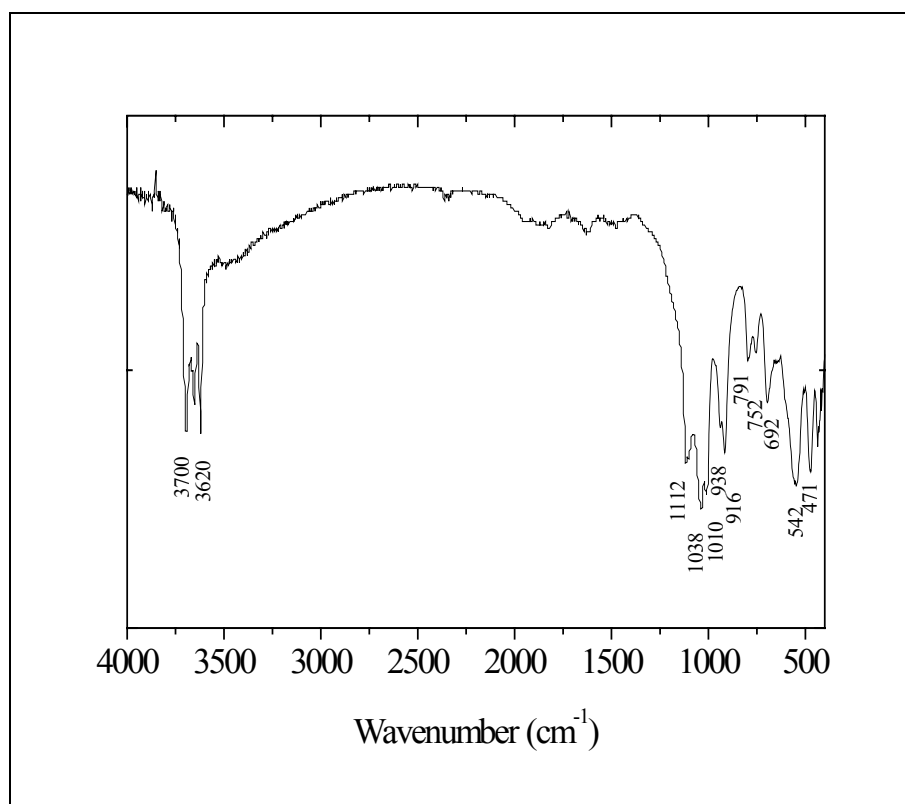


Figure 4.5. FTIR spectra of natural kaolinite used in our studies

The FTIR spectrum of kaolinite is given in Fig. 4.5. Kaolins can be readily distinguished from other clays by differences in position and relative intensities of their OH stretching bands. The OH stretchings occurring around the 3700-3620 cm⁻¹ doublet are characteristic for kaolin clays. The feature near 3700 cm⁻¹ lies well separated from those of most other mineral bands. The OH deformation bands near 938-916 cm⁻¹ are also typical for the kaolin group minerals and arise from vibrations of the inner and inner surface OH groups within the clay matrix. Other features appearing in the spectrum belong to a variety of Al-O and Si-O stretching and bending vibrations. (Russell and Fraser 1994 p.52, 53, 54, 55).

The FTIR spectrum of clinoptilolite is given in Fig. 4.6. The fact that zeolites are significantly hydrated is illustrated by the discrete water absorption bands in the 3500 and 1640 cm⁻¹ region. These bands, which were centered at 3450 and 1633, refer to

water molecules associated with Na and Ca in the channels and cages in the of the zeolite structure. [Wilson 1994 p.45]. As can be seen from the figure, other bands appear near 1204, 1057, 799 and 471 cm^{-1} . The 1111 cm^{-1} band arises from asymmetric stretching vibration modes of internal T-O bonds in TO_4 tetrahedra (T=Si and Al). The 799 and 471 cm^{-1} bands are assigned to the stretching vibration modes of O-T-O groups and the bending vibration modes of T-O bonds, respectively. [Tanaka et al. 2003 p.719]

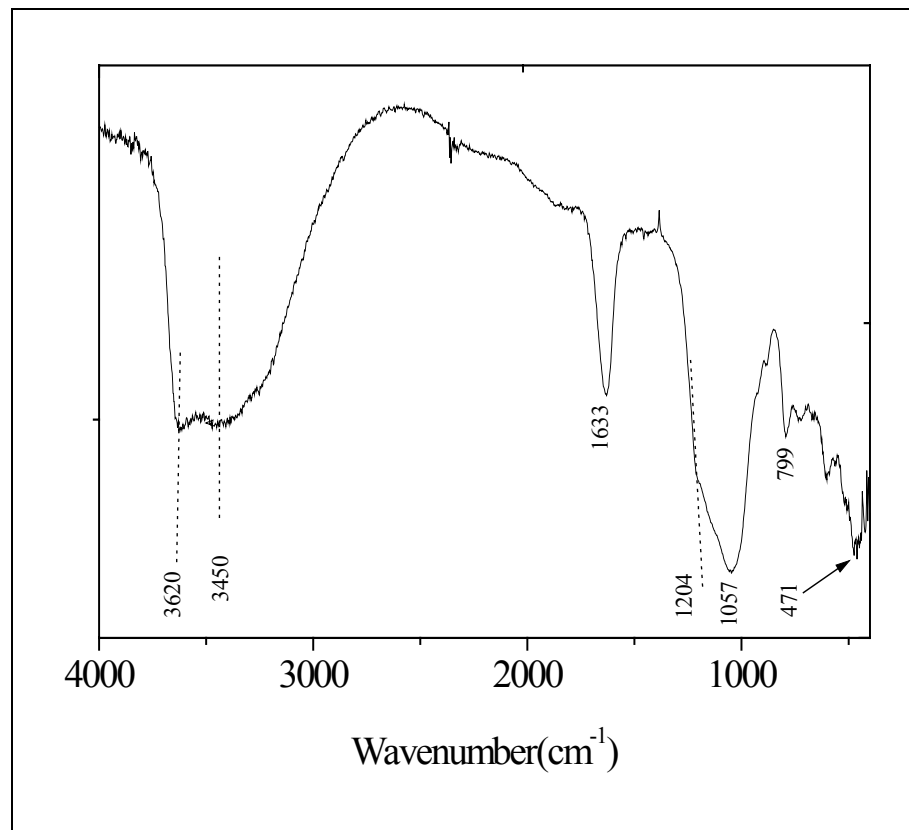


Figure 4.6. FTIR spectrum of clinoptilolite used in this work

4.2 Kinetic Analysis of Sorption

The kinetic studies of sorption were carried out for different initial concentrations of 10, 50, and 100 mg/L of CsCl and $\text{Sr}(\text{NO}_3)_2$ on kaolinite and clinoptilolite minerals. The variation of the sorbed amounts of Cs^+ and Sr^{2+} on kaolinite at a temperature of 25°C is provided in Figs.4.7 and 4.8. Similarly, the variation of the sorbed amounts of both cations on clinoptilolite is given in Figs. 4.9 and 4.10.

According to the results, equilibrium of sorbed Sr^{2+} (or Cs^+) was achieved within the first few hours of mixing on both kaolinite and clinoptilolite. The same experiments were repeated at a temperature of 60°C . These plots are represented in Appendix A. Apart from the change in the sorbed amounts, no significant change in the shape of the curves was observed.

It is interesting to note that in the sorption of Cs^+ and Sr^{2+} on kaolinite, in particular at highest loadings, fast accumulation of ions takes place at the surface of kaolinite during the initial stages of sorption followed by a partial desorption that leads to attainment of equilibrium. The same behavior was not documented for sorption on clinoptilolite, the thing probably stemming from the difference in the nature of sorption sites on these minerals, and consequently the difference in the types of barriers that stand against sorption in each case. A further discussion on this topic is provided in a coming section devoted to analysis of film and pore diffusions.

Quantitatively, the results of the percentage sorption at equilibrium are given in Table 4.2 decreased with the increase in initial concentration.

Table 4.2. % Sorption values at different initial concentrations

Sample	T ($^\circ\text{C}$)	10 mg/L	50 mg/L	100 mg/L	500 mg/L
Cs-kaolinite	25	30	29	40	28
	60	37	26	30	25
Cs-clinoptilolite	25	94	95	95	91
	60	90	92	93	89
Sr-kaolinite	25	47	17	16	13
	60	59	19	18	31
Sr-clinoptilolite	25	93	71	48	53
	60	94	73	71	63

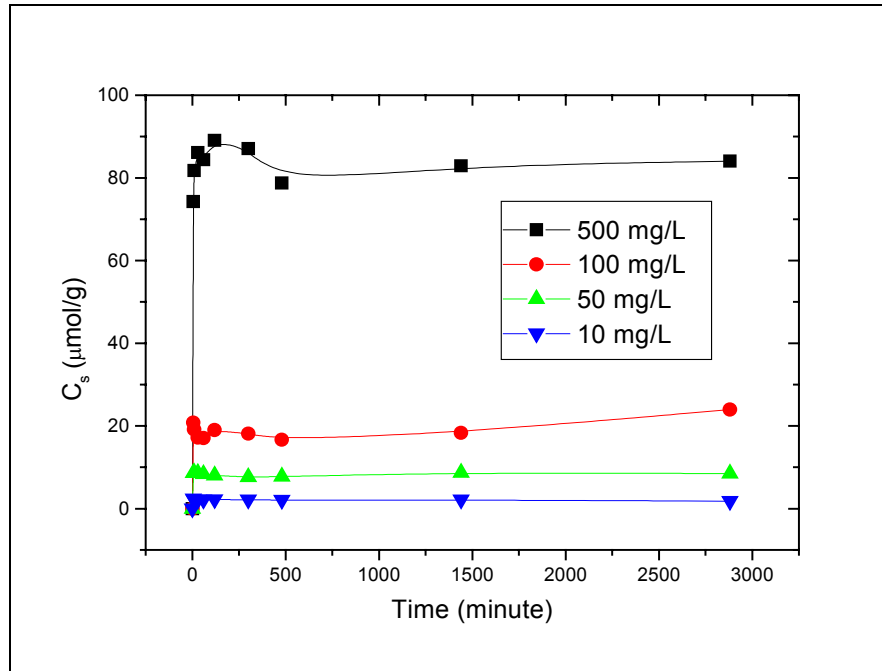


Figure 4.7. Variation of the sorbed amount of Cs^+ ($\mu\text{mol/g}$) on kaolinite with time at 25°C

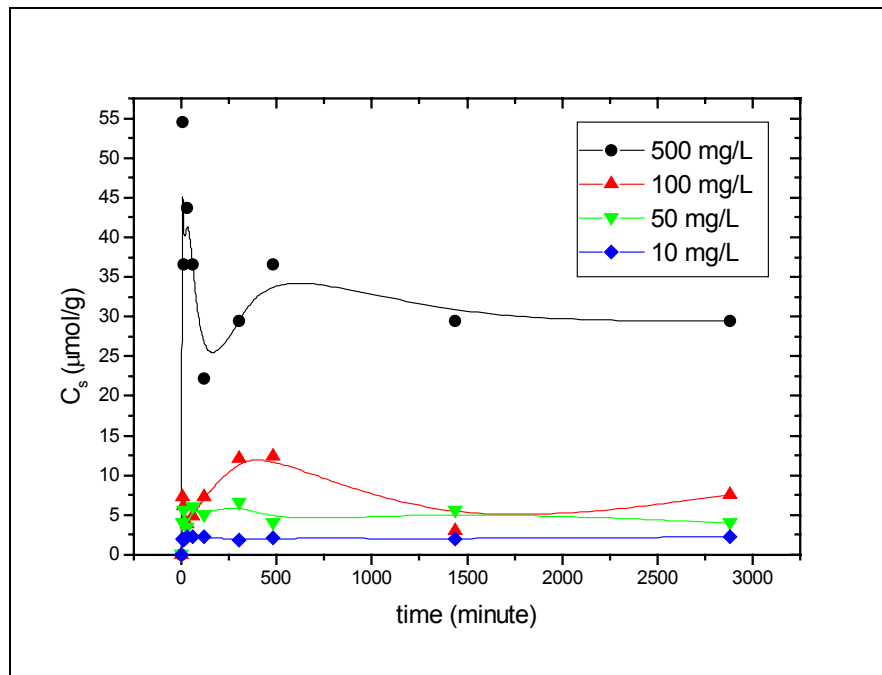


Figure 4.8. Variation of the sorbed amount of Sr^{2+} ($\mu\text{mol/g}$) on kaolinite with time at 25°C

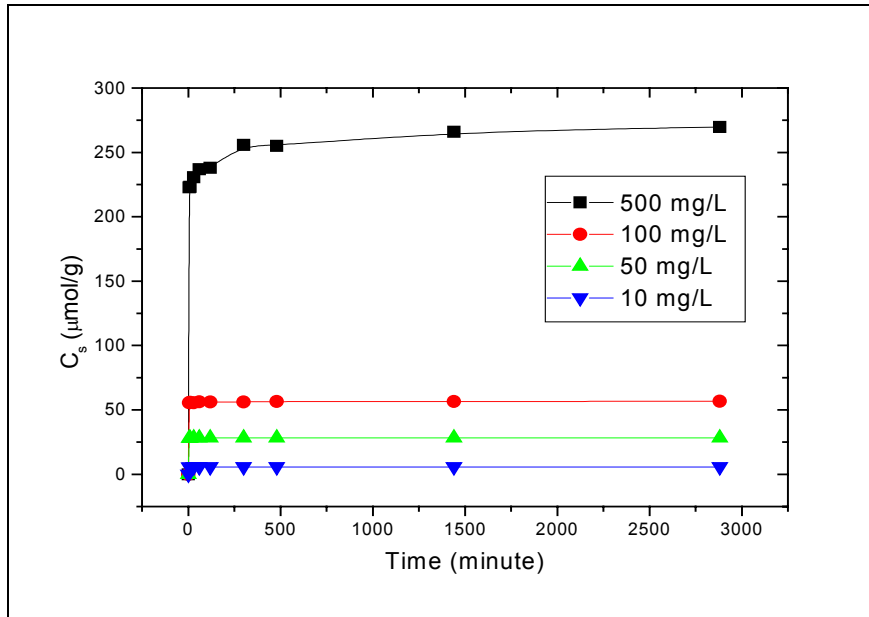


Figure 4.9. Variation of the sorbed amount of Cs⁺ (µmol/g) on clinoptilolite with time at 25°C

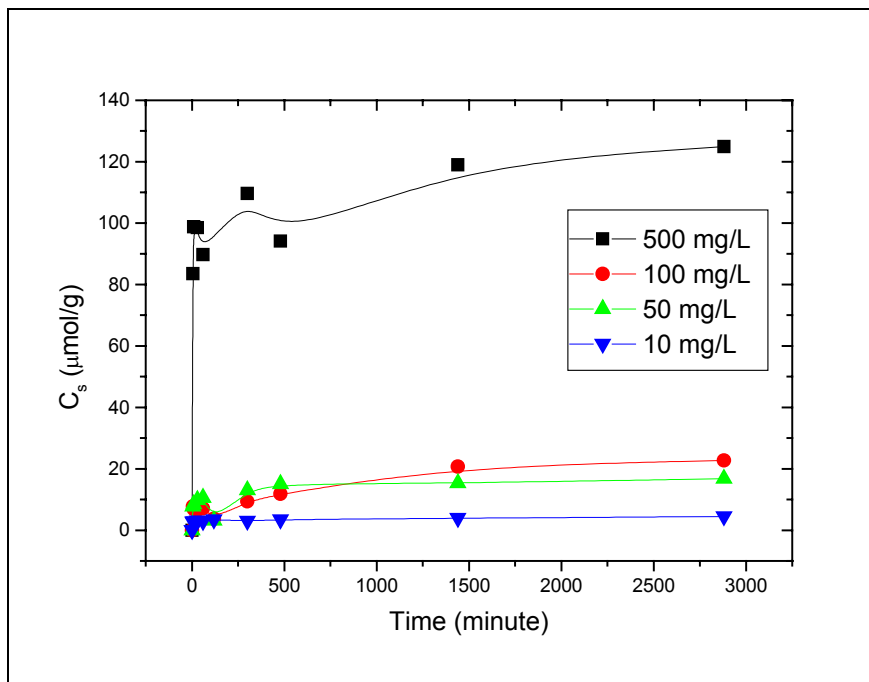


Figure 4.10. Variation of the sorbed amount of Sr²⁺ (µmol/g) on clinoptilolite with time at 25°C

4.2.1 Determination of Rate Equations and Activation Energies

The kinetic data was further used in the determination of the rate constants and activation energies of sorption. In order to calculate the “apparent” rate constant, the following pseudo first order equation (Kannan and Sundaram 2001 p.31) and pseudo second order equation (Ho and Mckay 2000 p.736) were used:

$$\frac{1}{[C]_s} = \left(\frac{k_1}{[C]_e}\right)\left(\frac{1}{t}\right) + \frac{1}{\{C\}_e} \quad (4-1)$$

$$\frac{t}{[C]_s} = \left(\frac{1}{k_2[C]_e^2}\right) + \left(\frac{1}{[C]_e}\right)t \quad (4-2)$$

Where $[C]_s$ is the concentration of sorbed ion on the solid at time t ($\mu\text{mol/g}$), $[C]_e$ is the concentration of sorbed ion at equilibrium, k_1 and k_2 are the pseudo first order rate constant and pseudo second order rate constant ($\text{g}/\mu\text{mol} \cdot \text{min}$), respectively. In the above equations, $[C]_s$ was calculated using the following equation, as given in section 3:

$$[C]_s = ([C]_o - [C]_l) * (V / M) \quad (3-3)$$

where $[C]_o$ is the initial concentration ($\mu\text{mol/L}$), V is the volume of the solution (L), and M is the mass of the solid (g).

The pseudo first order kinetics did not yield linear plots for the sorption data at 25°C and 60°C . On the other hand, equation (4-2) was adequately followed by the sorption data of both of Cs^+ and Sr^{2+} on kaolinite and clinoptilolite, as shown below.

The plot using second order kinetics of Cs^+ and Sr^{2+} sorption on kaolinite and clinoptilolite are given in Figs. 4.11, 4.12, 4.13, and 4.14. As shown in these figures, almost perfect linear fits were obtained with correlation coefficients close to unity for all concentrations. The constants C_e (equilibrium coverage) and k_2 (apparent rate constant) are obtained from the slope and intercept of t/q_t against t plots. The values of these constants are given in Table 4.3. The values of these constants were calculated from the linear fits corresponding to the highest concentration, i.e. 500 mg/L of CsCl and $\text{Sr}(\text{NO}_3)_2$. The plots drawn for the second order kinetics at 60°C are given in Appendix B.

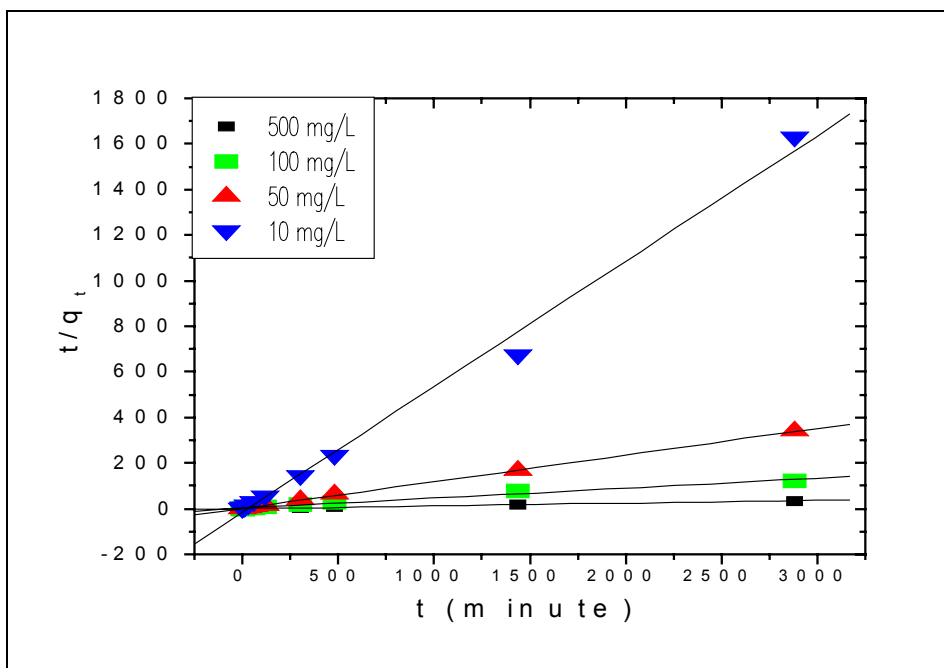


Figure 4.11. Corresponding linear fit for the variation of the sorbed amount of Cs^+ on kaolinite with time, using the pseudo-second order equation at 25C

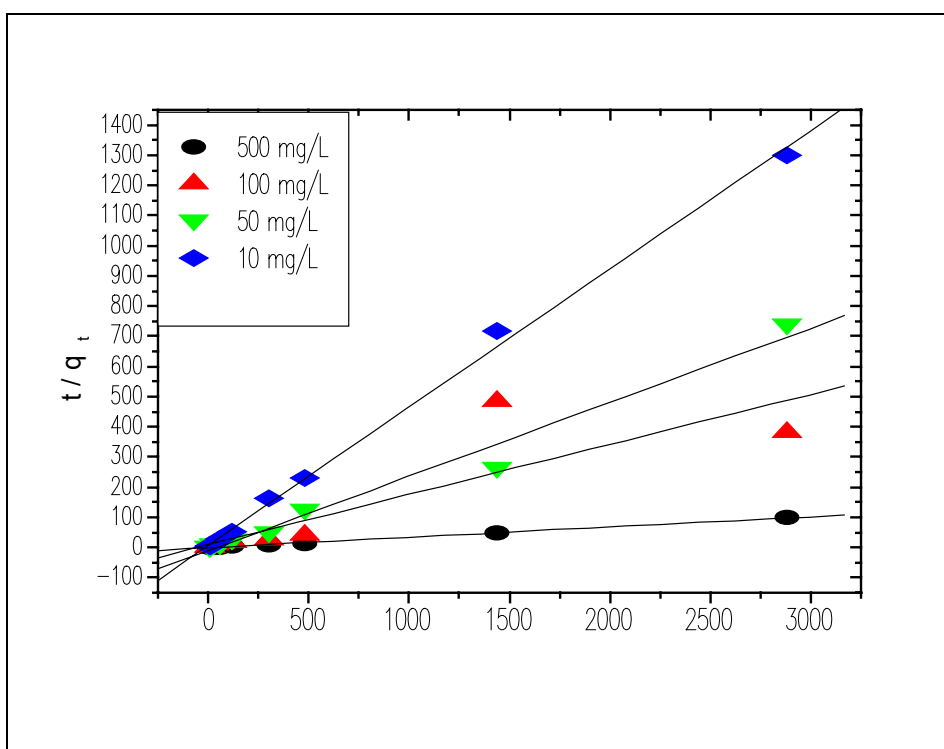


Figure 4.12. Corresponding linear fit for the variation of the sorbed amount of Sr^{2+} on kaolinite with time, using the pseudo-second order equation at 25C

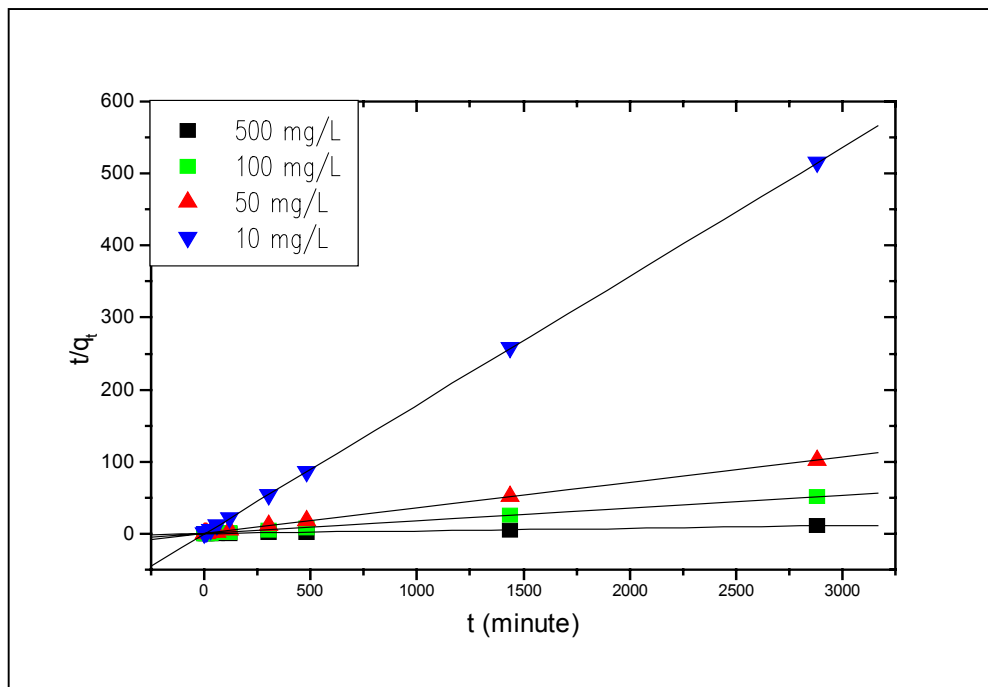


Figure 4.13. Corresponding linear fit for the variation of the sorbed amount of Cs⁺ on clinoptilolite with time, using the pseudo-second order equation at 25C

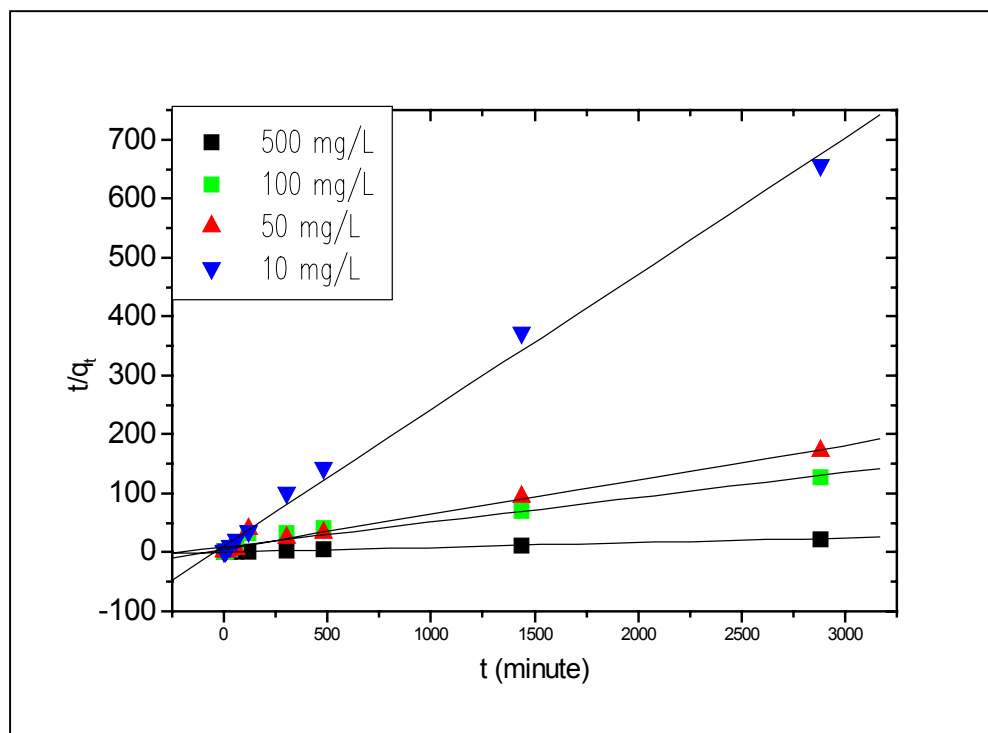


Figure 4.14. Corresponding linear fit for the variation of the sorbed amount of Sr²⁺ on clinoptilolite with time, using the pseudo-second order equation at 25C

Although equation (4-2) was applied widely by many authors to describe different sorption data on several types of sorbate/sorbent systems, it must be stressed that an important limitation on the applicability of this equation is that the equation would lead to a perfect linearity even if the sorbed amount does not show any variation with time. Moreover, there is a possibility of obtaining a negative intercept (the rate constant has a negative value) even in a case where the linear correlation coefficient might be 1.0. Due to this, we have chosen to apply equation (4-2) for the sorption data at initial concentration of Sr(NO₃)₂ (or CsCl) of 500 mg/L only, the concentration at which the uptake by the solids showed a gradual increase with time leading to equilibrium. This comment was included in a recent publication on the topic by our group (Shahwan et al. 2004).

As stated above, the values of the linear correlation coefficients (k_2) and $[C]_e$ obtained at the initial concentration of Sr(NO₃)₂ (or CsCl) of 500 mg/L only, and temperatures of 25°C and 60°C re shown in Table 4.3. The k_2 values indicates that the sorption of Cs⁺ is faster than of Sr²⁺ on both of kaolinite and clinoptilolite. This could be resulting from the larger mobility of Cs⁺ ions in aqueous media as a result of the smaller hydration energy of this cation compared to that of Sr²⁺ (hydration energies are -276 kJ/mol and -1443 kJ/mol for cesium and strontium, respectively). Moreover, for each of Cs⁺ and Sr²⁺ sorption, the uptake of these ions by kaolinite is observed to be faster than that of clinoptilolite, indicating that the sorption sites on the former mineral is more easily accessible than those on the latter.

The activation energy of sorption (E_a ; kJ/mol) can be calculated, as discussed in section 3, using the following equation:

$$\ln \frac{k_2(T_2)}{k_2(T_1)} = -\frac{E_a}{R} \left(\frac{1}{T_2} - \frac{1}{T_1} \right) \quad (3-36)$$

Here, R is the perfect gas constant (8.3145 J/mol.K), $k_2(T_1)$ and $k_2(T_2)$ are, respectively, the rate constants at two different temperatures. The activation energy can be thought of as the minimum kinetic energy required for a particular reaction to occur, and as such, it provides a measure of the energetic barrier that the sorbate ions have to overcome prior to being fixed by the sorption sites. The calculated values of E_a are provided in Table 4.3. As seen from the table, the values related with sorption of both ions on kaolinite are smaller than the ones related with fixation on clinoptilolite,

indicating that the energetic barrier against sorption on kaolinite is easier to overcome when compared with that on clinoptilolite. In all cases, the E_a values are below the energies corresponding to chemisorption barriers (usually > 40 kJ/mol), suggesting that a sort of physisorption mechanism is operative where the attractive forces are of van der Waals type in addition to weak electrostatic forces accompanying most ion-exchange reactions.

Table 4.3. The values of k_2 and $[C]_e$ obtained from the linear fits of the experimental data to the second order rate equation

Sample	Temperature ($^{\circ}$ C)	$[C]_e$ (μ mol/g)	k_2 (g/ μ mol*min)	R	E_a (kJ/mol)
Cs-loaded kaolinite	25	84	$6.0 \cdot 10^{-3}$	0.9999	11.6
	60	85	$3.7 \cdot 10^{-3}$	0.9991	
Cs-loaded clinoptilolite	25	270	$3.8 \cdot 10^{-4}$	0.9999	15.3
	60	262	$7.3 \cdot 10^{-4}$	0.9997	
Sr-loaded kaolinite	25	29	$3.6 \cdot 10^{-4}$	0.9994	8.5
	60	68	$2.5 \cdot 10^{-4}$	0.9836	
Sr-loaded clinoptilolite	25	125	$3.3 \cdot 10^{-4}$	0.9981	17.3
	60	148	$1.5 \cdot 10^{-4}$	0.9994	

4.2.2 Determination of Diffusion Parameter

As discussed previously, the k_2 values show that the sorption on kaolinite is faster than that on clinoptilolite, the thing due to the fact that the sorption sites of kaolinite are placed mainly on surface and edge locations which are more easily accessible. That is it would be enough for Sr^{2+} (or Cs^+) ions to reach the boundary sorption layer to overcome the film diffusion barrier on kaolinite, and finally undergo the exchange reaction that leads to fixation on the sorption sites. In the case of clinoptilolite, in addition to surface sites, there are sorption sites inside the channels of the mineral. Thus it is necessary for Sr^{2+} (or Cs^+) ions to additionally overcome the pore diffusion barrier before reaching the internal sorption sites and undergo the exchange reaction.

The effect of intraparticle diffusion on sorption was tested using the following equation as given in section 3, (Kannan and Sundaram 2001 p.32, Özcan, A.S. and Özcan, A. 2004 p.4):

$$[C]_s = k_p * t^{1/2} + C \quad (3-35)$$

where k_p is the intraparticle diffusion rate constant ($g/\mu\text{mol}*\text{min}$) and C is a constant related to the boundary layer thickness. The value of C gives an idea about the boundary layer thickness, i.e. the larger the intercept, the greater is the boundary layer effect.

This equation is useful in revealing whether particle diffusion is effective in the course of the sorption process, and thus allows for a comparison of particle diffusion with film diffusion.

The plots of the sorption data of Cs^+ and Sr^{2+} on kaolinite using equation (3-35) are shown in Figures 4.15 and 4.16, respectively. As implied by the two figures, no linear behavior was observed over the studied time range. This is indicative that intraparticle diffusion has no role to play in the sorption case of kaolinite. This seems to be inline with the fact that the sorption sites on kaolinite are situated at the outer surface of the clay, which possesses a tight interlayer structure that greatly hinders for diffusion of sorbate ions within the lattice of the clay. Thus, it might be argued that film diffusion is the main resistance against sorption on kaolinite. However, in light of the observations reported earlier and shown in Figures 4.7 and 4.8, it is possible to conclude that the fast accumulation of ions followed by partial desorption that lead to equilibrium, means that the exchange reaction (intrinsic sorption) on kaolinite sites is slower than the transfer rate of Cs^+ and Sr^{2+} ions from the bulk of the solutions to the boundary layer. This is probably due to the competition between the sorbate ions towards the limited number of sorption sites on kaolinite.

The same results were also verified for the concentrations of 100, 50, and 10 mg/L of CsCl and $\text{Sr}(\text{NO}_3)_2$, as shown in Appendix C.

On the other hand, the sorption data of Cs^+ and Sr^{2+} on clinoptilolite seemed to lead to a linear behavior at the initial stages of sorption (time $< \sim 100$ minutes) followed by a curved portion leading to a plateau as shown in Figures 4.17 and 4.18.

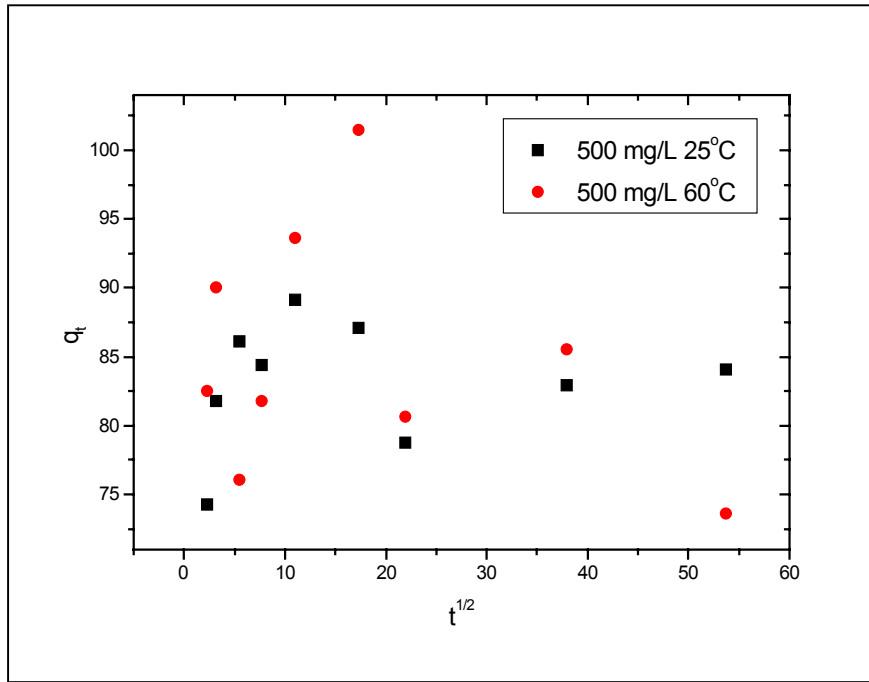


Figure 4.15. Intraparticle diffusion plots of sorbed Cs^+ on kaolinite at 25°C and 60°C

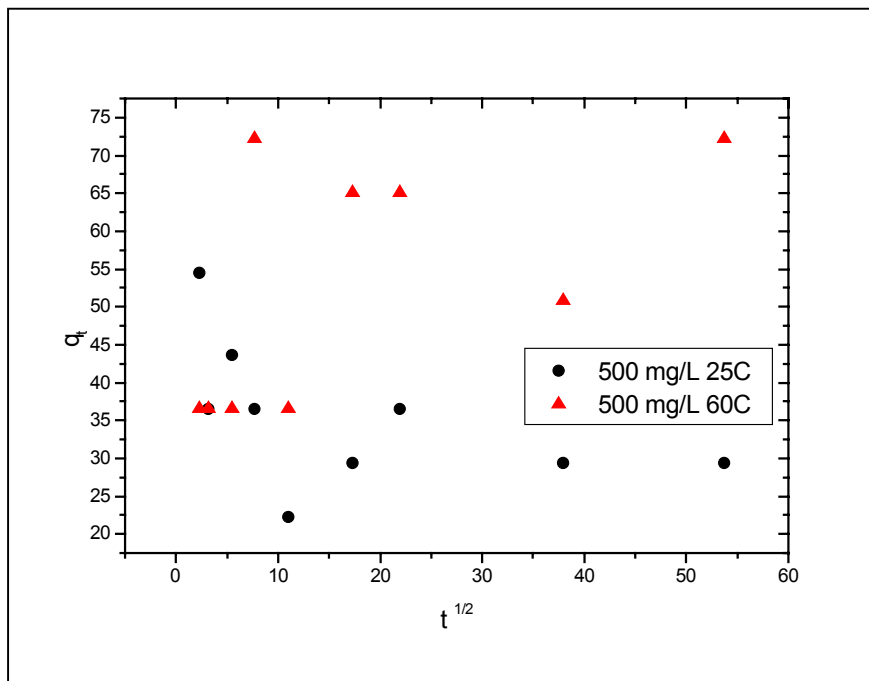


Figure 4.16. Intraparticle diffusion plots of sorbed Sr^{2+} on kaolinite at 25°C and 60°C

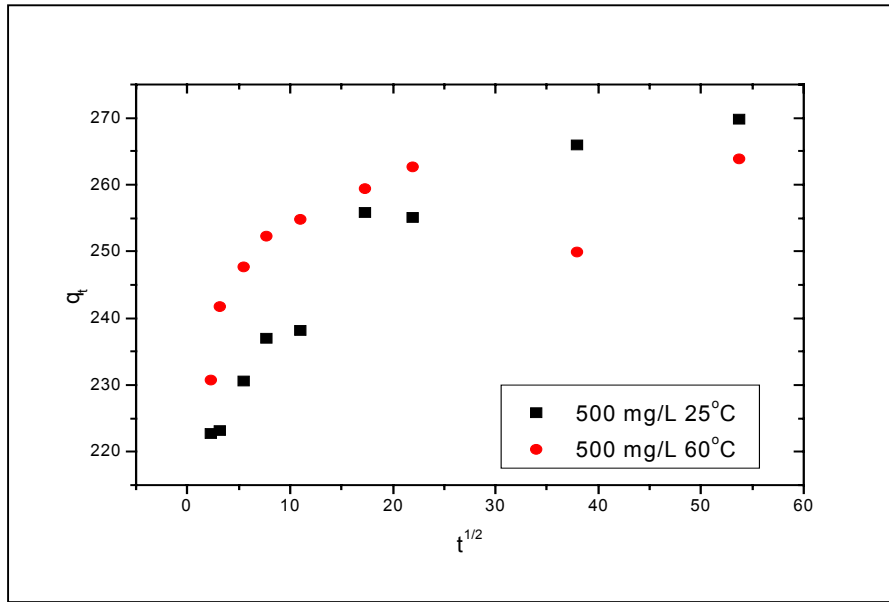


Figure 4.17. Intraparticle diffusion plots of sorbed Cs^+ on clinoptilolite at 25°C and 60°C

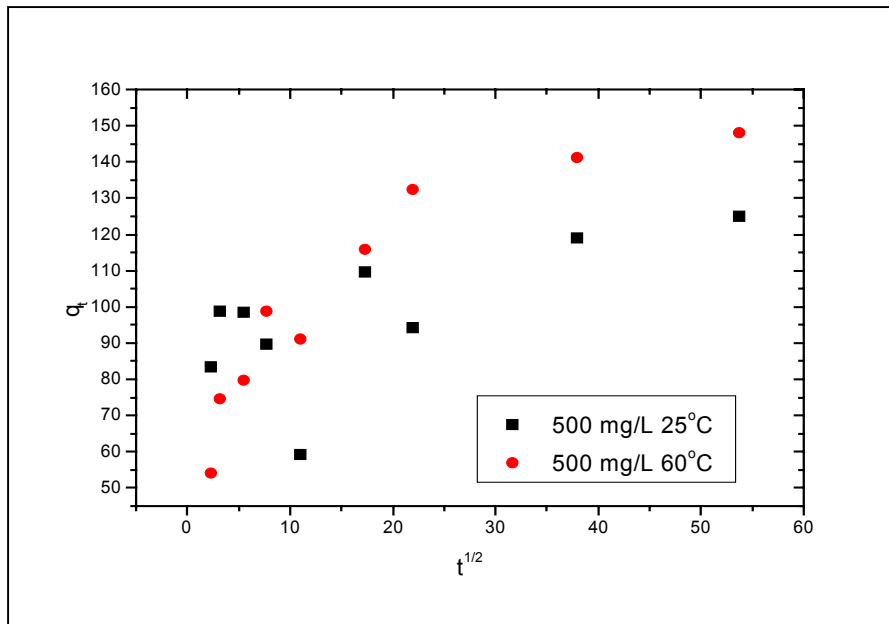


Figure 4.18. Intraparticle diffusion plots of sorbed Sr^{2+} on clinoptilolite at 25°C and 60°C

Similar behaviors were also observed for the sorption data corresponding to other initial concentrations of 100, 50, and 10 mg/L as shown in Appendix C.

This suggests that the pore diffusion affects the initial uptake steps of Cs^+ and Sr^{2+} by clinoptilolite, but it is not the rate determining step. It is reported that intraparticle diffusion can be considered as the rate determining step if a straight line that passes through the origin is obtained upon plotting $[\text{C}]_s$ versus $t^{1/2}$ (Özcan, A.S. and Özcan, A. 2004 p.5). The linear portions in Figures 4.17 and 4.18 yielded k_p values of 1.96 and 2.46 $\text{g}/\mu\text{mol}\cdot\text{min}$ for Cs^+ sorption on clinoptilolite at 25°C and 60°C, respectively. In the case of Sr^{2+} sorption on clinoptilolite, the k_p values were 1.54 and 3.79 $\text{g}/\mu\text{mol}\cdot\text{min}$ for at 25°C and 60°C, respectively. In both cases, the linear correlation coefficients were close to unity indicating the applicability of intraparticle diffusion model. Based on these results it might be concluded that although intraparticle diffusion is important, the film diffusion contributes also to the barriers standing against sorption of both cations on clinoptilolite.

It is important to note that, although the existence of intraparticle diffusion that limits the accessibility of Cs^+ and Sr^{2+} ions to the internal sites of clinoptilolite and as a result could make the uptake of clinoptilolite slower than that of kaolinite, the presence of those internal sites in clinoptilolite is believed, at the same time, to be responsible for the higher sorption capacity of this mineral due to the large surface area they provide. This can be validated from the higher uptake on clinoptilolite relative to that on kaolinite as demonstrated by the values of $[\text{C}]_e$ presented in Table 4.3.

4.3 Sorption Isotherm Models

Sorption isotherms are mathematical models that describe the distribution of the sorbate specie among liquid and solid phases, based on a set of assumptions that are related to the heterogeneity/homogeneity of the solid surface, the type of coverage, and the possibility of interaction between the sorbate specie.

The sorption data of Cs^+ and Sr^{2+} ions were examined using three types of the most widely used isotherms; Langmuir isotherm model, Freundlich isotherm model, and Dubinin-Radushkevich isotherm model. The description of these models was given earlier in Chapter 3, section 3-2.

The results indicated that our sorption data of Cs^+ and Sr^{2+} on kaolinite and clinoptilolite are well described by Freundlich and Dubinin-Radushkevich (D-R) isotherm models. Both models are adequate to explain the sorption on heterogeneous

surfaces, and allows for any plausible interactions between the sorbed specie, but while Freundlich isotherm does not predict any sorption capacity, i.e., no limitation on the extent of multiplayer sorption, D-R isotherm predicts a maximum sorption capacity for the fixed sorbates. Alternatively, Langmuir isotherm model did not yield a linear behavior of the sorption data of both Sr²⁺ and Cs⁺ on both kaolinite and clinoptilolite. Hence, this model is inadequate for describing the sorption data, as it assumes the sorption sites to be entirely homogeneous, with no interaction between the sorbate entities that can reach a maximum of single monolayer coverage. Langmuir isotherm plots are given in Appendix D and linear correlation coefficients are shown in Table 4.4.

Table 4.4. The linear correlation coefficients (R-values) obtained from Langmuir isotherm plots

Sample	Temperature (°C)	R values
Cs-loaded clinoptilolite	25	0.84128
	60	0.56237
Cs-loaded kaolinite	25	0.16971
	60	0.63418
Sr-loaded clinoptilolite	25	0.49363
	60	0.52841
Sr-loaded kaolinite	25	0.51332
	60	0.213

4.3.1 Freundlich Isotherm Model

Freundlich Isotherm in its linear form is given by the equation:

$$\log [C]_s = \log k + n \log [C]_l \quad (3-13)$$

The Isotherm parameters obtained by fitting the data of sorption are described by assuming that the elemental concentrations in solid and liquid are in equilibrium at the end of the experiment (48 hours). The magnitude of the Freundlich parameter k gives quantitative information on the relative sorption affinity towards the sorbed cation and the magnitude of constant n provides information about linearity of sorption. Nonlinear behavior of sorption indicates that the sorption energy barrier increases exponentially with increasing fraction of filled sites on the clay.

The linear fits of the sorption data of Cs⁺ and Sr²⁺ on kaolinite and clinoptilolite at 25°C and 60°C are given in Figures 4.19, 4.20, 4.21, and 4.22. The values of the Freundlich constants obtained from these plots are provided in Table 4.5.

Table 4.5. Freundlich parameters, n and k, obtained from the plots of Cs⁺ and Sr²⁺ uptake by kaolinite and clinoptilolite at 25°C and 60°C

Sample	Temperature (°C)	Freundlich Constants		
		n	k	R
Cs-kaolinite	25	0.99	45	0.9877
	60	0.87	15	0.9964
Sr-kaolinite	25	0.58	1	0.9594
	60	0.69	4	0.8877
Cs-clinoptilolite	25	0.87	402	0.9876
	60	0.96	702	0.9917
Sr-clinoptilolite	25	0.53	4	0.9599
	60	0.60	10	0.9836

According to the n values in Table 4.5, the deviation from linear sorption is higher in the case of Sr²⁺ uptake by both of kaolinite and clinoptilolite. The magnitude of k values indicate that both minerals favors the sorption of Cs⁺ over that of Sr²⁺. Moreover, clinoptilolite is seen to possess higher sorption affinity towards Cs⁺ or Sr²⁺ compared with kaolinite.

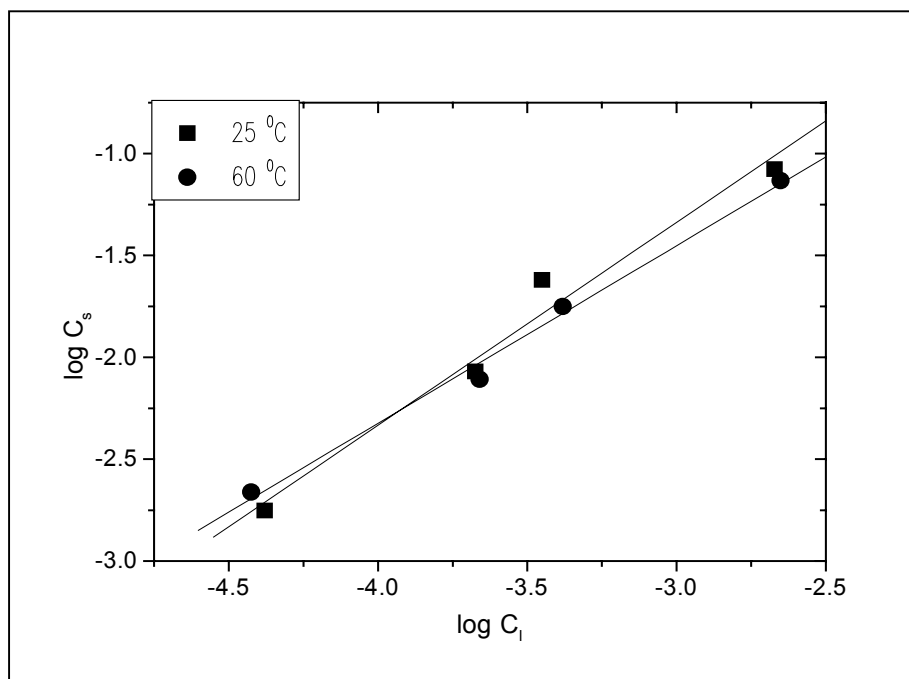


Figure 4.19. Freundlich isotherm model plots of Cs^+ sorbed by kaolinite at 25°C and 60°C

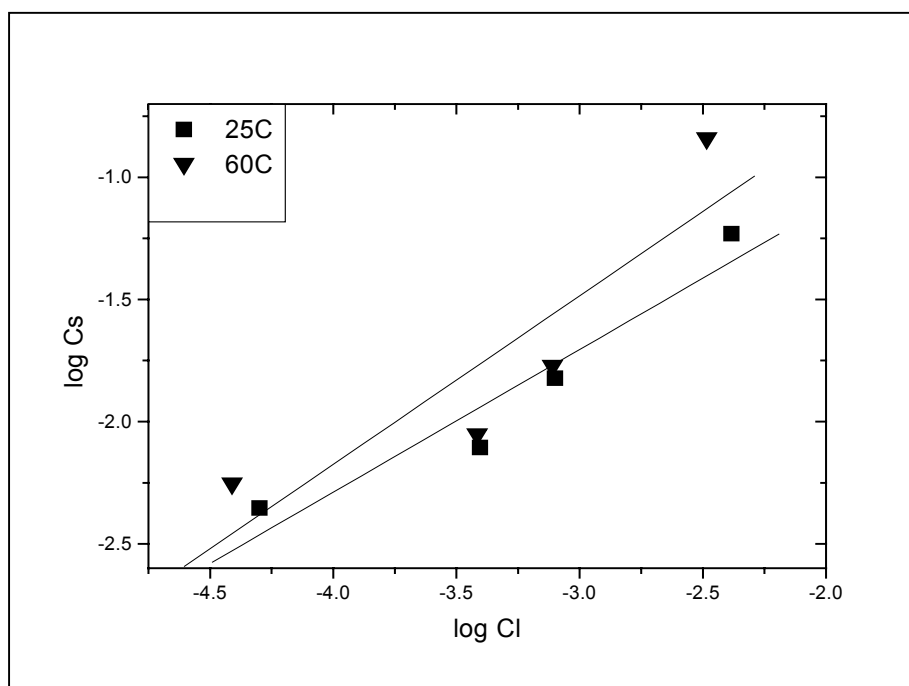


Figure 4.20. Freundlich isotherm model plots of Sr^{2+} sorbed by kaolinite at 25°C and 60°C

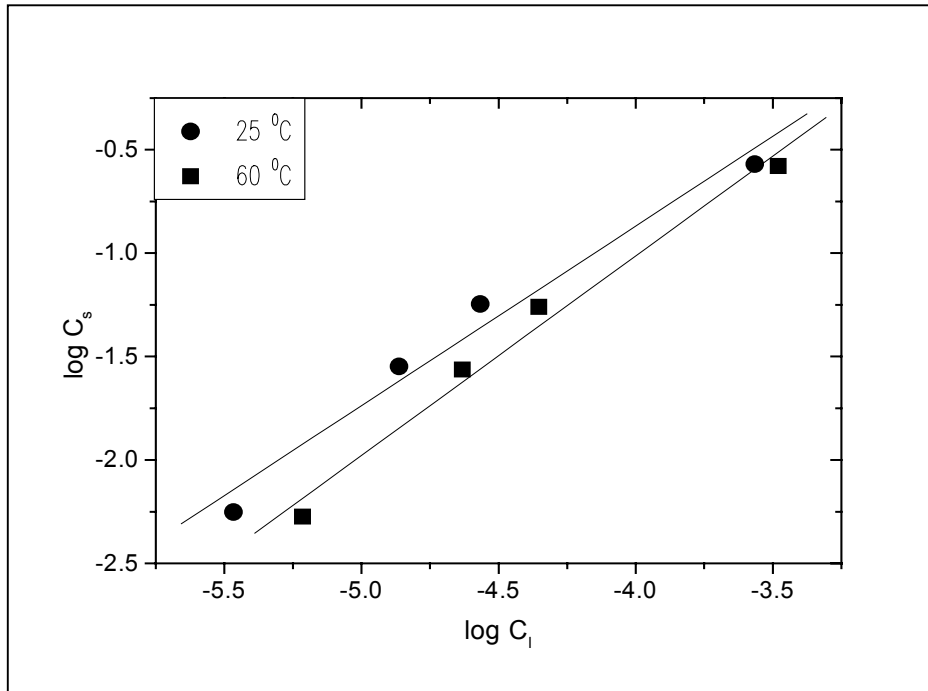


Figure 4.21. Freundlich isotherm plots of Cs^+ sorbed by clinoptilolite at 25°C and 60°C

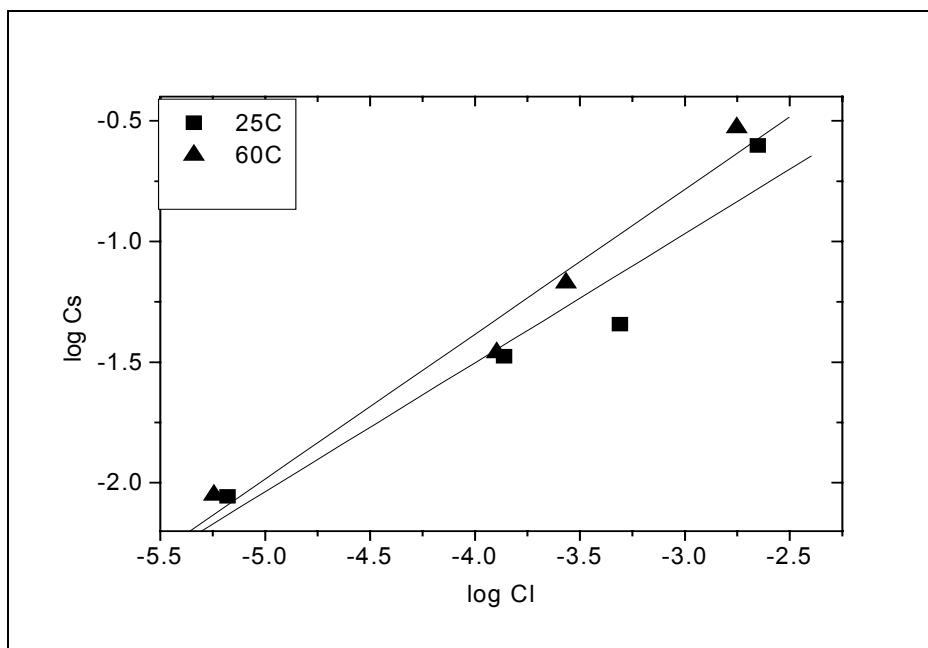


Figure 4.22. Freundlich isotherm plots of Sr^{2+} sorbed by clinoptilolite at 25°C and 60°C

4.3.2 D-R Isotherm Model

The linearized D-R isotherm model is described by the equation:

$$\ln [C]_s = \ln C_m - K\varepsilon^2 \quad (3-15)$$

The magnitude of D-R parameter C_m indicates the sorption capacity and K gives information about sorption energy E . The values of C_m and K are evaluated from the intercepts and slopes of plot of $\ln C_s$ vs. ε^2 . The D-R plots corresponding to sorption of Cs^+ and Sr^{2+} on kaolinite and clinoptilolite for the contact time of 48 hours and temperatures of 25°C and 60°C are given in Figures. 4.23, 4.24, 4.25, and 4.26. The values of D-R constants are also presented in Table 4.6.

Table 4.6. D-R parameters, K , C_m , and E , obtained from the plots of Cs^+ and Sr^{2+} uptake by kaolinite and clinoptilolite at 25°C and 60°C

Sample	Temperature (°C)	D-R Constants			R
		K	C_m (meq/100g)	E (kJ/mol)	
Cs-kaolinite	25	0.0100	0.90	7.1	0.9915
	60	0.0069	0.45	8.5	0.9891
Sr-kaolinite	25	0.0059	0,12	9.17	0.9289
	60	0.0053	0,24	9.71	0.8429
Cs-clinoptilolite	25	0.0069	5.27	8.5	0.9960
	60	0.0064	6.57	8.9	0.9980
Sr-clinoptilolite	25	0,0046	0.40	10.42	0.9337
	60	0.0041	0.68	10,99	0.9615

According to the D-R isotherm parameters K , C_m and E in Table 4.6 the sorption capacity of clinoptilolite is bigger than that of kaolinite. The C_m values confirm the prediction of Freundlich isotherm that both minerals are more effective in the removal of Cs^+ compared to Sr^{2+} . The magnitude of the mean sorption energy (E) is useful for estimating the type of sorption reaction taking place. In our study we have found E values for both Sr^{2+} and Cs^+ sorption on kaolinite and clinoptilolite to be within

the range of 8-16 kJ/mol, reported to correspond to ion-exchange reactions (Abusafa and Yücel 2002 p.111, Atun et al. 1996 p.438, Mishra and Tiwary 1999 p.362).

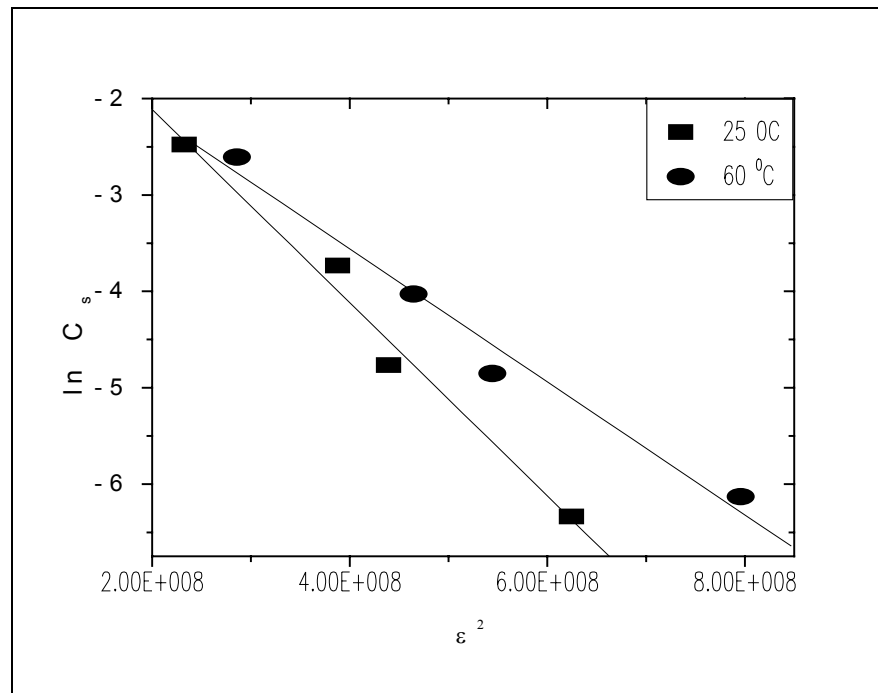


Figure 4.23. D-R isotherm plots of Cs^+ sorbed by kaolinite at 25°C and 60°C

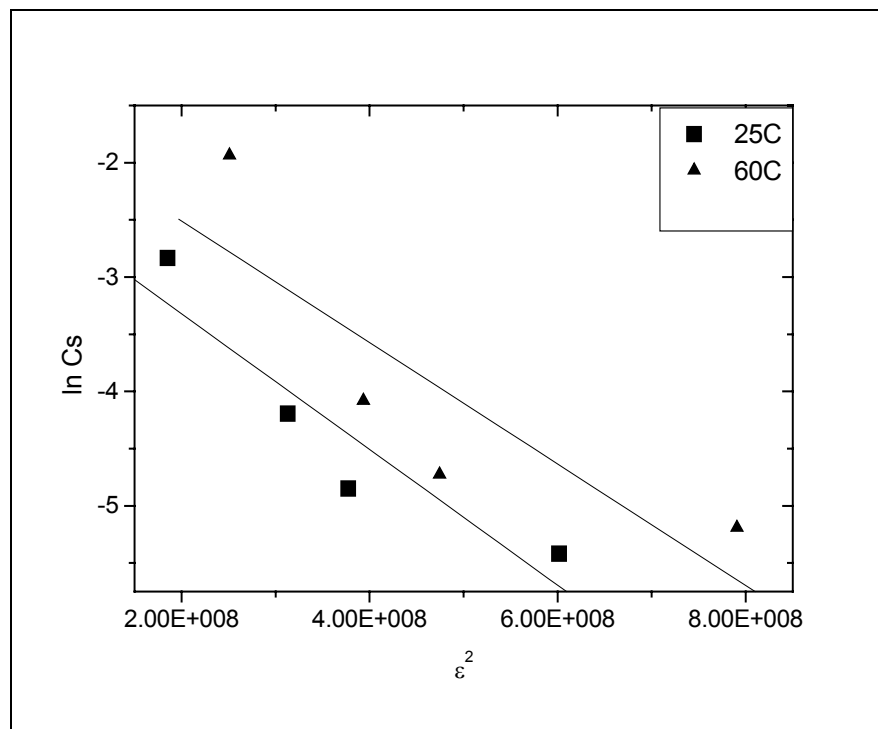


Figure 4.24. D-R isotherm plots of Sr^{2+} sorbed by kaolinite at 25°C and 60°C

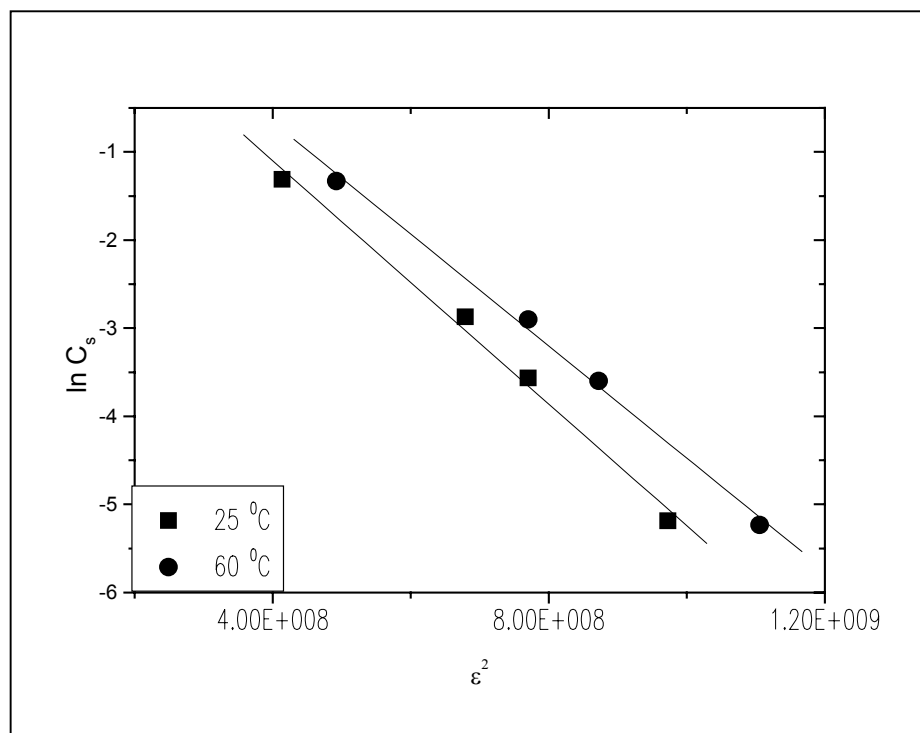


Figure 4.25. D-R isotherm plots of Cs^+ sorbed by clinoptilolite at 25°C and 60°C

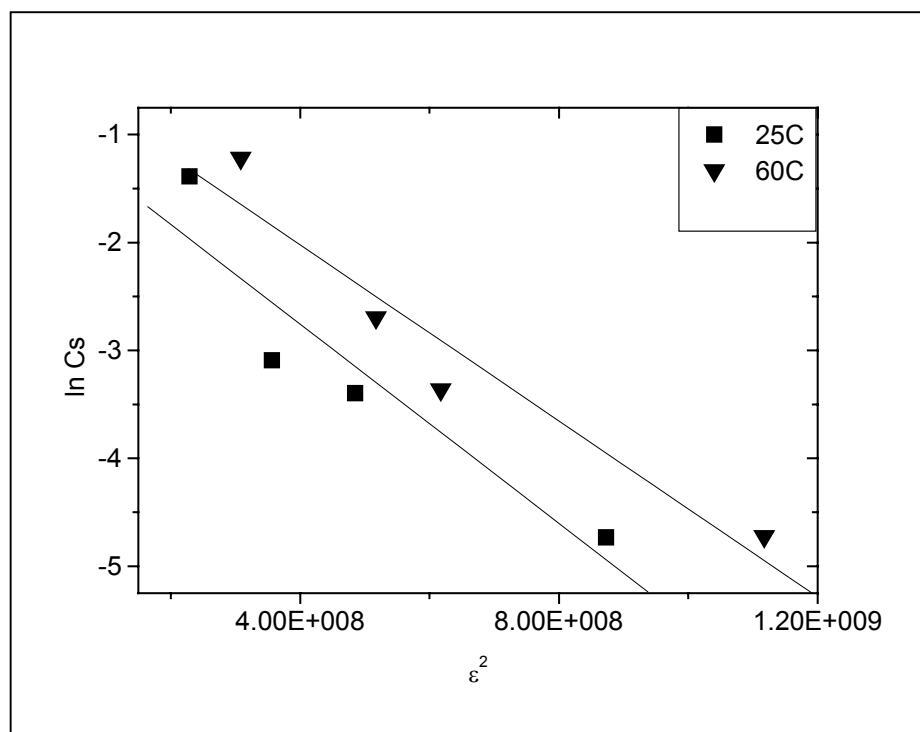


Figure 4.26. D-R isotherm plots of Sr^{2+} sorbed by clinoptilolite at 25°C and 60°C

4.4 Determination of Thermodynamic Parameters

The thermodynamic parameters, ΔH^0 , ΔS^0 , and ΔG^0 of sorption are useful in defining whether the sorption reaction is endothermic or exothermic, comment on the stability of the system undergoing sorption, and the spontaneity of the sorption process. As was outlined in Chapter 3, these parameters can be calculated using the following equations:

$$\Delta G^0 = -RT \ln R_d \quad (3-20)$$

$$\Delta G^0 = \Delta H^0 - T \Delta S^0 \quad (3-21)$$

$$\Delta H^0 = R \ln \frac{R_d(T_2)}{R_d(T_1)} \left(\frac{1}{T_1} - \frac{1}{T_2} \right)^{-1} \quad (3-22)$$

The distribution ratio, R_d (mL/g), in the above equation is an empirical equilibrium constant that is valid at particular initial concentration and reaction conditions. The R_d value, which refer to the ratio of the equilibrium concentration of the sorbate on the solid to its concentration in the liquid are given in Tables 4.7 and 4.8 for the sorption of Cs^+ on kaolinite and clinoptilolite and that of Sr^{2+} on the two minerals, respectively. These values were calculated from the data corresponding to all studied concentrations at temperatures of 25°C and 60°C at and a mixing period of 48 hours.

Table 4.7. The R_d values (mL/g) corresponding to Cs^+ sorption on kaolinite and clinoptilolite

[C] _o of CsCl (mg/L)	Cs-loaded Kaolinite		Cs-loaded Clinoptilolite	
	25 °C	60°C	25 °C	60°C
500	40	33	992	797
100	68	43	2091	1238
50	40	36	2069	1173
10	43	58	1639	875

Table 4.8. The Rd values (mL/g) corresponding to Sr²⁺ sorption on kaolinite and clinoptilolite

[C] ₀ of Sr(NO ₃) ₂ (mg/L)	Sr-loaded Kaolinite		Sr-loaded Clinoptilolite	
	25 °C	60°C	25 °C	60°C
500	14	44	112	168
100	19	22	93	249
50	20	23	243	273
10	88	144	1328	1556

Based on the values provided above for the distribution ratios and utilizing equations 3-20, 3-21, and 3-22, the standard enthalpy change, ΔH^0 , standard entropy change, ΔS^0 , and standard Gibbs energy of sorption, ΔG^0 were calculated. The values of ΔH^0 , ΔS^0 , and ΔG^0 obtained for Cs⁺ and Sr²⁺ uptake on kaolinite and clinoptilolite are summarized in Table 4.9.

Table 4.9. Values of ΔH^0 , ΔS^0 , and ΔG^0 calculated from the sorption data of Cs⁺ and Sr²⁺ on kaolinite and clinoptilolite

Sample	ΔH^0 (kJ/mol)	ΔS^0 (J/mol.K)	ΔG^0 (kJ/mol)	
			298 K	333 K
Cs-kaolinite	-6.3	11.4	-9.5	-10.3
Sr-kaolinite	11.3	63.5	-8.1	-9.3
Cs-clinoptilolite	-11.4	23.2	-18.3	-19.1
Sr-clinoptilolite	9.8	78.5	-13.6	-16.3

It is obvious from Table 4.9 that all the sorption cases involve negative standard Gibbs energy changes. The negative ΔG^0 values in both kaolinite and clinoptilolite indicate that the sorption of Cs⁺ and Sr²⁺ is spontaneous. The magnitudes of ΔG^0 are within the 8-16 kJ/mol range which is reported to stand for ion-exchange type of sorption mechanisms.

The standard enthalpy changes of the uptake of Cs^+ on both of kaolinite and clinoptilolite are negative. An exothermic behavior means that lower sorption temperatures are favored. The reason for this behavior could originate from thermal destabilization which cause an increase in the mobility of Cs^+ on the surface of the solid with increasing temperature, thus enhancing the desorption steps. The parallel increase in the mobility of Cs^+ ions in the solution body, which makes a positive contribution to sorption, is expected to be insignificant, since the ion already has a high mobility stemming from the weak hydration forces of water molecules ($\Delta H_{\text{hyd}}^0(\text{Cs}^+) = -276$ kJ/mol) caused by the low charge density (charge/size) of Cs^+ ions. The exothermic behavior of Cs^+ sorption on other types of sorbents was also reported by other authors (Shahwan and Erten 2002 p.119)

Interestingly, positive ΔH^0 values were obtained for Sr^{2+} sorption on kaolinite and clinoptilolite indicating that the uptake processes are endothermic. Metal ions with high hydration energies are well solvated in water. For these cations to be able to travel through solution and reach the sorption sites, it is necessary for them first to be stripped out of their hydration shell, a process known as dehydration process and requires energy. If the dehydration energy exceeds the exothermicity associated with the sorption of a metal ion on a solid surface, then the overall energy balance will lead to an endothermic behavior. After sorption it is assumed that the environment of the metal ions is less aqueous than it was in the solution state. In the case of Sr^{2+} , the hydration energy is -1443 kJ/mol, a value which is larger than the one mentioned above for Cs^+ , thus the mobility of Sr^{2+} is more hindered compared to that of Cs^+ , and increasing this mobility will require enhancing the dehydration steps, the thing achieved by increasing the temperature. The endothermic behavior of the sorption of a number of cations on various solids was also reported in a number of studies (Saeed and Ahmed.2004 p.294, Shahwan 2000 p.97, 98, Ishfaq et al. 1997 p.178, Mishra and Tiwari 2002 p.424).

In all cases, positive standard entropy changes are observed, as seen from Table 4.8. These values correspond to entropy changes in the system (adsorption medium), and a positive value indicates that more mobility is generated with in the system as a result of the sorption process. Normally, one might expect that the entropy change of the system be negative as a result of a sorption reaction, since such reaction leads to transferring the sorbate ions from a disordered state in the solution to a more ordered state when fixed by the sorbent. However, two other factors could outweigh this decrease in the disorder. One of them could probably be referred to the dehydration

steps that would increase the mobility of the ions and that of the surrounding water molecules within the body of the solution. Another reason might stem from the larger number of species leaving the sorbent when a sorbate is exchanged for them, in particular if the charge of that sorbate exceeds those of the ones depleted out of the sorbent matrix, e.g. two monovalent ions exchanged for one divalent ion. Both of the above factors are more significant in the case of Sr^{2+} than in the case of Cs^+ , the thing reflected in higher ΔS^0 values accompanying the sorption of the former. Similar observations were reported for other ions on different sorbents (Özcan A.S. and Özcan A. 2004 p.7, Saeed and Ahmed 2004 p.293, 294, Mishra and Tiwary 1999 p.362, 363, Shahwan and Erten 2002 p.119, 120, Ishfaq et al. 1997 p.178).

4.5 Desorption Studies

In order to check the sorption stability of Cs^+ and Sr^{2+} ions fixed by kaolinite and clinoptilolite, desorption experiments were performed. 0.1 g of solid samples prepared initially by sorption experiments with initial concentrations of CsCl and $\text{Sr}(\text{NO}_3)_2$ of 10 mg/L and 50 mg/L, were contacted with 10 mL tap water and shaken for periods ranging from 10 minutes up to 7 days at controlled temperatures of 25°C and 60°C. At the end of shaking period, the desorption percentage of Cs^+ from clinoptilolite did not exceed 7%, while it amounted to more than 30% in the case of kaolinite, indicating a more stable fixation by clinoptilolite.

Table 4.10. The percentage desorption values for Cs^+ sorption on both kaolinite and clinoptilolite

Sample	T (°C)	10 min.	4 hours	24 hours	168 hours
50 mg/L Cs-clinoptilolite	25	9.7	5.3	5.6	5.4
	60	6.5	6.3	6.0	3.4
10 mg/L Cs-clinoptilolite	25	5.8	6.0	6.5	5.4
	60	6.6	7.5	7.3	6.6
50 mg/L Cs-kaolinite	25	32.2	32.2	27.9	39.8
	60	34.2	37.6	35.7	37.1
10 mg/L Cs-kaolinite	25	20.4	35.3	29.3	41.6
	60	28.3	27.3	30.1	29.7

The results indicated that the percentage desorption of Sr²⁺ in the case of clinoptilolite did not exceed 8%, while it amounted to more than 10% in the case of kaolinite. In light of these findings, the sorption of Sr²⁺ on kaolinite seems to be more stable than that of Cs⁺. In both Cs⁺ and Sr²⁺ desorption, clinoptilolite indicates a more stable fixation compared with kaolinite.

Table 4.11. The percentage desorption values for Sr²⁺ sorption on both kaolinite and clinoptilolite

Sample	T (°C)	10 min.	4 hours	24 hours	168 hours
50 mg/L Sr-clinoptilolite	25	0.2	0.7	1.1	1.4
	60	1.6	2.0	2.0	1.3
10 mg/L Sr-clinoptilolite	25	6.2	5.2	3.6	3.1
	60	7.7	7.5	5.7	5.7
50 mg/L Sr-kaolinite	25	1.7	2.9	6.1	8.7
	60	0.4	0.5	4.8	5.2
10 mg/L Sr-kaolinite	25	8.2	6.2	8.8	10.3
	60	13.9	13.1	11.9	11.5

4.6 Surface Characterization

4.6.1 Characterization of Cs- and Sr-Loaded Kaolinite

Kaolinite samples loaded with Cs⁺ and Sr²⁺ ions were characterized using XRPD, SEM/EDS, and FTIR. The characterization was performed for the samples prepared by reacting 50 mL aliquots of 500 mg/L solutions of CsCl and Sr(NO₃)₂ with 0.50 g of kaolinite or clinoptilolite for 48 hours at 25°C.

SEM/EDS analysis was performed to detect any morphological changes and to elucidate the distribution of the two ions on the surface of kaolinite. The results of the SEM analysis no observable change in the morphology of kaolinite particles upon sorption.

The EDS characterization was performed in two modes; one as spot analysis of a total of eleven points selected randomly on the surface, and the other by recording electronic maps of elements that constitutes the surface of kaolinite. The results of the spot analysis are provided in Tables 4.12 and 4.13 for Cs- and Sr-loaded kaolinite, respectively. The electron maps of Cs⁺ and Sr²⁺ are also compared with those of Al and Si, the major structural elements in kaolinite, as demonstrated in Figures 4.27, 4.28.

As seen from the figure, the signals of Al coincide with those of Si as both elements are skeletal entities in the same layers constructing the matrix of kaolinite and as such they are associated with each other. The signals of Cs and Sr on kaolinite seem to have some localization. In order to reveal the extent of any localization, EDS spot analysis was performed. The EDS findings (see Tables 4.12 and 4.13) indicate higher variation in the Cs signals compared to those of Sr. This can be figured out from the higher relative standard deviation which amounts to %50 in the case of Cs, compared with %28 in the case of Sr. It must be noted that EDS analysis correspond to about 2 μm depth across the surface of the mineral and that the percentage error might exceed %50 for elements whose atomic percentage is less than 5.

The EDS results proved the existence of elements like Na, K, Mg, and Ca which are usually not contained within kaolinite. The source of such elements is probably of non kaolinitic origin, and could be originating from minor quantities of a smectitic clay, the presence of which, as a distinct phase, is hard to detect using XRPD, as the detection limit of this technique is usually above 5 percent.

Table 4.12. EDS findings of the atomic percentages of O, Si, Al, Ca, Mg, Na, K, and Cs in Cs-loaded kaolinite

Atomic Percentages in Cs-Loaded Kaolinite									
Spot No	O	Na	Mg	Al	Si	K	Ca	Cs	Others
1	63.14	0.81	0.5	14.13	16.23	0.18	0.59	0.23	3.82
2	63.9	0.65	0.5	13.11	16.82	0.08	0.24	0.13	4.25
3	66.61	0.59	0.39	13.35	13.81	0	0.14	0	4.94
4	66.02	0.7	0.42	12.98	13.94	0.05	0.17	0.05	5.55
5	63.2	0.64	0.46	13.02	16.05	0.16	0.3	0.13	5.8
6	65.79	0.79	0.53	12.89	13.85	0.05	0.57	0.07	5.21
7	65.72	0.67	0.47	11.57	16.22	0.12	0.3	0.17	4.55
8	64.98	0.53	0.42	14.24	14.59	0	0.1	0.14	5.01
9	64.11	0.6	0.54	14.86	14.29	0.14	0.17	0.17	4.88
10	64.66	0.72	0.36	13.94	14.27	0.14	0.91	0.14	4.55
11	65.53	0.86	0.43	13.48	13.55	0.08	0.09	0.12	5.7
Mean	64.88	0.69	0.46	13.42	14.87	0.09	0.33	0.12	4.93
St. Dev.	1.17	0.10	0.06	0.88	1.20	0.06	0.26	0.06	0.62

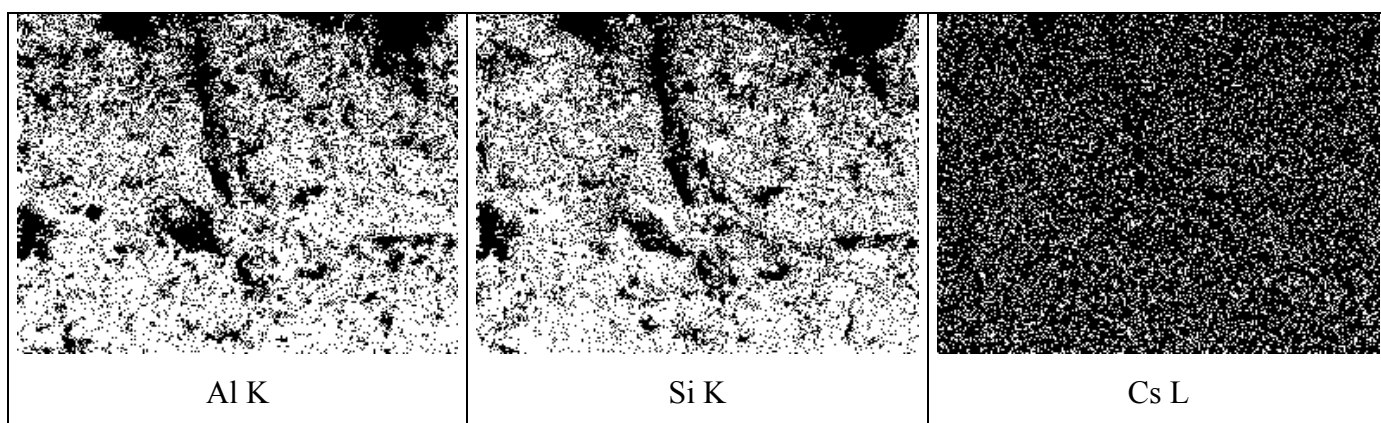


Figure 4.27. EDS mapping images showing the distribution of elements Al, Si, and Cs on the surface of Cs-loaded kaolinite

Table 4.13. EDS findings of the atomic percentages of O, Si, Al, Ca, Mg, Na, K, and Sr in Sr loaded kaolinite

Atomic Percentages in Sr-Loaded Kaolinite									
Spot No	O	Na	Mg	Al	Si	Ca	K	Sr	Others
1	62.27	0.42	0.28	14.29	16.39	0.7	0.12	0.88	4.26
2	58.3	0.31	0.26	9.91	24.73	0.52	0.19	1.43	4.36
3	64.24	0.46	0.37	13.3	14.94	1.02	0.03	1.25	4.39
4	65.61	0.58	0.41	11.65	14.31	0.63	0.24	0.78	5.78
5	66.6	0.47	0.3	12.52	13.86	0.46	0.09	1	4.71
6	66.5	0.44	0.3	9.66	17.42	0.12	0	1.13	4.43
7	67.73	0.62	0.36	11.02	15.03	0.37	0.12	0.63	4.11
8	67.38	0.62	0.36	12.66	12.71	0.26	0.09	0.57	5.34
9	66.01	0.5	0.33	12.78	13.97	0.42	0.15	0.85	4.99
10	67.02	0.57	0.38	11.78	14.1	0.21	0.14	0.87	4.95
11	64.22	0.27	0.26	8.43	20.31	0.18	0.19	0.72	5.42
Mean	65.08	0.48	0.33	11.64	16.16	0.44	0.12	0.92	4.79
St. Dev.	2.77	0.12	0.05	1.75	3.53	0.27	0.07	0.26	0.54

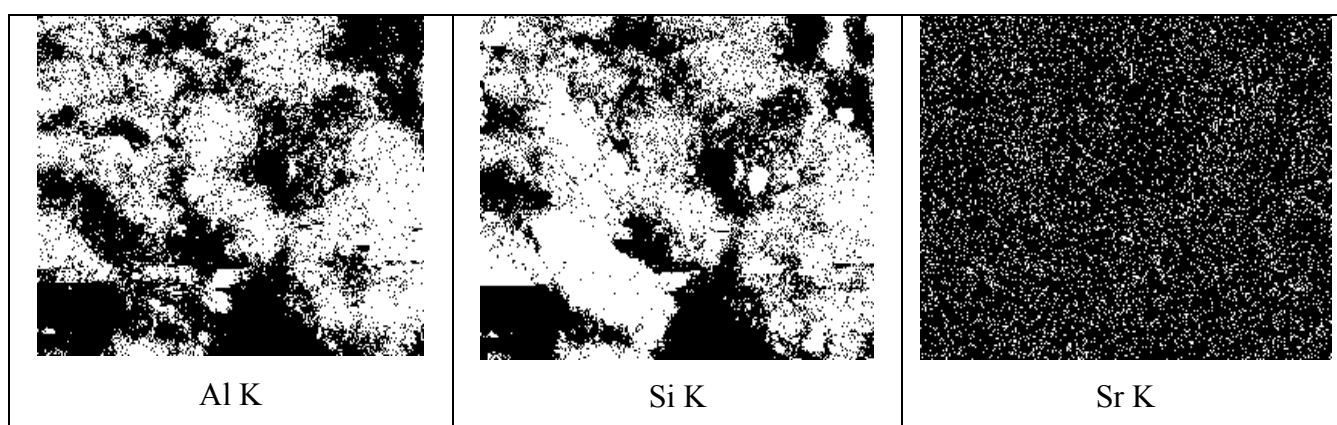


Figure 4.28. EDS mapping images showing the distribution of elements Al, Si, and Sr on the surface of Sr-loaded kaolinite

XRPD was used to reveal any plausible changes in kaolinite structure upon sorption of Cs^+ and Sr^{2+} ions. The patterns indicated no significant change in the peak positions, peak intensities, or FWHM of the peaks corresponding to kaolinite basic reflections. This was also supported by the FTIR spectra, which revealed that no detectable change existed in the vibrational bands of kaolinite as a result of loading with Cs^+ and Sr^{2+} ions. This result is expected as the sorption sites are situated on the surface and edge parts of the matrix of this clay type. As stated previously, kaolinite interlayer space is inaccessible to sorption due to the strong H-bonds that act against any expansion of the interlayer region, the thing necessary to allow for the diffusion of sorbate ions inside, like it is the case in the clay mineral known as montmorillonite.

In order to check the effect of interlayer expansion on the uptake capacity of kaolinite, the clay was intercalated with dimethylsulfoxide (DMSO) to increase the interlamellar space of kaolinite by breaking up the hydrogen bonds tightly interlinking the kaolinite lamellae. The DMSO-intercalated kaolinite samples were then exposed to Cs^+ and Sr^{2+} solution, and the amount of sorbed ions under these conditions was compared with those obtained earlier, when no DMSO intercalation of kaolinite is performed.

XRPD was used to follow the intercalation process of kaolinite by DMSO solution. Typical XRPD diagrams of kaolinite prior to and following treatment with DMSO are given in Fig. 4.29. According to these diagrams, upon intercalation, the characteristic 001 and 002 reflections of kaolinite changed from 0.71 and 0.35 nm to 1.12 and 0.37 nm, respectively, thus confirming the expansion of the interlayer space of the clay. Fig. 4.29 (c) shows that DMSO was readily removed from kaolinite structure upon exposure with Cs^+ ions. Similar observations were also seen in the case of exposure to Sr^{2+} ions. In the sorption experiments carried out with DMSO-intercalated kaolinite, the concentrations of CsCl and $\text{Sr}(\text{NO}_3)_2$ were 100 mg/L and 500 mg/L at temperatures of 25°C and 60°C for the contact time of 24 hours. Compared with the percentage sorption on natural kaolinite, the percentage sorption of Cs^+ on DMSO-intercalated kaolinite for initial concentrations of 100 mg/L and 500 mg/L CsCl , increased, respectively, from 35 to 41, and from 27 to 33. On the other hand, the percentage sorption of Sr^{2+} on DMSO-intercalated kaolinite for the initial concentrations of 100 and 500 mg/L of $\text{Sr}(\text{NO}_3)_2$, increased from 17 to 58, and from 22 to 45, respectively. These results show that the interlayer space of kaolinite is better accessible to Sr^{2+} ions, as revealed by the higher increase in the percentage sorption

upon expansion using DMSO molecules. Alternatively, such an expansion in the interlayer space of kaolinite did not yield a significant increase in the sorption capacity of the clay towards Cs^+ , indicating that the surface and edge sites of the clay are more favored for this ion.

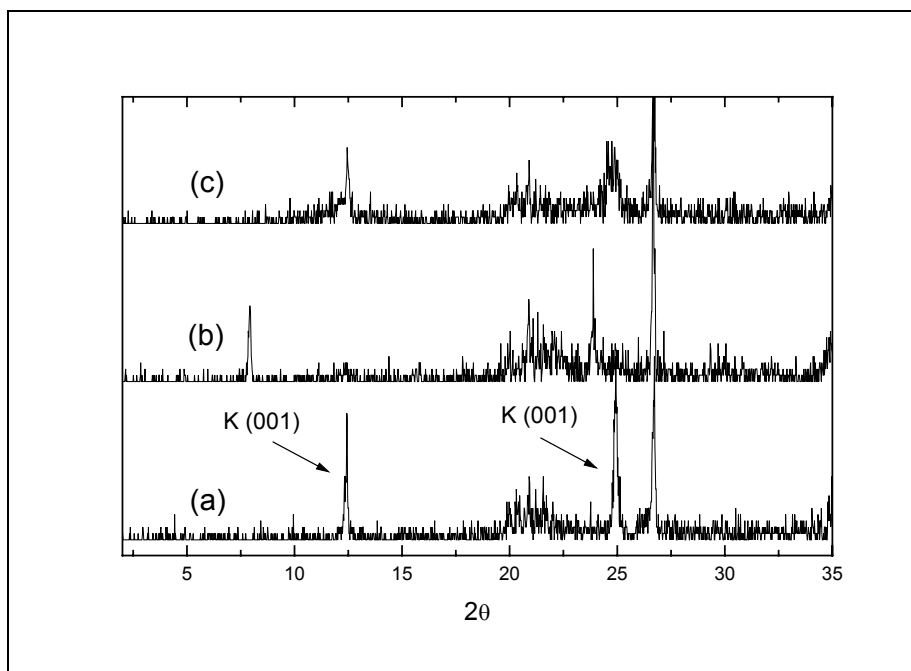


Figure 4.29. XRPD diagrams of: (a) natural kaolinite, (b) DMSO-treated kaolinite, (c) DMSO-intercalated kaolinite after loading with Cs^+ ions

4.6.2 Characterization of Cs- and Sr-Loaded Clinoptilolite

Like in the case of kaolinite, the samples of Cs- and Sr-loaded clinoptilolite were characterized using XRPD, FTIR, and SEM/EDS techniques. The XRPD and FTIR characterization revealed no detectable changes in the structure of the mineral as a result of loading with both cations. Clinoptilolite, is a mineral that is reported to withstand chemical changes, unless the pH is lowered to 1 unit or lower. Thus sorption of Cs⁺ and Sr²⁺, which was carried out around neutral pH conditions is not expected to cause significant structural changes in the matrix of this mineral. SEM micrographs revealed also no change in the particle morphology of loaded clinoptilolite.

The elemental compositions of Cs- and Sr-loaded clinoptilolite, obtained using EDS, are provided in Tables 4.12 and 4.13, respectively. Furthermore, the EDS mapping results for the same samples are shown in Figures 4.30 and 4.31.

Table 4.14. EDS findings of the atomic percentages of Al, Si, O, Na, K, Mg, Ca, and Cs in Cs-loaded clinoptilolite

% Atomic Composition of Cs-Loaded Clinoptilolite									
Spot No	O	Na	Mg	Al	Si	K	Ca	Cs	Others
1	61.24	0.7	0.9	5.32	23.59	1.24	0.84	0.65	4.77
2	61.88	0.62	0.81	5.11	22.75	1.21	1.09	0.77	5.13
3	60.44	0.75	0.95	5.05	23.94	1.16	0.85	0.68	5.47
4	61.2	0.89	0.92	5.34	23.35	1.33	0.89	0.79	4.63
5	61.73	0.6	1.09	5.14	22.86	1.36	1.13	0.76	4.76
6	60.81	0.81	0.99	5.17	22.92	1.31	0.86	0.77	5.67
7	61.16	0.84	1.19	5.35	23.6	1.2	0.95	0.7	4.4
8	60.75	0.69	1.05	5.5	23.71	1.5	1.18	0.91	4.01
9	60.75	0.75	1.14	5.68	23.53	1.41	0.92	0.95	4.11
10	62.42	0.94	0.98	5.29	21.75	1.16	1.43	0.69	4.8
11	60.95	0.76	0.98	5.29	22.54	1.41	1.03	0.76	5.64
Mean	61.21	0.76	1.00	5.29	23.14	1.30	1.02	0.77	4.85
St. Dev.	0.59	0.11	0.11	0.18	0.64	0.11	0.18	0.09	0.57

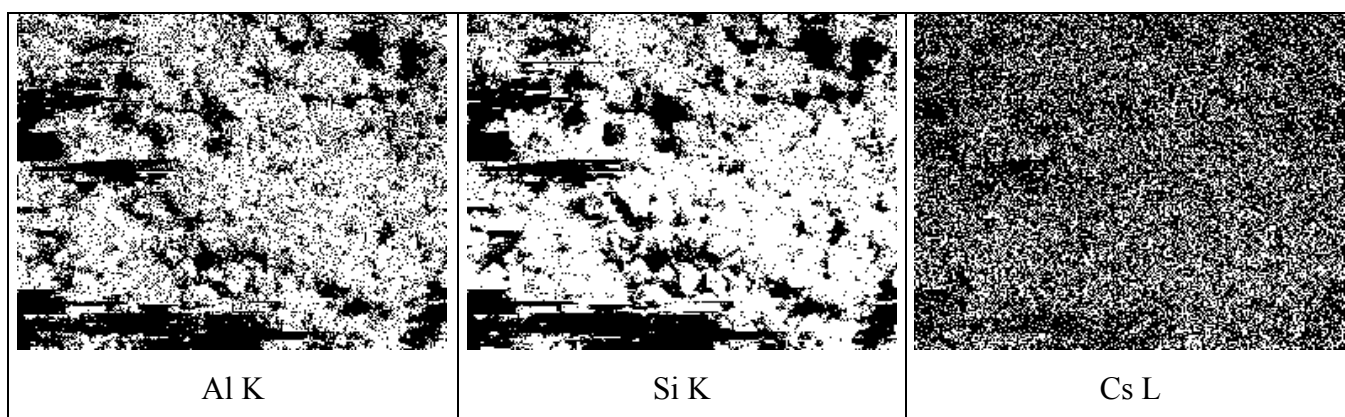


Figure 4.30. EDS mapping images showing the distribution of elements Al, Si, and Cs on the surface of Cs-loaded clinoptilolite

Table 4.15. EDS findings of the atomic percentages of Al, Si, O, Na, K, Mg, Ca, and Sr in Sr loaded clinoptilolite

% Atomic Composition of Sr-Loaded Clinoptilolite									
Spot No	O	Na	Mg	Al	Si	Ca	K	Sr	Others
1	65.34	0.8	0.75	5.03	19.87	0.67	0.97	1.16	5.03
2	61.56	0.61	0.9	5.16	22.41	0.85	1.32	1.78	4.87
3	60.84	0.5	0.82	5.19	23.38	0.95	1.44	1.4	4.57
4	60.68	0.81	1.16	5.26	22.17	0.79	1.43	1.31	5.57
5	63.23	0.91	0.74	4.79	21.26	0.89	1.03	1.46	5.22
6	62.59	0.55	0.89	5.06	20.64	0.75	1.3	1.64	5.97
7	63	0.89	0.79	5.03	21.32	0.86	1.45	1.67	4.45
8	62.14	0.86	0.84	5.3	21.92	0.86	1.28	1.8	4.57
9	62.02	0.79	0.93	5.15	21.08	1.17	1.27	1.44	5.67
10	63.18	0.65	1.01	5	22.3	0.85	1.1	1.09	4.51
11	61.46	0.81	0.87	5.25	21.79	0.93	1.36	1.42	5.44
Mean	62.37	0.74	0.88	5.11	21.65	0.87	1.27	1.47	5.08
St. Dev.	1.32	0.14	0.12	0.15	0.96	0.13	0.17	0.23	0.53

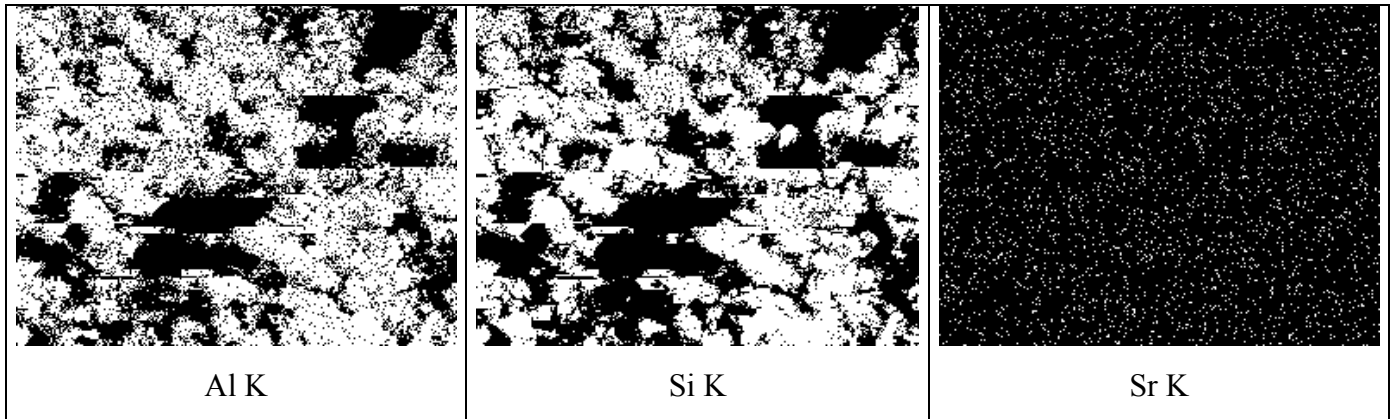


Figure 4.31. EDS mapping images showing the distribution of elements Al, Si, and Sr on the surface of Sr-loaded clinoptilolite

The higher uptake capacity of clinoptilolite is evident from the higher atomic percentage compared with kaolinite. The Cs and Sr signals, as well as those of Al and Si, are showing higher variation with location in the case of kaolinite, as can be seen from the higher values of S.D., the thing that might be referred to the higher heterogeneity of the natural kaolinite sample compared to clinoptilolite.

CHAPTER 5

CONCLUSIONS

Batch studies were performed to investigate kinetic, thermodynamic, and surface characterization of the sorption of Cs^+ and Sr^{2+} ions on natural minerals of kaolinite and clinoptilolite under different initial concentrations, times and temperatures. Based on the findings of these studies, the following main conclusions can be obtained:

1. Clinoptilolite have higher sorption capacity towards Sr^{2+} and Cs^+ ions compared with kaolinite. In addition, both of kaolinite and clinoptilolite are showing higher fixation ability of Cs^+ compared to Sr^{2+} , within the experimental conditions of this study.
2. The sorption data of both of Sr^{2+} and Cs^+ on kaolinite and clinoptilolite did not obey the pseudo first order kinetics and did fit to the pseudo-second order kinetics. The calculated rate constants of sorption showed that sorption on kaolinite is faster and is marked by lower activation energies barriers for both cations.
3. Whereas the intraparticle diffusion seems to play no rule in the sorption of Sr^{2+} and Cs^+ on kaolinite, this type of diffusion seems to be important for clinoptilolite, in particular, at the initial stages of sorption. However, intraparticle diffusion is not the rate determining step, and hence film diffusion is expected to be effective.
4. Langmuir isotherm model did not correlate well with the sorption data. On the contrary, Freundlich and D-R isotherm models described the sorption data adequately, indicating that sorption is taking place on heterogeneous sites and that multiplayer sorption is possible.
5. While the uptake of Cs^+ on both minerals is exothermic, that of Sr^{2+} uptake is endothermic. This fact can be understood based on the energy of hydration. In all cases, positive standard entropy changes were obtained, suggesting that sorption leads to increasing the mobility of the involved specie. The values of

standard Gibbs free energy change indicated the spontaneity of the sorption processes, with energy values corresponding to electrostatic type of interactions.

6. Expanding the interlayer space of kaolinite using DMSO enhanced slightly the uptake of Cs^+ , suggesting that the surface and edge sides of kaolinite are more energetically favored for the uptake of this cation. More enhancement was, however, observed in the case of Sr^{2+} , the thing that must be further clarified on a mechanistic basis.
7. The percentage desorption of Cs^+ from clinoptilolite did not exceed 7% while it amounted to more than 30% in kaolinite, indicating a more stable fixation on clinoptilolite. The results indicated that in the case of desorption of Sr^{2+} from kaolinite ranged between 5-11 and in the case of clinoptilolite, ranged between 1-6, indicating a more stable fixation on clinoptilolite.
8. Surface characterization studies indicated that the morphologies of kaolinite and clinoptilolite seem to be not effected upon sorption. In addition, EDS analysis demonstrated the higher fixation ability of clinoptilolite and revealed some localization in the sorbed Sr^{2+} and Cs^+ on the surfaces of both minerals, with localization on kaolinite being larger, probably as a result of the heterogeneous nature of this natural clay.

REFERENCES

- Abusafa, A., Yücel, H. 2002. "Removal of ^{137}Cs from aqueous solutions using different cationic forms of a natural zeolite: clinoptilolite," *Separation and Purification Technology*. Vol. 28, pp. 103-107, 110-111.
- Armbruster, T. 2001. "Clinoptilolite-heulandite: applications and basic research," *Studies in Surface Science and Catalysis*. Vol. 135, pp. 13-15.
- Atun, G., Bilgin, B., Mardinli, A. 1996. "Sorption of cesium on montmorillonite and effects of salt concentration," *Journal of Radioanalytical and Nuclear Chemistry*. Vol. 211, pp. 435, 438, 440-442.
- Atun, G., Kilislioglu, A. 2003. "Adsorption behavior of cesium on montmorillonite-type clay in the presence of potassium ions," *Journal of Radioanalytical and Nuclear Chemistry*. Vol. 258, pp. 605-606, 609-610.
- Bagosi, S., Csetenyi, L. J. 1999. "Immobilization of caesium-loaded ion exchange resins in zeolite-cement blends," *Cement and Concrete Research*. Vol. 29, pp. 479-480.
- Cahn, R. W., Haesen, P., Kramer, E.J. 1994. "Silicate Ceramics" , in *Materials Science and Technology* edited by M.V. Swain (VCH, Germany), pp. 54-59.
- Chorover, J., Choi, S., Amistadi, M. K., Karthikeyan, K.G., Crosson, G., Mueller, K. T. 2003. "Linking cesium and strontium uptake to kaolinite weathering in simulated tank waste leachate," *Environmental Science & Technology*. Vol. 37, pp. 2200-2202.
- Christie, T., Brathwaite, B., Thompson, B. 2002. "Mineral commodity report 23-zeolites," *New Zealand Mining*. Vol. 31, p. 16.
- Cui, D., Eriksen, T. E. 1997. "On the sorption of Co and Cs on stripa granite fracture-filling material," *Radiochimica Acta*. Vol. 79, pp.31, 34.
- Erten, H. N., Aksoyoglu, S., Göktürk, H. 1988. "Sorption / desorption of Cs on clay and soil fractions from various regions of Turkey," *The Science of the Total Environment*. Vol. 69, pp. 272,273.

Formica, J., 1997 . “X-Ray Diffraction”, in *Handbook of Instrumental Techniques for Analytical Chemistry*, edited by Settle, F.A. (Prentice Hall PTR), pp. 340-343.

Goodman, B. A. 1986. “Adsorption of metal ions and complexes on aluminosilicate minerals,” *American Chemical Society*. Vol. 86, pp. 342-346.

Groenewold, G. S., Ingram, J. C., McLing, T., Gianotto, A. K. 1998. “Cs⁺ speciation on soil particles by TOF-SIMS imaging,” *Analytical Chemistry*. Vol. 70, pp. 534-535.

Grütter, A., Von gunten, H. R., Rössler, E. 1986. “Sorption, desorption, and isotope exchange of cesium (10^{-9} – 10^{-3} M) on chlorite,” *Clays and Clay Minerals*. Vol. 34, pp. 677, 678, 679.

Grütter, A., Von gunten, H. R., Kohler, M., Rössler, E. 1990. “Sorption, desorption and exchange of cesium on glaciofluvial deposits,” *Radiochimica Acta*. Vol. 50, pp. 177, 179, 182, 183.

Hakem, N., Fourest, B., Guillaumont, R., Marmier, N. 1996. “Sorption of iodine and cesium on some mineral oxide colloids,” *Radiochimica Acta*. Vol. 74, p.225.

Ho, Y. S., Mckay, G. 2000. “The kinetics of sorption of divalent metal ions onto sphagnum moss peat,” *Wat. Res.* Vol. 34, pp. 736-739.

Ishfaq, M. M., Karim, H. M. A., Khan, M. A. 1997. “A radiochemical study on the thermodynamics of cesium adsorption on potassium copper nickel hexacyanoferrate(II) from aqueous solutions,” *Journal of Radioanalytical and Nuclear Chemistry*. Vol. 222, pp. 178, 179, 180.

Ivanov, V. A., Timofeevskaja, V. D., Gavlina, O. T., Gorshkov, V. I. 2003. “Dual-temperature reagent-less ion-exchange separations of alkali metals salts on zeolites,” *Microporous and Mesoporous Materials*. Vol. 65, pp. 257-260, 262, 263.

Jedinakova, V. 1998. “Migration of radionuclides in the environment,” *Journal of Radioanalytical and Nuclear Chemistry*. Vol. 229, pp. 13-17.

Jinzhou, D., Wenming, D., Xiangke, W., Zuyi, T. 1996. “Sorption and desorption of radiostrontium on calcareous soil and its solid components,” *Journal of Radioanalytical and Nuclear Chemistry*. Vol. 203, p. 31.

Kannan, N., Sundaram, M. M. 2001. “Kinetics and mechanism of removal of methylene blue by adsorption on various carbons-a comparative study,” *Dyes and Pigments*. Vol. 51, pp. 27-34.

Karnland, O., Pusch, R. 1990. "Development of clay characterization methods for use in repository design with application to a natural Ca-bentonite clay containing a redox front," *SKB Technical Report*. Vol. 90, p. 11.

Kleven, R., Alstad, J. 1996. "Interaction of alkali, alkaline-earth and sulphate ions with clay minerals and sedimentary rocks," *Journal of Petroleum Science and Engineering*. Vol. 15, pp. 181-182, 185, 194.

Lawes, G., "SEM-Instrumentation", in *Scanning Electron Microscopy and X-Ray Microanalysis*, edited by A.M. James (John Wiley & Sons, London), pp. 1-20, 78-79.

Levine, I. N., 1988. "Reaction Kinetics and Surface Chemistry", in *Physical Chemistry*, Edited by Misler, K.S., Tenney, S. (McGraw Hill, third edition, Singapore), pp. 372, 373, 537, 538, 539, 540.

Lieser, K. H., Steinkopff, Th. 1989. "Sorption equilibria of radionuclides or trace elements in multicomponent systems," *Radiochimica Acta*. Vol. 47, p. 55.

Lim, C. H., Jackson, M. L., Koons, R. D., Helmke, P. A. 1980. "Kaolins : sources of differences in cation – exchange capacities and cesium retention," *Clays and Clay Minerals*. Vol. 28, pp. 223, 226.

Liu, D., Hsu, C., Chuang, C. 1995. "Ion-exchange and sorption kinetics of cesium and strontium in soils," *Appl. Radiat. Isot.* Vol. 46, pp. 839-843.

Likar, A., Omahen, G., Lipoglavsek, M., Vidmar, T. 2001. "A theoretical description of diffusion and migration of ¹³⁷ Cs in soil," *Journal of Environmental Radioactivity*. Vol. 57, pp. 191, 199.

Mishra, S. P., Tiwary, D. 1999. "Ion exchangers in radioactive waste management. Part XI. Removal of barium and strontium ions from aqueous solutions by hydrous ferric oxide," *Applied Radiation and Isotopes*. Vol. 51, pp. 359-363.

Mishra, S. P., Tiwari, D. 2002. "Inorganic ion exchangers in radioactive waste management. Part XII: Removal behavior of stannic and zirconium phosphates for strontium," *Journal of Radioanalytical and Nuclear Chemistry*. Vol. 253, p. 421.

Molva, M., "Removal of phenol from industrial wastewaters using lignitic coals" MSc. Thesis, Environmental Engineering, İzmir Institute of Technology, İzmir, 2004

O'Connor, D. J., Sexton, B.A. 1992. "Electron Microscope Techniques for Surface Characterization", in *Surface Analysis Methods in Materials Science*, edited by R.St. C. Smart (Springer, Berlin), pp. 13-15, 87-99.

Oscarson, D. W., Watson, R. L., Miller, H. G. 1987. "The interaction of trace levels of cesium with montmorillonitic and illitic clays," *Applied Clay Science*. Vol. 2, pp.29, 38.

Özcan, A.S.,Özcan, A. 2004. "Adsorption of acid dyes from aqueous solutions onto acid-activated bentonite," *Journal of Colloid and Interface Science.*, p. 5

Parkman, R. H., Charnock, J. M., Livens, F. R., Vaughan, D. J. 1998. "A study of the interaction of strontium ions in aqueous solution with the surfaces of calcite and kaolinite," *Geochimica et Cosmochimica Acta*. Vol. 62, pp. 1481-1485, 1490, 1491.

Patakfalvi, R., Oszko, A., Dekany, I. 2003. "Synthesis and characterization of silver nanoparticle / kaolinite composites," *Colloids and surfaces*. Vol. 220, pp. 45-48.

Poinssot, C., Baeyens, B., Bradbury, M. H. 1999. "Experimental and modelling studies of caesium sorption on illite," *Geochimica et Cosmochimica Acta*. Vol. 63, pp. 2, 3, 7, 8.

Polat, M., "A review of the theory of interactions between particles dispersed in aqueous media, I. The electrical double layer", İzmir Institute of Technology, İzmir

Rouquerol, F. 1999. *Adsorption by Powders and Porous Solids*, (Academic Press, London), pp. 1-21, 355-361, 378-382.

Russell, J.D., Fraser, A.R., 1994. "Infrared Methods" in *Clay Mineralogy: Spectroscopic and Chemical Determinative Methods*, edited by M.J. Wilson, (Chapman&Hall, London), pp. 18-21, 45-49.

Saeed, M.M., Ahmed, M. 2004. "Retention, kinetics and thermodynamics profile of cadmium adsorption from iodide medium onto polyurethane foam and its separation from zinc bulk," *Analytica Chimica Acta*. Vol. 525, pp.292, 294, 296.

Shahwan, T., "Radiochemical and spectroscopic studies of cesium, barium, and cobalt sorption on some natural clays" PhD Thesis, Bilkent University, Ankara, 2000

Shahwan, T., Sayan, S., Erten, H. N., Black, L., Hallam, K. R., Allen, G. C. 2000. "Surface spectroscopic studies of Cs⁺, and Ba²⁺ sorption on chlorite-illite mixed clay," *Radiochim. Acta.* Vol. 88, pp. 681-684.

Shahwan, T., Erten, H. N. 2002. "Thermodynamic parameters of Cs⁺ sorption on natural clays," *Journal of Radioanalytical and Nuclear Chemistry*. Vol. 253, pp. 115-119.

Shahwan, T., Atesin, A. C., Erten, H. N., Zararsiz, A. 2002. "Uptake of Ba²⁺ ions by natural bentonite and CaCO₃: A radiotracer, EDXRF and PXRD study," *Journal of Radioanalytical and Nuclear Chemistry*. Vol. 254, pp. 563-566.

Shahwan, T., Akar, D., Erođlu, A.E. 2004. "Physicochemical characterization of the retardation of aqueous Cs⁺ ions by natural kaolinite and clinoptilolite minerals,"

Tanaka, H., Yamasaki, N., Muratani, M., Hino, R. 2003 "Structure and formation process of (K, Na) – clinoptilolite," *Materials Research Bulletin*. Vol. 38, p. 719.

Toprak, R., Girgin, İ. 2000. "Removal of chromium from leather industry waste water by activated clinoptilolite," *Turk J Engin Environ Sci*. Vol. 24, p. 344.

Tsai, S., Ouyang, S., Hsu, C. 2001. "Sorption and diffusion behavior of Cs and Sr on Jih-Hsing bentonite," *Applied Radiation and Isotopes*. Vol. 54, p. 213.

Türkman, A., Aslan, Ş., Ege, İ. 2001. "Lead removal from wastewaters by natural zeolites," *DEÜ Mühendislik Fakültesi Fen ve Mühendislik Dergisi* Cilt: 3, p.14.

Tyson, J. F., Haswell, S.J. 1991 . "Basic Principles and Instrumental Requirements and Optimisation", in *Atomic Absorption Spectrometry*, edited by S.J. Haswell (Elsevier, Amsterdam), pp. 9-10, 14-17,21-40.

(a) Valcke, E., Engels, B., Cremers, A. 1997. "The use of zeolites as amendments in radiocaesium- and radiostrontium- contaminated soils: A soil-chemical approach. Part I: Cs-K exchange in clinoptilolite and mordenite," *Zeolites*. Vol. 18, pp. 209, 211.

(b)Valcke, E., Engels, B., Cremers, A. 1997. "The use of zeolites as amendments in radiocaesium- and radiostrontium- contaminated soils: A soil-chemical approach. Part II: Sr-Ca exchange in clinoptilolite and mordenite, and zeolite A," *Zeolites*. Vol. 18, pp. 212-216.

JR Weber, W. J., McGinley, P. M., Katz, L. E. 1991. "Sorption phenomena in subsurface systems: concepts, models and effects on contaminant fate and transport," *Wat. Res.* Vol. 25, No. 5, pp. 500-507.

Welz, B., Sperling, M. 1998. *Atomic Absorption Spectrometry*, (Überlingen), pp. 103-105, 113, 149-171

Wenming, D., Xiangke, W., Xiaoyan, B., Aixia, W., Jingzhou, D., Zuyi, T. 2001. "Comparative study on sorption / desorption of radioeuropium on alumina, bentonite and red earth: effects of pH, ionic strength, fulvic acid, and iron oxides in red earth," *Applied Radiation and Isotopes*. Vol. 54, pp. 603-604.

Westrich, H. R., Brady, P. V., Cygan, R. T., Gruenhagen, S. E., Anderson, H. L., Nagy, K. L. 1998. "Characterization of Retardation Mechanisms in Soil," , pp. 4, 8-12, 15-19.

Wilson M.J., 1994. *Clay Mineralogy: Spectroscopic and Chemical Determinative Methods*. (Chapman and Hall) , pp 52-55.

Woods, R. M. and Gunter, M. E. 2001. "Na-and Cs-exchange in a clinoptilolite-rich rock: Analysis of the outgoing cations in solution," *American Mineralogist*. Vol. 86, p.428.

WEB_1, 2001, ATSDR-ToxFAQs™ -Cesium, 27.04.2004. <http://www.atsdr.cdc.gov/tfacts157.html>

WEB_2, 2001, ATSDR-ToxFAQs™ :Strontium – Draft for public comment, 27.04.2004. <http://www.atsdr.cdc.gov/tfacts159.html>

WEB_3, 2001, CDC Radiation Emergencies / Radioisotope Brief: Cesium - 137 (Cs-137), 27.04.2004. <http://www.bt.cdc.gov/radiation/isotopes/cesium.asp>

WEB_4, 2001, CDC Radiation Emergencies / Radioisotope Brief: Strontium -90 (Sr-90), 27.04.2004. <http://www.bt.cdc.gov/radiation/isotopes/strontium.asp>

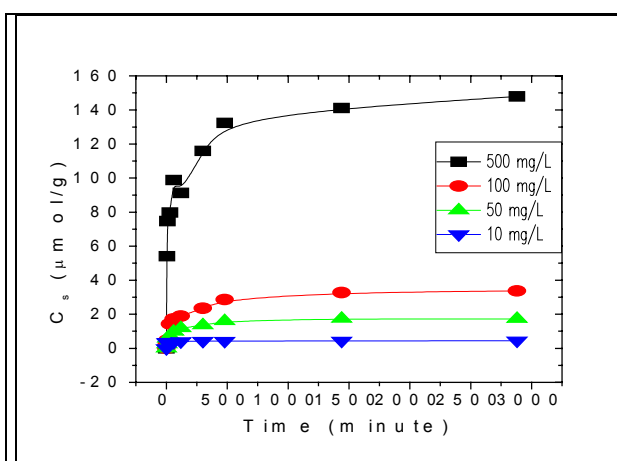
WEB_5, 2003, Mining Sector in Turkey, 01.01.2005. http://www.maden.org.tr/yeni3/english/mining_sector_in_turkey/miningsectorinturkey%202003.pdf

WEB_6, 1999, Kaolinite 01.01.2005 <http://cems.alfred.edu/courses/ces101/rawmat/sld011.htm>

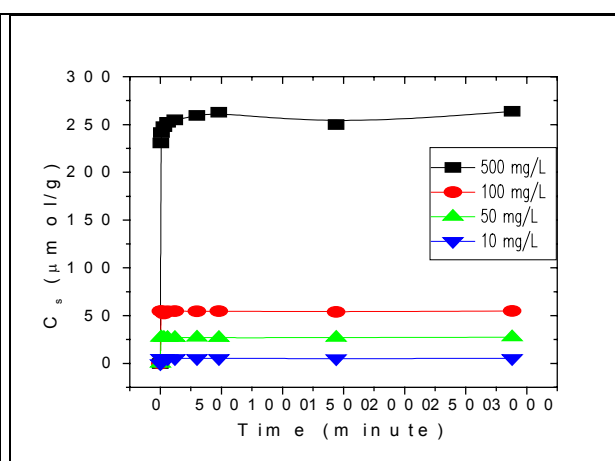
APPENDICES

APPENDIX A

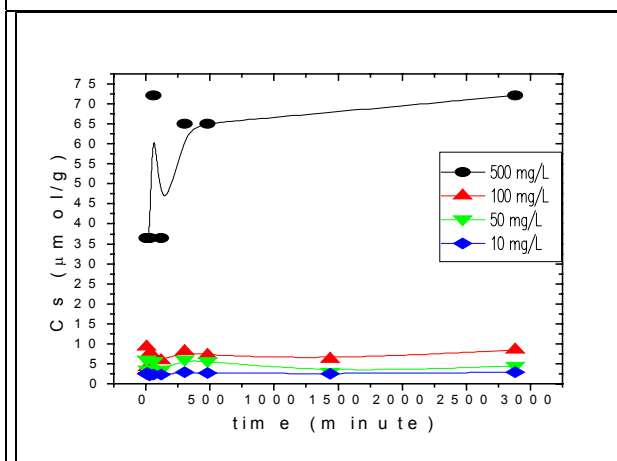
Variation of the sorbed amount of Sr^{2+} (or Cs^+) ($\mu\text{mol/g}$) on kaolinite and clinoptilolite at 60°C .



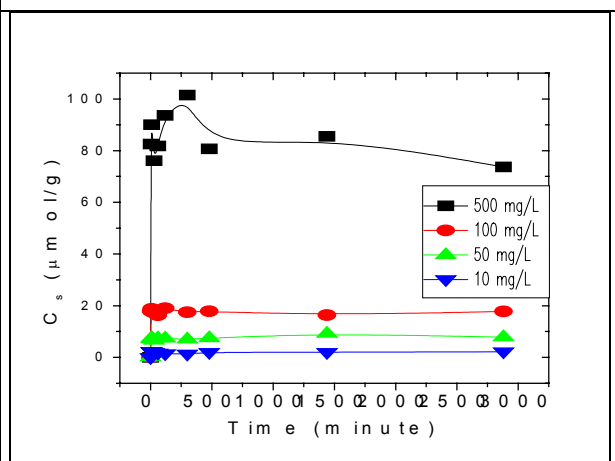
Sr-clinoptilolite 60°C



Cs-clinoptilolite 60°C



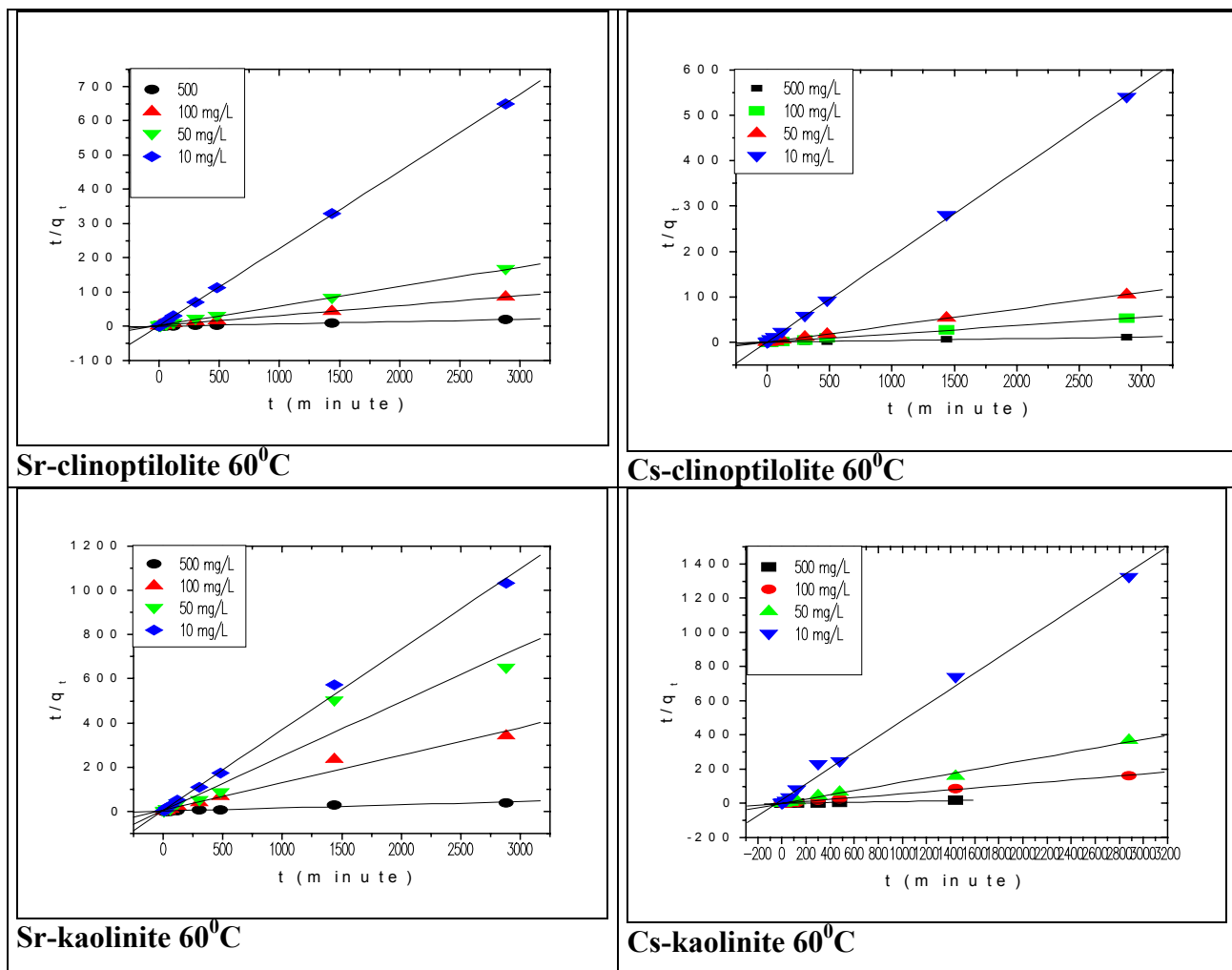
Sr-kaolinite 60°C



Cs-kaolinite 60°C

APPENDIX B

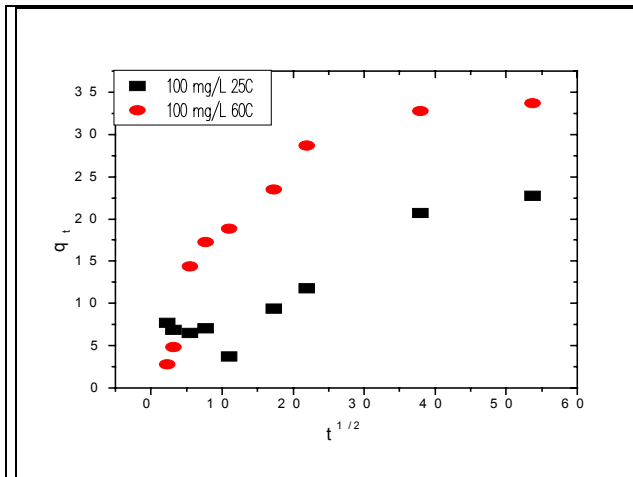
Corresponding linear fits using the pseudo-second order equation.



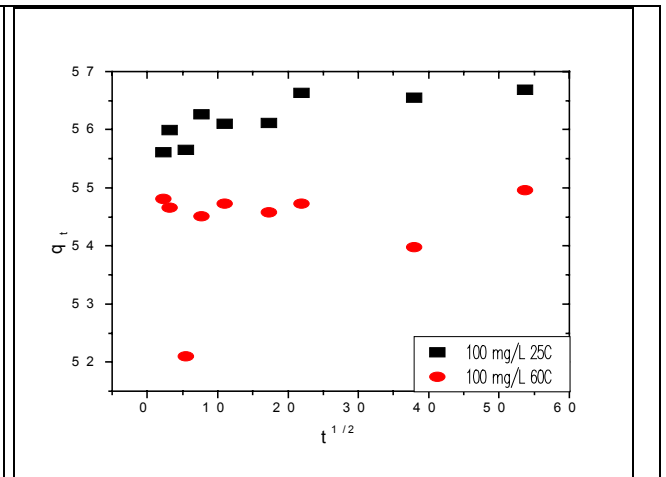
APPENDIX C

Intra-particle diffusion plots of sorbed ions at 25C and 60C.

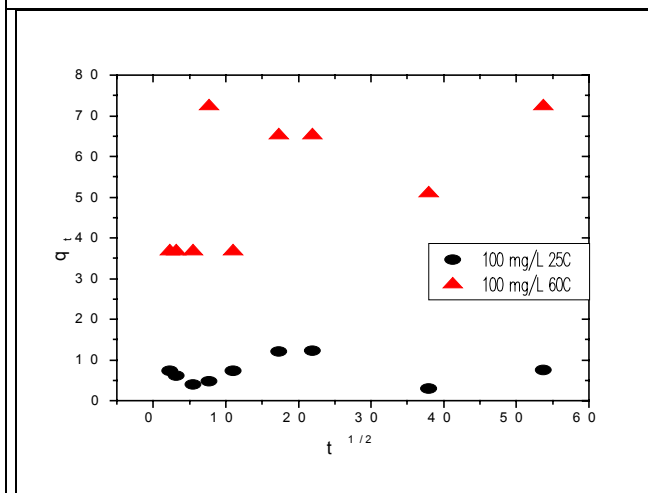
For 100 mg/L initial concentrations



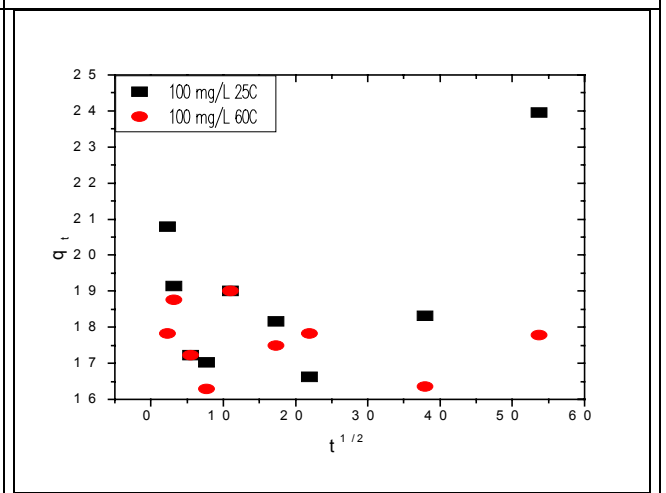
Sr-clinoptilolite



Cs-clinoptilolite

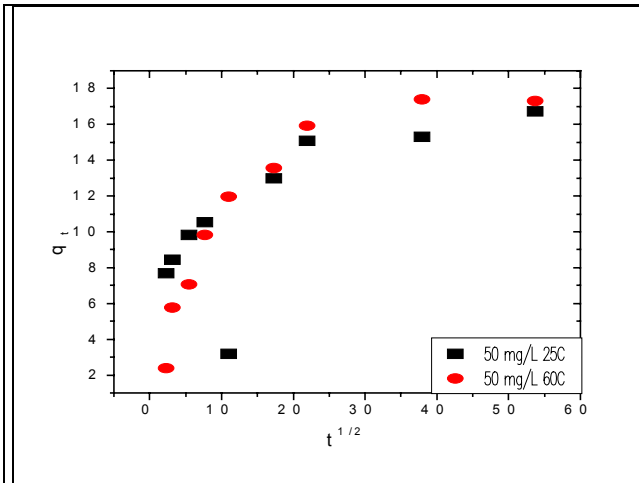


Sr-kaolinite

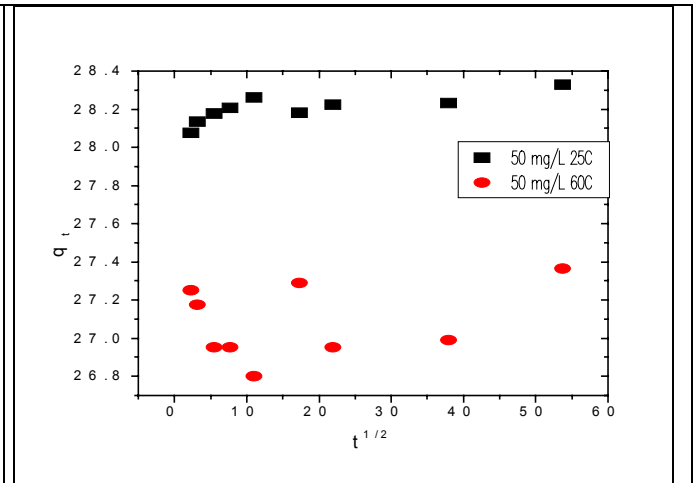


Cs-kaolinite

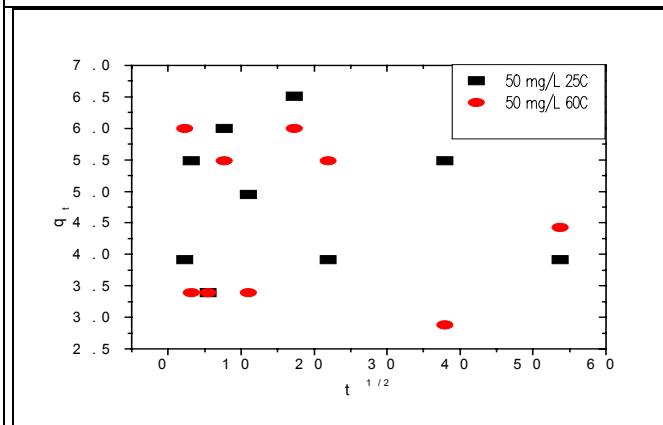
For 50 mg/L initial concentrations



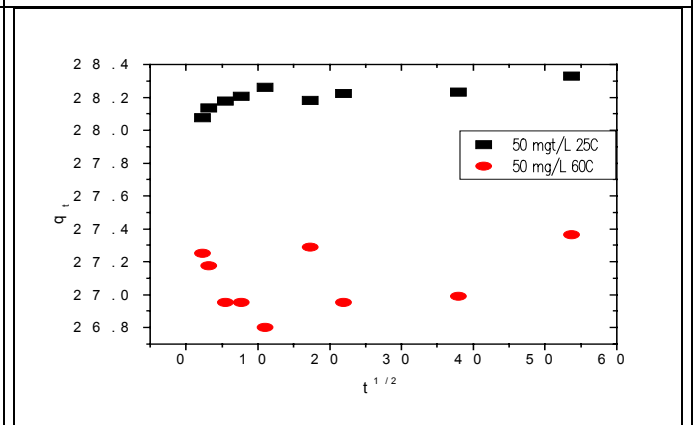
Sr-clinoptilolite



Cs-clinoptilolite

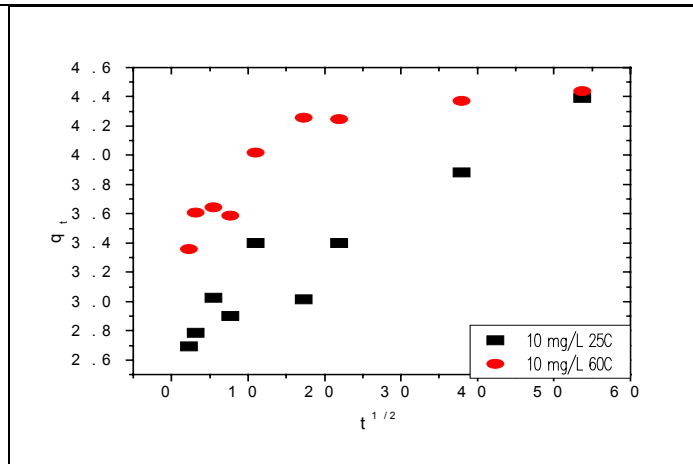


Sr-kaolinite

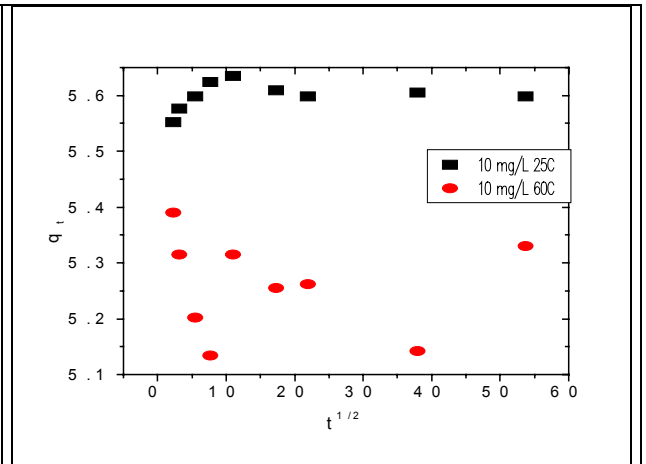


Cs-kaolinite

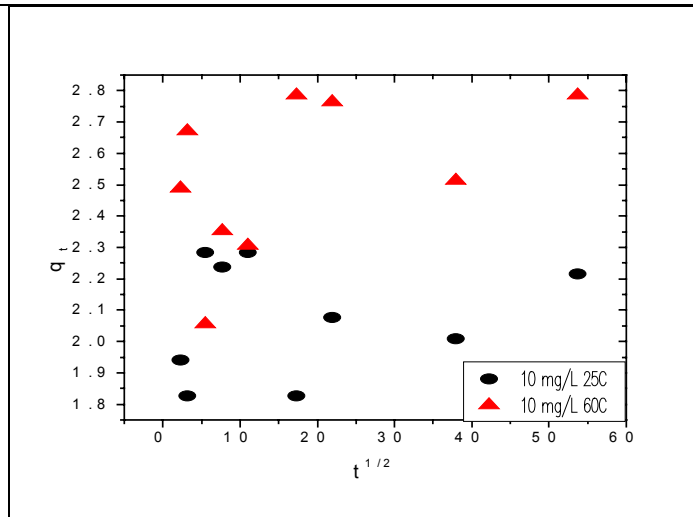
For 10 mg/L initial concentrations



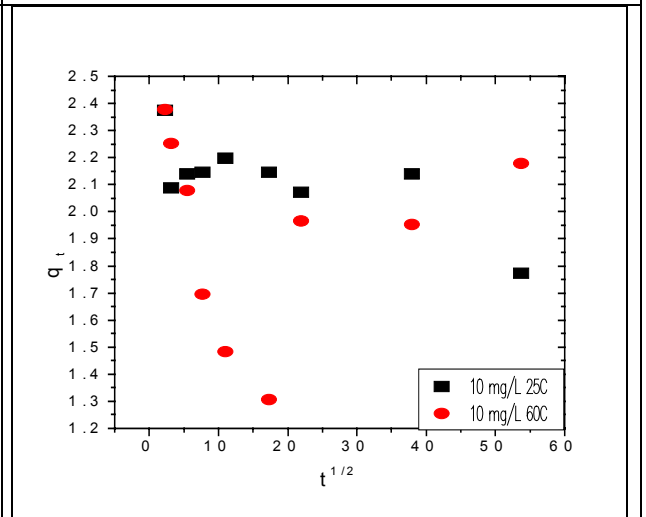
Sr-clinoptilolite



Cs-clinoptilolite



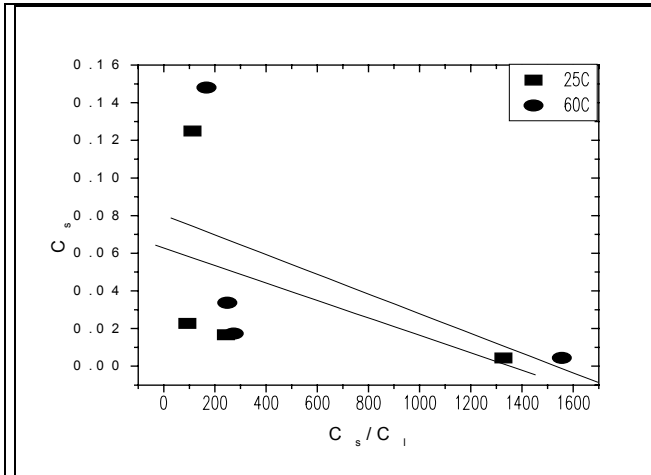
Sr-kaolinite



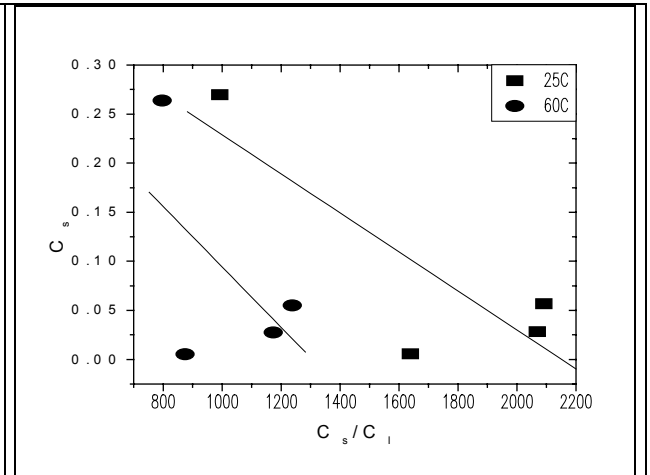
Cs-kaolinite

APPENDIX D

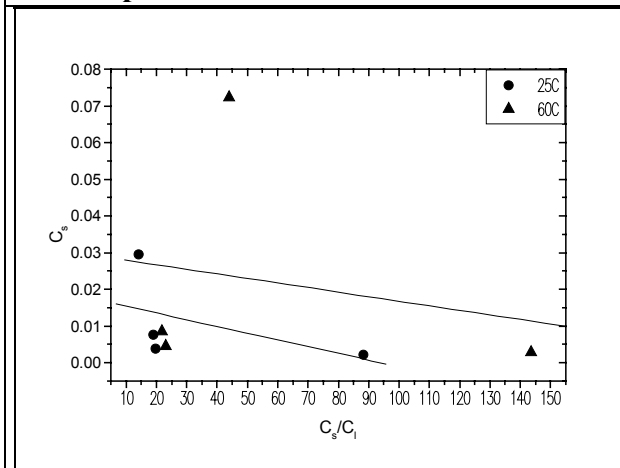
Langmuir isotherm plots of sorbed ions by clinoptilolite and kaolinite at 25C and 60C.



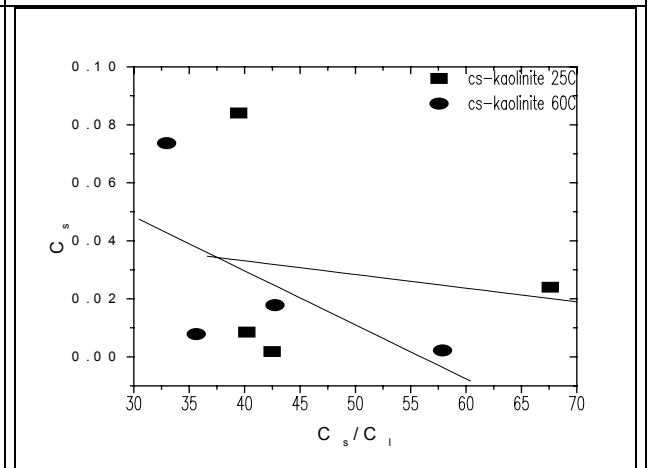
Sr-clinoptilolite



Cs-clinoptilolite



Sr-kaolinite



Cs-kaolinite